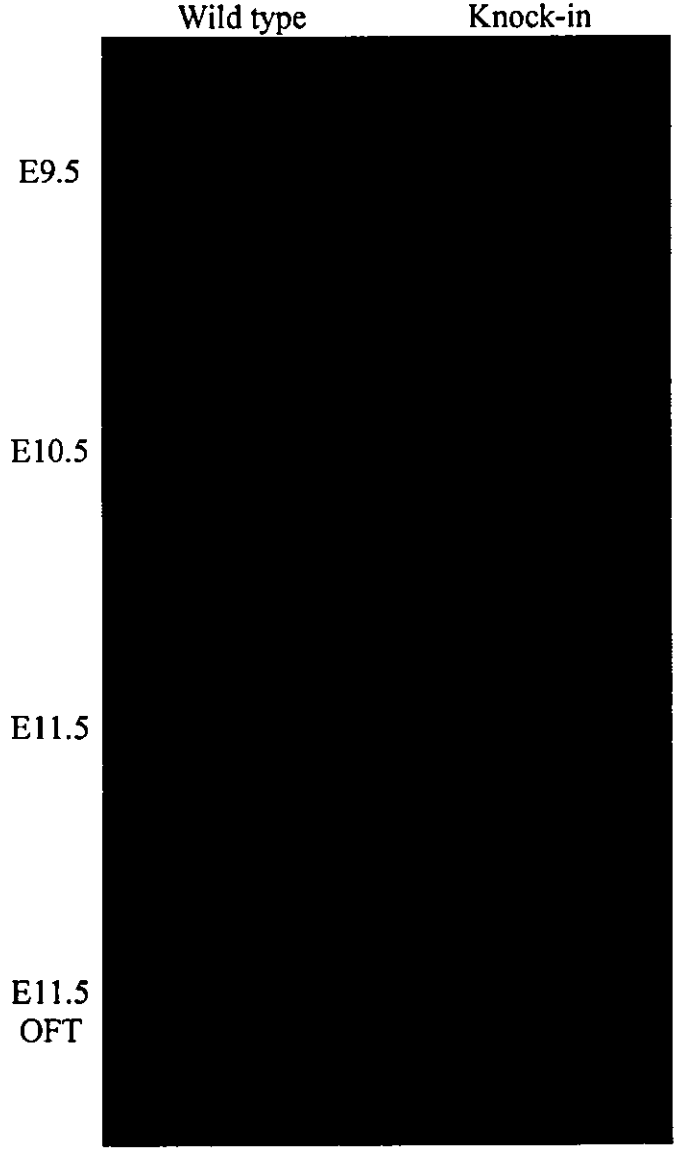

FIG. 3. Expression of *Hand1/eHAND* in wild-type and *Hand1/eHAND* KI embryos. In wild-type embryos, *Hand1/eHAND* was expressed in the outer curvature of the LV at E9.5 (arrows in panel A). Weak expression was observed in the outer curvature of the RV at E10.5 and E11.5 (C, E, and G). *Hand1/eHAND* expression was also detected in the distal part of the OFT (G). Note the absence of *Hand1/eHAND* expression in the IVG (arrowheads in panels A, C, and E). In *Hand1/eHAND* KI embryos, *Hand1/eHAND* was expressed in the whole ventricle, including the inner curvature, as well as in the AVC and the proximal part of the OFT (B, D, F, and H). In spite of the ectopic *Hand1/eHAND* expression, the inner curvature, AVC, or OFT did not expand outwards in *Hand1/eHAND* KI embryos (D, F, and H). Bars, 200 μm.

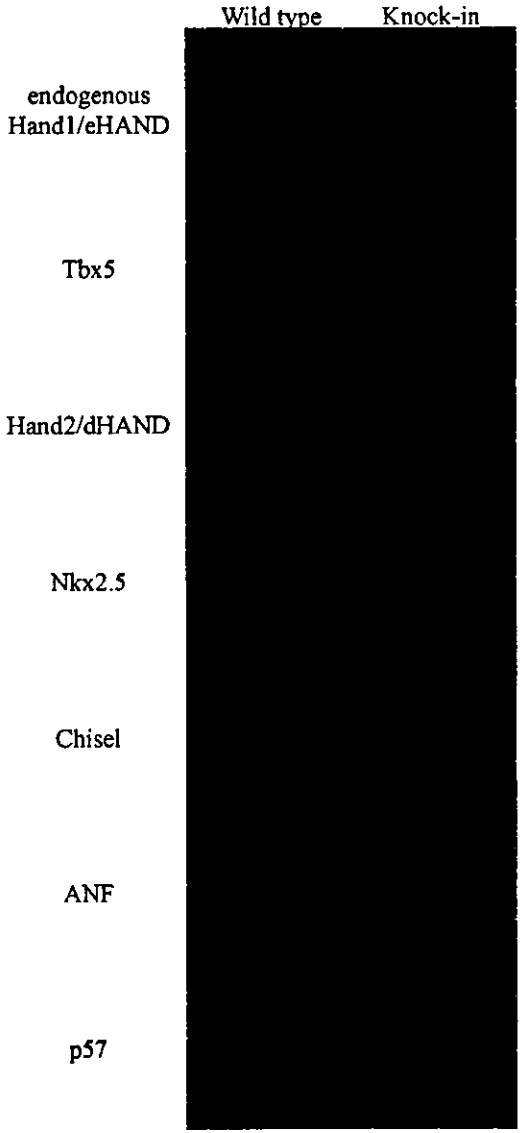

FIG. 4. Expression of cardiac transcription factors and molecular markers for the chamber myocardium. Expression of endogenous *Hand1/eHAND* (A and B), *Tbx5* (C and D), *Hand2/dHAND* (E and F), *Nkx2.5* (G and H), *Chisel* (I and J), *ANF* (K and L), and *p57* (M and N) are shown. Endogenous *Hand1/eHAND* expression was only detected in the left half of the ventricle in *Hand1/eHAND* KI embryos (B). The *Tbx5* expression

bryos overexpressing *Hand1/eHAND* in the RV by using the *MLC2V* promoter (Fig. 5A and B) (10, 18). As expected, the IVS formed normally in these transgenic embryos (Fig. 5D). Immunohistochemistry revealed FLAG-tagged Hand1/eHAND expression in the RV but not in the boundary region (Fig. 5C). These results indicated that the absence of *Hand1/eHAND* expression in the boundary region was critical for the proper formation of the IVS.

DISCUSSION

Septum formation is one of the critical steps in the transformation of a linear heart tube into a four-chambered heart. Morphologically, it has been pointed out that the boundary region between the LV and RV does not expand during the formation of the muscular IVS (Fig. 6A) (19). When the outer curvatures on each side of the narrow boundary region keep expanding, the two walls will eventually fuse, forming a septum (19). However, the molecular mechanism for expansion of the ventricular walls has never been elucidated. *Hand1/eHAND* KI embryos had a morphologically single ventricle, but there were distinctive LV and RV at the molecular level. Therefore, forced expression of *Hand1/eHAND* in the whole ventricle resulted in expansion of the entire ventricular wall including the boundary region (Fig. 6B). Although it is possible that overexpression of *Hand1/eHAND* may have affected the phenotype, the absence of *Hand1/eHAND* expression in the boundary region was critical in the development of the IVG and IVS (Fig. 6A) because transgenic embryos expressing *Hand1/eHAND* in the RV and LV, but not in the boundary region, exhibited normal formation of the IVS (Fig. 6C).

Ectopic expression of *Hand1/eHAND* in the entire RV resulted in more marked expansion of the outer curvature of the RV. Together with the result that *Hand1/eHAND* expression caused expansion of the boundary region, it is likely that *Hand1/eHAND* is involved in expansion of the ventricular walls. Then, which gene(s) regulate ballooning of the RV during normal cardiac development? Specific hypoplasia of the RV soon after cardiac looping in *Hand2/dHAND* knock-out embryos suggested a role of *Hand2/dHAND* in the expansion of the RV (21). Notably, *Hand2/dHAND* expression was also absent in the boundary region (Fig. 4E), thus suggesting a possibility that absence of *Hand1/eHAND* and *Hand2/dHAND* expression in the boundary region may be essential for the IVG and IVS formation (Fig. 6A).

Does *Hand1/eHAND* control the DV patterning of the embryonic heart? Interestingly, *Chisel* and *ANF*, molecular markers for the working myocardium (7), were ectopically expressed in the inner curvature and/or the AVC in *Hand1/eHAND* KI embryos. However, the inner curvature or the AVC did not expand morphologically. These results indicated that *Hand1/*

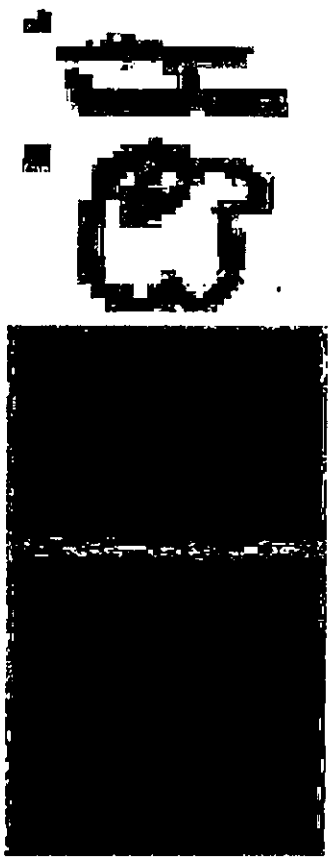

FIG. 5. *MLC2V-Hand1/eHAND* transgenic mice. (A) Schematic representation of the transgene. (B) The *MLC2V* promoter drives transgene expression in the RV and OFT but not in the boundary region. (C) Immunohistochemistry with an anti-FLAG antibody revealed FLAG-tagged Hand1/eHAND protein expression in the RV but not in the IVS. (D) In *MLC2V-Hand1/eHAND* transgenic embryos, the IVS formed normally. Av, AvaII; E, EcoRI. Bars, 100 μm.

gradient with higher expression in the LV was not disturbed in *Hand1/eHAND* KI embryos (D). Expression of *Hand2/dHAND* in the RV (E) was almost abolished in *Hand1/eHAND* KI embryos (F). Note the absence of *Hand2/dHAND* expression in the IVG in wild-type embryos (arrowhead in panel E). *Nkx2.5* expression was comparable between wild-type (G) and *Hand1/eHAND* KI (H) embryos. *Chisel* expression was also detected in the inner curvature and AVC in *Hand1/eHAND* KI embryos (J). Note the absence of *ANF* expression in the IVG (arrowhead in panel K) and inner curvature (arrow in panel K) in wild-type embryos (K). *ANF* expression was up-regulated in the RV and inner curvature in *Hand1/eHAND* KI embryos (L). *ANF* was also expressed at the region where the IVS was expected to form (arrowhead in panel L). Expression of *p57* was detected only in the trabecular layer both in wild-type and *Hand1/eHAND* KI embryos (M and N). Bars, 200 μm.

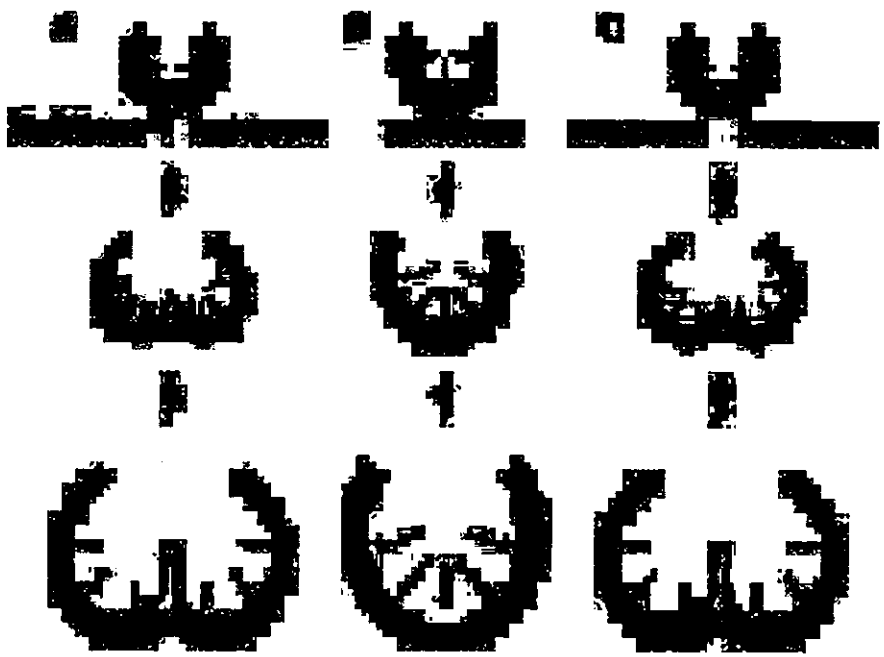

FIG. 6. Schematic presentation of ventricular expansion and IVS formation. (A) IVS formation in normal hearts. The outer curvatures of the LV and RV expand outwards. For the proper formation of the IVS, the boundary region should not expand. *Hand1/eHAND* and *Hand2/dHAND* may regulate expansion of the LV and RV, respectively. Note the absence of *Hand1/eHAND* and *Hand2/dHAND* expression in the boundary region. (B) In *Hand1/eHAND* KI hearts, the boundary region also expanded outward. As a result, the IVS did not form properly. (C) In *MLC2V-Hand1/eHAND* transgenic embryos, while the *Hand1/eHAND* transgene was expressed in the RV and endogenous *Hand1/eHAND* was expressed in the LV, *Hand1/eHAND* expression was absent in the boundary region. In these transgenic embryos, the boundary region did not expand outwards and the IVS formed normally.

eHAND regulated expression of molecular markers for the working myocardium but that additional gene(s) normally expressed in the outer curvature may be required for expansion of the chamber walls together with *Hand1/eHAND*.

The results of this study also gave insight into the hierarchical and combinatorial molecular cascade that controls cardiac development. Forced expression of *Hand1/eHAND* in the RV down-regulated *Hand2/dHAND* expression. It is possible that expression of *Hand2/dHAND* in the LV may be suppressed by high expression of *Hand1/eHAND* in the normal embryonic heart. However, *Hand1/eHAND* expression in the whole ventricles did not disturb the *Tbx5* expression gradient or endogenous *Hand1/eHAND* expression. Therefore, it is unlikely that *Hand1/eHAND* is the most upstream gene that specifies the LV myocyte lineage.

Between E10.5 and E11.5, cardiac myocytes undergo rapid cell division, resulting in doubling of cardiac mass (11). By E10.5, *Hand1/eHAND* KI embryos were indistinguishable from wild-type embryos except that they lacked the IVG and IVS. At E11.5, the compact zone layer of the *Hand1/eHAND* KI hearts were thin, suggesting that heart failure due to poor development of the compact zone layer may have caused the embryonic lethality. What is the mechanism for thin myocardium in *Hand1/eHAND* KI embryos? N-*myc*, *TEF-1*, and *p57* were normally expressed in *Hand1/eHAND* KI embryos, suggesting that there may be other mechanism(s). At E11.5, *Hand1/eHAND* expression was obviously down-regulated in wild-type embryos, while strong expression of *Hand1/eHAND* persisted in *Hand1/eHAND* KI embryos. Thus, down-regulation of *Hand1/eHAND* at the mid-stage of cardiac development may be important for the proper formation of the compact zone myocardium. Although it may seem inconsistent that *Hand1/eHAND* enhanced expansion of the ventricular chambers at E10.5 but that overexpression of *Hand1/eHAND* at E11.5 disturbed proliferation of the compact zone myocardium, fine-tuning of *Hand1/eHAND* expression at each stage may be required for the proper development of the embryonic heart. It is also possible that different mechanisms may exist to regulate expansion of the ventricular chambers and thickening of ventricular walls.

Recently, Takeuchi et al. reported that *Tbx5* may determine the position of the IVS in chicken and mouse embryonic hearts (22). When *Tbx5* was overexpressed in the whole ventricles, the *Hand1/eHAND* expression domain was expanded to the RV, resulting in a lack of IVS formation. Their study suggested that *Tbx5* may control *Hand1/eHAND* expression and that in the chicken heart, the boundary of the *Tbx5* and *Tbx20* expression domains may determine the position of the IVS (22). Together with the results of our study, it was likely that the function of *Tbx5* in the expansion of the ventricular walls and the IVS formation in murine hearts was mediated through eHAND. Moreover, since *Tbx20* is uniformly expressed in the LV and RV (12) and *Tbx5* is not expressed in the boundary region between the LV and RV in the normal murine hearts, the absence of *Tbx5* and *Hand1/eHAND* expression in the boundary region may be critical in the proper formation of the IVS in murine cardiac development.

In summary, expression of *Hand1/eHAND* enhanced expansion of chamber walls, and absence of *Hand1/eHAND* expression in the boundary region may be essential for the proper formation of the IVG and IVS. Moreover, additional factors normally expressed in the outer curvature may determine the DV patterning of the embryonic heart in concert with *Hand1/eHAND*.

ACKNOWLEDGMENTS

We gratefully acknowledge Keiko Kobayashi and Ayumi Hosotani for technical assistance. We also thank Benoit G. Bruneau for providing a cDNA probe.

This work was supported by research grants from the Ministry of Education, Science, Sports, and Culture of Japan (grants 13045019, 13832003, and 15590738 [to M.T.] and 12CE2006 and 13307034 [to T.K.]), research grants from the Ministry of Health, Labor, and Welfare of Japan (Comprehensive Research on Aging and Health grant no. H14-choju-012 [to T. Kita]), and the grant provided by the Ichiro Kanehara Foundation (to M.T.).

REFERENCES

1. **Biben, C., and R. P. Harvey.** 1997. Homeodomain factor Nkx2-5 controls left/right asymmetric expression of bHLH gene eHand during murine heart development. Genes Dev. 11:1357–1369.
2. **Bruneau, B. G.** 2002. Transcriptional regulation of vertebrate cardiac morphogenesis. Circ. Res. 90:509–519.
3. **Bruneau, B. G., G. Nemer, J. P. Schmitt, F. Charron, L. Robitaille, S. Caron, D. A. Conner, M. Gessler, M. Nemer, C. E. Seidman, and J. G. Seidman.** 2001. A murine model of Holt-Oram syndrome defines roles of the T-box transcription factor Tbx5 in cardiogenesis and disease. Cell 106:709–721.
4. **Charron, J., B. A. Malynn, P. Fisher, V. Stewart, L. Jeannotte, S. P. Goff, E. J. Robertson, and F. W. Alt.** 1992. Embryonic lethality in mice homozygous for a targeted disruption of the N-myc gene. Genes Dev. 6:2248–2257.
5. **Chen, J., S. W. Kubalak, S. Minamisawa, R. L. Price, K. D. Becker, R. Hickey, J. Ross, Jr., and K. R. Chien.** 1998. Selective requirement of myosin light chain 2v in embryonic heart function. J. Biol. Chem. 273:1252–1256.
6. **Chen, Z., G. A. Friedrich, and P. Soriano.** 1994. Transcriptional enhancer factor 1 disruption by a retroviral gene trap leads to heart defects and embryonic lethality in mice. Genes Dev. 8:2293–2301.
7. **Christoffels, V. M., P. E. Habets, D. Franco, M. Campione, F. de Jong, W. H. Lamers, Z. Z. Bao, S. Palmer, C. Biben, R. P. Harvey, and A. F. Moorman.** 2000. Chamber formation and morphogenesis in the developing mammalian heart. Dev. Biol. 223:266–278.
8. **de Jong, F., S. Viragh, and A. F. Moorman.** 1997. Cardiac development: a morphologically integrated molecular approach. Cardiol. Young 7:131–146.
9. **Harvey, R. P.** 1999. Seeking a regulatory roadmap for heart morphogenesis. Semin. Cell Dev. Biol. 10:99–107.
10. **Henderson, S. A., M. Spencer, A. Sen, C. Kumar, M. A. Siddiqui, and K. R. Chien.** 1989. Structure, organization, and expression of the rat cardiac myosin light chain-2 gene. Identification of a 250-base pair fragment which confers cardiac-specific expression. J. Biol. Chem. 264:18142–18148.
11. **Kochilas, L. K., J. Li, F. Jin, C. A. Buck, and J. A. Epstein.** 1999. p57Kip2 expression is enhanced during mid-cardiac murine development and is restricted to trabecular myocardium. Pediatr. Res. 45:635–642.
12. **Kraus, F., B. Haenig, and A. Kispert.** 2001. Cloning and expression analysis of the mouse T-box gene tbx20. Mech. Dev. 100:87–91.
13. **Lamers, W. H., and A. F. Moorman.** 2002. Cardiac septation: a late contribution of the embryonic primary myocardium to heart morphogenesis. Circ. Res. 91:93–103.
14. **Moens, C. B., B. R. Stanton, L. F. Parada, and J. Rossant.** 1993. Defects in heart and lung development in compound heterozygotes for two different targeted mutations at the N-myc locus. Development 119:485–499.
15. **Nagy, A., C. Moens, E. Ivanyi, J. Pawling, M. Gertsenstein, A. K. Hadjantonakis, M. Pirity, and J. Rossant.** 1998. Dissecting the role of N-myc in development using a single targeting vector to generate a series of alleles. Curr. Biol. 8:661–664.
16. **Palmer, S., N. Groves, A. Schindeler, T. Yeoh, C. Biben, C. C. Wang, D. B. Sparrow, L. Barnett, N. A. Jenkins, N. G. Copeland, F. Koentgen, T. Mohun, and R. P. Harvey.** 2001. The small muscle-specific protein Csl modifies cell shape and promotes myocyte fusion in an insulin-like growth factor 1-dependent manner. J. Cell Biol. 153:985–998.
17. **Riley, P., L. Anson-Cartwright, and J. C. Cross.** 1998. The Hand1 bHLH transcription factor is essential for placentation and cardiac morphogenesis. Nat. Genet. 18:271–275.
18. **Ross, R. S., S. Navankasattusas, R. P. Harvey, and K. R. Chien.** 1996. An HF-1a/HF-1b/MEF-2 combinatorial element confers cardiac ventricular specificity and established an anterior-posterior gradient of expression. Development 122:1799–1809.
19. **Sadler, T. W.** 2004. Langman's medical embryology, 9th ed. Lippincott William & Wilkins, Baltimore, Md.
20. **Srivastava, D., and E. N. Olson.** 2000. A genetic blueprint for cardiac development. Nature 407:221–226.
21. **Srivastava, D., T. Thomas, Q. Lin, M. L. Kirby, D. Brown, and E. N. Olson.** 1997. Regulation of cardiac mesodermal and neural crest development by the bHLH transcription factor, dHAND. Nat. Genet. 16:154–160.
22. **Takeuchi, J. K., M. Ohgi, K. Koshiba-Takeuchi, H. Shiratori, I. Sakaki, K. Ogura, Y. Saijoh, and T. Ogura.** 2003. Tbx5 specifies the left/right ventricles and ventricular septum position during cardiogenesis. Development 130:5953–5964.
23. **Tanaka, M., Z. Chen, S. Bartunkova, N. Yamasaki, and S. Izumo.** 1999. The cardiac homeobox gene Csx/Nkx2.5 lies genetically upstream of multiple genes essential for heart development. Development 126:1269–1280.
24. **Thomas, T., H. Yamagishi, P. A. Overbeek, E. N. Olson, and D. Srivastava.** 1998. The bHLH factors, dHAND and eHAND, specify pulmonary and systemic cardiac ventricles independent of left-right sidedness. Dev. Biol. 196:228–236.

Critical Roles of CXC Chemokine Ligand 16/Scavenger Receptor that Binds Phosphatidylserine and Oxidized Lipoprotein in the Pathogenesis of Both Acute and Adoptive Transfer Experimental Autoimmune Encephalomyelitis[1]

Noriko Fukumoto,* Takeshi Shimaoka,* Harutoshi Fujimura,† Saburo Sakoda,‡ Makoto Tanaka,§ Toru Kita,¶ and Shin Yonehara[2]*

The scavenger receptor that binds phosphatidylserine and oxidized lipoprotein (SR-PSOX)/CXCL16 is a chemokine expressed on macrophages and dendritic cells, while its receptor expresses on T and NK T cells. We investigated the role of SR-PSOX/CXCL16 on acute and adoptive experimental autoimmune encephalomyelitis (EAE), which is Th1-polarized T cell-mediated autoimmune disease of the CNS. Administration of mAb against SR-PSOX/CXCL16 around the primary immunization decreased disease incidence of acute EAE with associated reduced infiltration of mononuclear cells into the CNS. Its administration was also shown to inhibit elevation of serum IFN-γ level at primary immune response, as well as subsequent generation of Ag-specific T cells. In adoptive transfer EAE, treatment of recipient mice with anti-SR-PSOX/CXCL16 mAb also induced not only decreased clinical disease incidence, but also diminished traffic of mononuclear cells into the CNS. In addition, histopathological analyses showed that clinical development of EAE correlates well with expression of SR-PSOX/CXCL16 in the CNS. All the results show that SR-PSOX/CXCL16 plays important roles in EAE by supporting generation of Ag-specific T cells, as well as recruitment of inflammatory mononuclear cells into the CNS. ***The Journal of Immunology*****, 2004, 173: 1620–1627.**

Multiple sclerosis (MS)[3] and its animal model, experimental autoimmune encephalomyelitis (EAE), are type I (Th1)-polarized T cell-mediated autoimmune diseases of the CNS (1, 2). In both diseases, Th1 autoreactive T cells for self-Ags in the CNS are initially generated (3, 4), and then circulating leukocytes including the autoreactive T cells penetrate the blood brain barrier. Finally, the penetrated leukocytes induce damage of myelin, resulting in impaired nerve conduction and paralysis (2). However, the mechanisms of generation of autoreactive Th1 T cells, recruitment of leukocytes into the CNS, and accumulation of the leukocytes in the CNS before and during clinical disease are not well understood.

Chemokines are a family of cytokines exhibiting selective chemoattractant properties for target leukocytes. Based on the motif of the first two cysteines, chemokines have been classified into four highly conserved but distinct subfamilies: CC, CXC, C, and CX3C chemokines (5). Chemokines play an important role in recruitment of leukocytes at the site of initial immunoreactions induced by such as infection as well as infiltration of leukocytes into the site of inflammation during the T cell-mediated inflammatory conditions (3, 6). Various chemokine members have been implicated as candidates involved in the immunopathology of EAE. CCL2/MCP-1, CCL3/MIP-1α, and CXCL1/IFN-γ-inducible protein-10 (IP-10) were reported to be expressed in the CNS in acute rat and murine EAE models (7, 8). T cell clones, which could induce adoptive transfer EAE, were reported to express CCR5, a receptor for CCL3/MIP-1α.

MIP-1α was demonstrated to play a functionally significant role in pathogenesis of mouse EAE by analyses that administration of neutralizing polyclonal Ab for MIP-1α suppressed severity of clinical EAE through partial inhibition of recruitment of inflammatory mononuclear cells including Th1 T cells into the CNS (7). In the case of IP-10, two contradictory results were reported (9, 10). Administration of neutralizing Ab against IP-10 partially decreased or increased clinical and histological disease incidence and severity, as well as infiltration of mononuclear cells into the CNS. As for MCP-1, gene-disrupted mice of MCP-1 and its receptor, CCR2, were shown to be completely resistant to development of EAE by inability of monocyte to be recruited into the CNS (9, 11, 12). Recruitment of monocytes into the CNS by MCP-1 must play an essential rule in EAE, while it has not been clear whether chemokines other than MIP-1α and IP-10 are involved in the infiltration of autoreactive T cells into the CNS.

Recently, polyclonal Ab against CCL20/MIP-3α was reported to partially suppress clinical EAE by inhibiting sensitization of naive lymphocytes to myelin Ags through inhibition of naive dendritic cells (DCs) trafficking or by inhibiting exit of sensitized lymphocytes from the draining lymph nodes (13). However, it has not been clear what chemokines are involved in the generation of Th1-polarized autoreactive T cells in primary immune response in EAE.

Recently, we and others identified a novel transmembrane protein that was designated as SR-PSOX (scavenger receptor that binds phosphatidylserine and oxidized lipoprotein) and CXCL 16, respectively (14–16). Interestingly, SR-PSOX/CXCL16 was shown to possess two different biological activities, scavenger receptor and chemokine activities. SR-PSOX/CXCL16 is the ligand for Bonzo/CXCR6 expressed on naive and active CD8 T cells, Th1-polarized activated CD4, and naive and activated NK T cells (14, 15). SR-PSOX/CXCL16 was shown to have chemoattractant activity for activated T cells, but not naive CD8 T cells (15). Cell surface-anchored SR-PSOX/CXCL16 with a transmembrane domain shows not only scavenger receptor activity but also cell adhesion activity against CXCR6-expressing cells, while membrane metalloprotease-cleaved soluble SR-PSOX/CXCL16 shows chemokine activity for CXCR6-expressing cells (17, 18). Bonzo/CXCR6, a receptor of SR-PSOX/CXCL16, was reported to be expressed on a subset of Th1 T cells but not on Th2 T cells, and its expression has been regarded as a differential marker of Th1-polarized T cells (19). Furthermore, expression of Bonzo/CXCR6 was confirmed in myelin basic protein-reactive T cell lines with IFN-γ-producing activity (20).

In this study, we investigated in vivo effects of neutralizing anti-SR-PSOX/CXCL16 mAb in both acute and adoptive transfer EAE. SR-PSOX/CXCL16 was clearly shown to play an important role in different two phases of EAE: IFN-γ-production at primary immune response followed by generations of myelin basic protein-specific T cells and recruitment of mononuclear cells into the CNS.

Materials and Methods

Mice and Ag

C57BL/6J mice were purchased from CLEA Japan (Tokyo, Japan) and housed under the specific pathogen-free condition. Myelin oligodendrocyte glycoprotein peptide (MOG_{35-55}; MEVGWYRSPFSRVVHLYRNGK), which was used for Ags inducing acute EAE, was synthesized by Toray Research Center (Kamakura, Japan), and purity was determined to be >95% by reversed-phase HPLC.

Anti-mouse SR-PSOX/CXCL16 mAbs

We generated anti-SR-PSOX/CXCL16 mAb IgG1 12-81 as described previously (18). This Ab did not cross any other chemokines, which could be expected. Anti-human SR-PSOX mAb IgG1 22-19-12 was generated and characterized as described previously (17). Both mAbs were provided by Sankyo (Tokyo, Japan).

Chemotaxis and calcium mobilization assays

Chemotaxis assay using transwell plates with 5-μm pore size membrane (Corning Japan, Tokyo, Japan) and calcium mobilization assays were performed as described previously (18, 21).

Effect of anti-SR-PSOX/CXCL16 mAb on soluble SR-PSOX/CXCL16-binding to CXCR6-expressing cells

CXCR6-expressed L1.2 cells (17) were incubated for 1 h on ice with mouse SR-PSOX/CXCL16-Fc (1 μg/ml), which was preincubated with anti-SR-PSOX mAbs 12-81 (5 μg/ml) or control rat IgG for 30 min on ice. For determining the quantity of cell-bound SR-PSOX/CXCL16-Fc, cells were stained with PE-labeled goat anti-human-Fc and analyzed by flow cytometry using Epics XL (Beckman Coulter, Fullerton, CA).

Expression analysis of CXCR6 on spleen T cells

Spleen cells were prepared from mice on day 4 after immunization of MOG_{35-55}, and cultured for 4 days in the presence or absence 25 μg/ml MOG_{35-55}. Cells were incubated for 1 h on ice with mouse SR-PSOX/CXCL16-Fc (1 μg/ml), followed by staining with PE-labeled goat anti-human-Fc, together with FITC-labeled anti-mouse CD4 mAb or FITC-labeled anti-mouse CD8 mAb (BD Biosciences, San Diego, CA) as described previously (18), and then analyzed by flow cytometry.

Active induction of EAE with MOG peptides and clinical evaluation

Six to 9-wk-old female mice were immunized by s.c. injection into thighs of bilateral hind feet with 150 μg/mouse of MOG peptides in 0.15 ml of sterilized PBS emulsified with an equal volume of CFA containing 4 mg/ml *Mycobacterium tuberculosis* (BD Diagnostic Systems, Sparks, MD) (22, 23). Two hours before and 2, 4, and 7 days after the immunization, mice were injected with 500 μg anti-SR-PSOX/CXCL16 mAb or control rat IgG. The mice were i.v. injected with pertussis toxin (List Biological Laboratories, Campbell, CA) at day 0 and 2 after immunization. Animals were scored daily for 5 wk for clinical signs of EAE using the following criteria: 0, no clinical signs; 1, limp tail (tail paralysis); 2, complete loss of tail tonicity or abnormal gait; 3, partial hind limb paralysis; 4, complete hind limb paralysis; 5, forelimb paralysis or moribund; and 6, death (24).

Passive transfer of EAE

Spleen-cell suspension was prepared from mice 4 days after the immunization with MOG_{35-55} as described in acute EAE and cultured in RPMI 1640 containing 10% FCS and 25 μg/ml MOG_{35-55} for 4 days at 37°C. Cells were harvested, washed three times with PBS and transferred i.v. into normal C57BL/6 recipient mice ($1–2 \times 10^7$ viable cells/mouse). Animals were scored daily for 5 wk for signs of EAE using the above-described criterion (8, 13).

T cell proliferation assay

Spleen-cell suspension (5×10^6/ml) was prepared from mice on day 6 after immunization of MOG_{35-55}, and cultured in triplicate in 96-well flat-bottom plates (IWAKI, Tokyo, Japan) in the presence or absence of MOG_{35-55}. Cells were pulsed with 0.5 μCi/well [^{3}H]thymidine (Valeant Pharmaceuticals, Costa Mesa, CA) at 72 h after cultivation, and incubated further for 12 h. Cells were then harvested and incorporated radioactivity was measured using a MicroBeta PLUS liquid scintillation counter with software v3.3 (PerkinElmer Wallac, Gaithersburg, MD).

Quantification of IFN-γ by ELISA

IFN-γ in serum, which was prepared from MOG_{35-55}-immunized mice on 36, 48, 60, and 84 h after immunization, was quantified using a mouse IFN-γ ELISA kit (GE Medical Systems, Milwaukee, WI), and the data were measured using Wallac 1420 ARVO fluoroscan (PerkinElmer Wallac).

Spleen-cell suspension (5×10^6/ml) was prepared from mice on day 6 after immunization of MOG_{35-55}, and cultured in triplicate in 96-well flat-bottom plates (IWAKI) in the presence or absence of MOG_{35-55} for 48 h. IFN-γ in the culture supernatants was quantified using a mouse IFN-γ ELISA kit (Amersham Biosciences), and the data were measured using Wallac 1420 ARVO fluoroscan (PerkinElmer Wallac).

RT-PCR for SR-PSOX/CXCL16 and CXCR6 mRNA

Total RNA was extracted from PBS-perfused and snap-frozen spinal cords using a total RNA Purification System (Invitrogen Life Technologies, Carlsbad, CA). cDNA was synthesized and RNA was amplified using Ready-To-Go RT-PCR Beads (GE Medical Systems). CXCR6 was detected by using the forward primer, 5′-CACTCTGGAACAAAGCTACTGGGCT-3′, and reverse primer, 5′-AGGTGAGAGTGAGCATGGACA-3′, and CXCL16 was detected by using primers as previously described (14).

Histological assessment for EAE

Spinal cords from EAE-induced mice were dissected on day 15 after immunization and fixed in 4% neutral buffered formalin in PBS. Paraffin-embedded sections of 4-μm thickness were cut from the spinal cords and stained with H&E or with the myelin-specific Bodian and Luxol fast blue (25). For in situ hybridization, paraffin-embedded sections of spinal cords from EAE-induced mice were sliced and fixed on glass slides precoated with 3-aminopropyltriethoxysilane. Antisense and sense ^{35}S-labeled cDNA probes specific for mouse SR-PSOX/CXCL16 were prepared by in vitro transcription with T3/T7 RNA polymerase (Stratagene, La Jolla, CA). SR-PSOX/CXCL16 mRNA-positive cells were examined under fluorescence microscope. Data were collected in several independent visual fields (24).

*Graduate School of Biostudies and Institute for Virus Research, Kyoto University, Sakyo-ku, Kyoto, Japan; †Department of Neurology, Toneyama National Hospital, Osaka, Japan; ‡Department of Neurology, Graduate School of Medicine, Osaka University, Suita, Japan; and Departments of §Geriatric Medicine and ¶Cardiovascular Medicine, Graduate School of Medicine, Kyoto University, Kyoto, Japan

Received for publication November 26, 2003. Accepted for publication May 25, 2004.

The costs of publication of this article were defrayed in part by the payment of page charges. This article must therefore be hereby marked *advertisement* in accordance with 18 U.S.C. Section 1734 solely to indicate this fact.

[1] This work was supported in part by Grants-in-Aid from the Ministry of Education, Culture, Sports, Science and Technology of the Japanese Government. N.F. was supported by the 21st Century Center of Excellence Program of the Ministry of Education, Culture, Sports, Science and Technology of Japan to Graduate School of Biostudies and Institute for Virus Research, Kyoto University.

[2] Address correspondence and reprint requests to Dr. Shin Yonehara, Graduate School of Biostudies and Institute for Virus Research, Kyoto University, Shogoin Kawaracho 53, Sakyo-ku, Kyoto 606-8507, Japan. E-mail address: syonehar@virus.kyoto-u.ac.jp

[3] Abbreviations used in this paper: MS, multiple sclerosis; DC, dendritic cell; EAE, experimental autoimmune encephalomyelitis; IP-10, IFN-γ-inducible protein-10; MOG, myelin oligodendrocyte glycoprotein; SR-PSOX, scavenger receptor that binds phosphatidylserine and oxidized lipoprotein.

0022-1767/04/$02.00

Results

Characterization of anti-SR-PSOX/CXCL16 mAb 12-81

To characterize rat anti-mouse SR-PSOX/CXCL16 mAb 12-81, we examined inhibitory activity of the mAb against the chemotactic activity of soluble SR-PSOX/CXCL16 for CXCR6-expressing cells using the standard transwell assay. The number of cells that migrated into bottom wells was shown to decrease in accordance with the concentration of anti-SR-PSOX/CXCL16 mAb (Fig. 1*A*). Then, we examined whether the mAb inhibits direct binding of SR-PSOX/CXCL16 to its receptor, CXCR6. Direct binding of soluble SR-PSOX/CXCL16-Fc to CXCR6-expressing L1.2 cells was quantified by flow cytometry. Anti-SR-PSOX/CXCL16 mAb 12-81 was clearly shown to specifically inhibit direct binding of SR-PSOX/CXCL16-Fc to CXCR6-expressing cells (Fig. 1*B*). These results indicate that anti-SR-PSOX/CXCL16 mAb 12-81 can inhibit SR-PSOX/CXCL16-induced migration as well as direct binding of SR-PSOX/CXCL16 to CXCR6-expressing cells.

Anti-SR-PSOX/CXCL16 mAb-treated mice are resistant to induction of acute EAE

To determine the roles of SR-PSOX/CXCL16 on development of clinical EAE, we examined the in vivo activity of neutralizing anti-mouse SR-PSOX/CXCL16 mAb 12-81 against induction of clinical acute EAE. Mice, immunized with the encephalitogenic peptide MOG_{35-55} on day 0, were administrated with anti-SR-PSOX/CXCL16 mAb on day 0, 2, 4, and 7, and scored daily for signs of disease (Fig. 2*A*). As expected, mice treated with control rat IgG instead of anti-SR-PSOX/CXCL16 mAb developed clinical EAE with a mode incidence of 100%. In contrast, the clinical disease severity was dramatically decreased in anti-SR-PSOX/CXCL16 mAb-treated mice. Although the control mice developed severe EAE with a mean clinical score of 3.8 on day 18 after immunization, anti-SR-PSOX/CXCL16 mAb-treated mice developed disease with a significantly decreased mean clinical score of 1.3 on day 19 with associated delayed onset of the clinical disease. Interestingly, administration of anti-SR-PSOX/CXCL16 mAb on only day 0 and 2 after immunization of MOG_{35-55} was shown to be enough to induce delayed onset of clinical EAE while reduction of the disease severity was lower than administration on day 0, 2, 4, and 7 after immunization (data not shown). Administration of anti-SR-PSOX/CXCL16 mAb on day 4 and 7 after immunization did not affect clinical EAE. All the results indicate that in vivo neutralization of SR-PSOX/CXCL16 before the onset of clinical EAE significantly reduced the severity as well as early onset of acute EAE.

FIGURE 1. Characterization of anti-SR-PSOX/CXCL16 mAb 12-81. *A*, Effect on SR-PSOX/CXCL16-induced chemotaxis. Migration of CXCR6-expressing L1.2 cells to recombinant soluble SR-PSOX/CXCL16 (100 ng/ml) was quantified by chemotaxis assay using transwell plate as described previously (21). Neutralizing activity of anti-SR-PSOX/CXCL16 was analyzed by using CXCR6-expressing cells pretreated with indicated amounts of anti-SR-PSOX/CXCL16 mAb 12-81 or control rat IgG. Values in the absence of Ab were set as 100%. The data shown represent the mean ± SD ($n = 3$). *B*, Effect of SR-PSOX/CXCL16-binding to CXCR6-expressing cells. Binding of control Fc (dotted line) or soluble SR-PSOX/CXCL16-Fc (solid line) against CXCR6-expressing L1.2 cells was analyzed by flow cytometry. SR-PSOX/CXCL16-Fc was preincubated with control rat IgG (thin line) or anti-SR-PSOX/CXCL16 mAb 12-81 (bold line), as described in *Materials and Methods*.

Paucity of demyelinating lesions with inflammation in EAE mice treated with anti-SR-PSOX/CXCL16 mAb

Then, we histologically examined spinal cords of acute EAE-induced mice treated with or without anti-SR-PSOX/CXCL16 mAb (Fig. 2, *B–E*). Anti-SR-PSOX/CXCL16 mAb-treated mice showed no signs of histological EAE with demyelination and mononuclear cell infiltration, while there were numerous inflammatory and demyelinating lesions in the perivascular areas and parenchymal in spinal cord of control rat IgG-received mice that showed severe clinical EAE. These inflammatory lesions contain infiltrated mononuclear cells, while spinal cords of anti-SR-PSOX/CXCL16 mAb-treated mice lacked mononuclear cell infiltration and showed significantly decreased number of demyelinating lesions per section compared with the control mice. These results of histological analyses in anti-SR-PSOX/CXCL16 mAb-received mice correlate well with the absence of clinical EAE. Thus, inhibition of SR-PSOX/CXCL16 activities by anti-SR-PSOX/CXCL16 mAb 12-81 is efficient to suppress both clinical and histological EAE.

Decrease of MOG_{35-55}-specific T cell response in anti-SR-PSOX/CXCL16 mAb-treated mice

Because anti-SR-PSOX/CXCL16 mAb-treated mice were resistant to development of both clinical and histological EAE, we examined which phase was inhibited by administration of anti-SR-PSOX/CXCL16 mAb 12-81, generation of MOG_{35-55}-specific Th1-polarized T cells, or infiltration of MOG_{35-55}-specific T cells into the CNS. We analyzed generation of Ag-specific T cells in spleens of MOG_{35-55}-immunized mice. Spleen cells were prepared from mice on day 6 after immunization with MOG_{35-55}, and their MOG_{35-55}-specific in vitro proliferation and in vitro IFN-γ production were quantified by [^{3}H]thymidine incorporation assay (Fig. 3*A*) and by ELISA (Fig. 3*B*), respectively. Spleen T cells from control rat IgG-received mice showed robust and dose-dependent proliferative response in accordance with the amounts of added MOG_{35-55}. In contrast, spleen T cells from anti-SR-PSOX/CXCL16 mAb-treated mice did not show MOG_{35-55}-dependent increase of cell proliferative response in vitro (Fig. 3*A*). Moreover, MOG_{35-55}-dependent increase of in vitro IFN-γ production was not induced in spleen cells from anti-SR-PSOX/CXCL16 mAb-received mice, although MOG_{35-55}-induced dramatic increase of IFN-γ production was observed in spleen cells from control rat IgG-received mice (Fig. 3*B*). These results suggest that generation of MOG_{35-55}-specific T cells was inhibited by anti-SR-PSOX/CXCL16 mAb in primary in vivo immune response, because mice received MOG_{35-55} only once on day 0.

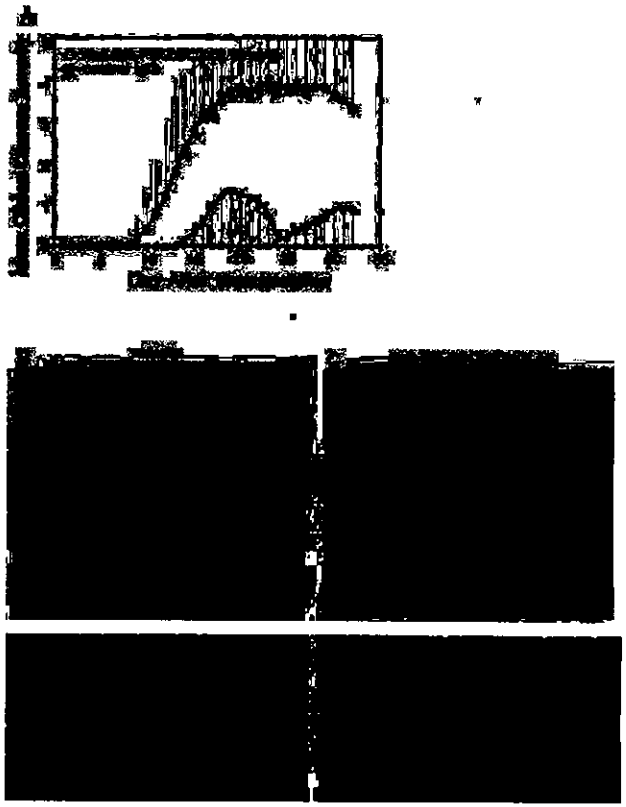

FIGURE 2. Effects of anti-SR-PSOX/CXCL16 mAb 12-81 on development of clinical disease in MOG_{35-55}-induced acute EAE. *A*, Development of MOG_{35-55}-induced clinical EAE. Mice were immunized with MOG_{35-55} and then received pertussis toxin as described in *Materials and Methods*. Results of mice receiving control rat IgG ($n = 7$) or anti-SR-PSOX/CXCL16 mAb ($n = 7$) are expressed as mean disease score ± SD. The data are representative of three independent experiments with essentially similar results; *, $p < 0.02$; **, $p < 0.01$ (Mann-Whitney U test). *B–E*, Histological examination. Spinal cords from EAE-induced mice treated with control rat IgG (*B* and *D*) or anti-SR-PSOX/CXCL16 mAb (*C* and *E*) were analyzed. Serial tissue sections were stained by Bodian and Luxol fast blue (*B* and *C*) and H&E (*D* and *E*) in each mouse. Demyelinating lesions (*B*) and lesions with infiltrated mononuclear cells (*D*) are indicated in control IgG-treated mice, while little demyelinating lesion (*C*) and lesions with only some extent of perivascular mononuclear cell infiltration (*E*) are indicated in anti-SR-PSOX/CXCL16 mAb-treated mouse. Scale bars, *B* and *C*, 150 μm; *D* and *E*, 200 μm.

Because EAE is a Th1-dominant autoimmune disease model, we also examined the amount of proinflammatory Th1 cytokine IFN-γ secreted in serum of mice immunized with MOG_{35-55}. IFN-γ is known to be involved in the pathogenesis of EAE at different points in the course of disease, including primary immune response (26, 27). At 48 and 60 h after primary immunization with MOG_{35-55}, amount of secreted IFN-γ was elevated in serum of mice receiving control rat IgG. In contrast, production of IFN-γ was vigorously suppressed in mice receiving anti-SR-PSOX/CXCL16 mAb (Fig. 3*C*). These observations suggest that anti-SR-PSOX/CXCL16 mAb inhibits generation of MOG_{35-55}-specific Th1 T cell by suppression of IFN-γ production in primary immune response.

Anti-SR-PSOX/CXCL16 mAb-treated mice are resistant to induction of adoptive transfer EAE

Next, we examined whether anti-SR-PSOX/CXCL16 mAb 12-81 could inhibit migration of MOG_{35-55}-specific activated T cells into the spinal cord. Then, effect of administrated anti-SR-PSOX/CXCL16 mAb was analyzed in adoptive transfer EAE, which is developed in recipient mice receiving MOG_{35-55}-specific activated T cells. Anti-SR-PSOX/CXCL16 mAb-treated mice receiving MOG_{35-55} peptide-specific T cells were indicated to manifest significantly delayed onset of clinical EAE at day 21 on average, while control rat IgG-treated mice showed onset of clinical EAE at day 13 on average (Fig. 4). In addition, anti-SR-PSOX/CXCL16 mAb-treated mice showed milder neurological impairment in histological EAE (data not shown). These results suggest that SR-PSOX/CXCL16 is relevant to onset of adoptive transfer EAE by inducing migration of MOG_{35-55}-specific T cells into CNS, because CXCR6, a receptor of SR-PSOX/CXCL16, was reported to be expressed on activated CD4$^+$, and naive and activated CD8$^+$ T cells (14, 15).

Then, we analyzed whether CXCR6 was actually expressed on activated T cells used in adoptive transfer EAE (Fig. 5). Although a small part of CD4$^+$ spleen T cells from unimmunized mice expressed increased amounts of CXCR6 after in vitro cultivation with MOG_{35-55}, the number of CXCR6-positive CD4$^+$ T cells was significantly larger in splenocytes of MOG_{35-55}-immunized mice than in unimmunized mice after in vitro cultivation with

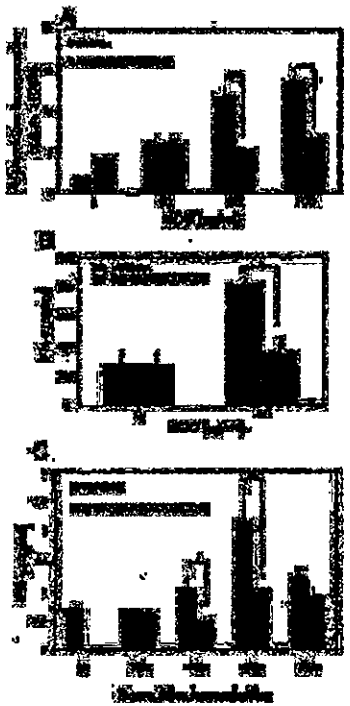

FIGURE 3. Effects of anti-SR-PSOX/CXCL16 mAb 12-81 on MOG_{35-55}-specific immune responses. *A* and *B*, Six days after administration of MOG_{35-55}, splenocytes were isolated from mice treated with anti-SR-PSOX/CXCL16 mAb (anti-SR-PSOX/CXCL16) or control rat IgG (vehicle). *A*, Incorporation of [^{3}H]thymidine by the splenocytes was measured after in vitro stimulation with MOG_{35-55}-peptide as described in *Materials and Methods*; *, $p < 0.002$; **, $p < 0.02$. *B*, Production of IFN-γ by the splenocytes was measured after in vitro stimulation with MOG_{35-55}-peptide as described in *Materials and Methods*; *, $p < 0.03$. *C*, Production of IFN-γ was quantified by ELISA in serum of MOG_{35-55}-injected mice treated with anti-SR-PSOX/CXCL16 mAb (anti-SR-PSOX/CXCL16) or rat IgG (vehicle). Serum was harvested at indicated hours after the immunization with MOG_{35-55}; *, $p < 0.002$; **, $p < 0.02$.

MOG_{35-55}. However, in $CD8^+$ spleen T cells, in vitro cultivation with MOG_{35-55} similarly increased expression of CXCR6 between MOG_{35-55}-immunized and -unimmunized mice. Thus, in vitro cultivation with MOG_{35-55} specifically augments expression of CXCR6 on $CD4^+$ T cells from MOG_{35-55}-immunzed mice, which may be relevant to onset and development of transfer EAE.

Expression of SR-PSOX/CXCL16 in spinal cord of EAE mice

Then, we ascertained the expression of SR-PSOX/CXCL16 in the CNS of EAE mice that might induce chemotaxis of MOG_{35-55}-specific activated T cells into the CNS. Expression of SR-PSOX/CXCL16 was analyzed in the spinal cords of EAE mice 14 days after immunization by in situ hybridization. SR-PSOX/CXCL16-expressing cells were observed around in the white matter of the spinal cord, while significant expression of SR-PSOX/CXCL16

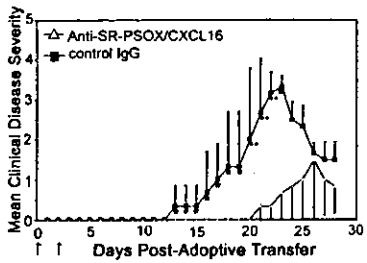

FIGURE 4. Effects of anti-SR-PSOX/CXCL16 mAb 12-81 on onset and development of adoptive transferred clinical EAE. Mice were immunized with MOG_{35-55} as described in Fig. 2, and splenocytes of the mice 4 days after the immunization were cultured with MOG_{35-55} for 4 days, and then, obtained MOG_{35-55}-specific T cell blasts were transferred into recipient B6 mice as described in *Materials and Methods*. Two hours before and 2 days after the transfer of encephalitogenic T cells, recipient mice were injected i.p. with 0.2 ml/mouse of PBS containing 500 μg of anti-SR-PSOX/CXCL16 mAb or control rat IgG (arrows). The data of mice receiving anti-SR-PSOX/CXCL16 mAb ($n = 6$) or control rat IgG ($n = 6$) are expressed as the mean clinical disease score ± SD; *, $p < 0.05$; **, $p < 0.002$. The data are representative of three independent experiments with similar results.

was not detected in control mice (Fig. 6, *B* and *C*). Next, we confirmed the expression of SR-PSOX/CXCL16 by RT-PCR in spinal cords of EAE mice. SR-PSOX/CXCL16 mRNA was shown to express at low level in spinal cords of mice 2, 4, and 6 days after immunization with MOG_{35-55}, while at detectable high level after onset of acute clinical EAE 14 days after immunization (Fig. 6*D*). The results suggested that a small increase of SR-PSOX/CXCL16 mRNA in the spinal cords preceded the development of clinical disease symptoms, which might have an affect on the disease onset, and its high expression was induced after disease onset.

From the observation that SR-PSOX/CXCL16 was highly produced in the CNS at the time of clinical EAE onset, we predicted that T cells in the CNS after induction of EAE would express CXCR6, the receptor for SR-PSOX/CXCL16. To ascertain this possibility, we analyzed CXCR6 mRNA level by RT-PCR in the spinal cords of EAE-induced mice. CXCR6 was shown to express in the CNS of acute clinical EAE 14 days after immunization, while expression of CXCR6 was not detected in mice 2, 4, and 6 days after immunization of MOG_{35-55} before onset of clinical EAE (Fig. 6*D*). Taken together, both SR-PSOX/CXCL16 and its receptor CXCR6 were expressed in the CNS during the development of acute EAE.

Discussion

EAE is a Th1-polarized T cell-mediated autoimmune disease of the CNS in appropriate strains of laboratory animals with a relapsing-remitting course that serves as a model for human MS. Th1-poralized T cells that are reactive to autoantigen in the CNS play an essential role in development of EAE (1, 2, 4). In EAE induced in this manuscript, such autoreactive Th1-poralized T cells were generated in peripheral lymphoid organ by s.c. immunization with MOG_{35-55} peptides, and EAE was caused by infiltration of mononuclear cells including the autoreactive T cells into the CNS. The present study demonstrates that administration of neutralizing mAb against transmembrane chemokine SR-PSOX/CXCL16 suppresses the development of both acute and adoptive transfer EAE by inhibiting the generation of the MOG_{35-55}-reactive T cells in

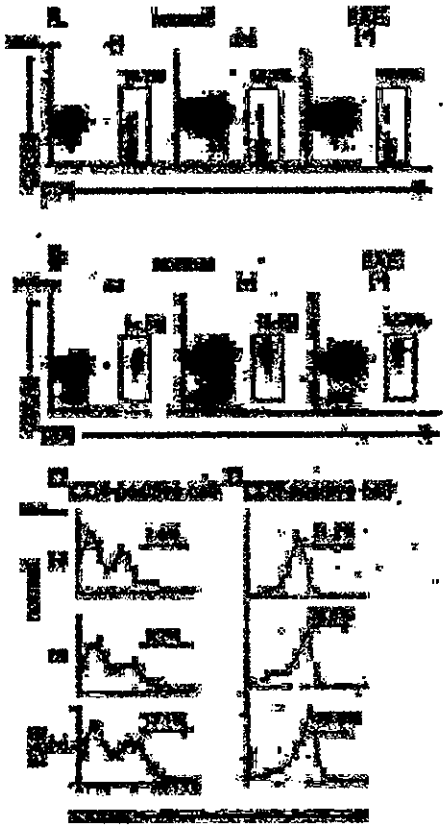

FIGURE 5. Expression of CXCR6 on MOG_{35-55}-specific activated CD4-positive and CD8-positive T cells. Mice were immunized with MOG_{35-55} as described in Fig. 2, and spleen cells of mice 4 days after immunization (EAE) or without immunization (normal) were analyzed before (−) and after (+) in vitro cultivation with MOG_{35-55} for 4 days. Cells were stained with SR-PSOX/CXCL16-Fc, followed by PE-labeled anti-human-Fc mAb together with anti-FITC-labeled CD4 mAb (*A* and *C*) or anti-FITC-labeled CD8 mAb (*B* and *D*), and then analyzed by two-dimensional flow cytometry (*A* and *B*). CD4-positive and CD8-positive cells in *A* and *B*, respectively, were gated, and the expression of CXCR6 was analyzed (*C* and *D*). The data are representative of three independent experiments with similar results.

periphery and the recruitment/accumulation of mononuclear cells, including MOG_{35-55}-reactive T cells, into the CNS, respectively. Thus, SR-PSOX/CXCL16 was suggested to play an important role in the development of EAE at different two phases: 1) generation of autoreactive Th1-polarized T cells and 2) its recruitment into and/or accumulation in the CNS.

In acute EAE, it was shown that SR-PSOX/CXCL16 was involved in generation of MOG_{35-55}-reactive T cells as well as production of IFN-γ in primary immune response against MOG_{35-55} peptides used as immunogen (Fig. 3). Because SR-PSOX/CXCL16 has been expressed on APCs such as DCs and macrophages (14, 15, 17), which play an important role in primary immune response, SR-PSOX/CXCL16 may be involved in generation of Th1-polarized T cells through supporting IFN-γ production in primary immune response. However, it has not been clarified which activity of SR-PSOX/CXCL16, scavenger receptor or chemokine activity, plays a role in generation of the MOG-reactive T cells, although it is possible that both activities coordinately function on the generation of the MOG-reactive T cells. As a scavenger receptor, SR-PSOX/CXCL16 on APCs may be able to support uptake and presentation of various Ags including MOG peptide. As a transmembrane chemokine, SR-PSOX/CXCL16 exerts chemotaxis-inducing activity against CXCR6-expressing cells after cleaving by membrane metalloprotease (18). CXCR6 was shown to express on naive CD8 T cells, Th1-polarized activated CD4 T cells, and naive and activated NK T cells (15). SR-PSOX/CXCL16 on DCs may play a role to induce chemotaxis of T and/or NK T cells. We are now analyzing a role of NK T cells in generation of the MOG-reactive T cells, because NK T cells with high expression of CXCR6 have been reported to support primary Th1-poralized immune response by producing high amounts of IFN-γ (28, 29). Involvement of NK T cells in the generation of Th1-inclined autoreactive T cells in EAE must be intimately examined in the near future.

In adoptive transfer EAE, SR-PSOX/CXCL16 was indicated to induce mononuclear cell traffic into the CNS. In addition, our data indicate that clinical disease severity of both acute and adoptive transfer EAE correlates well with expression levels of both SR-PSOX/CXCL16 and its receptor CXCR6 in spinal cords (Fig. 6*D*). Because 1) CXCR6 was expressed on both $CD4^+$ and $CD8^+$ T cells used in transfer EAE (Fig. 5); 2) CXCR6 was reported to express on a subset of Th1-polarized T cells but not on Th2 T cells or monocytes/macrophages (19); 3) SR-PSOX/CXCL16 was reported to have chemoattractant activity for activated T cells but not for monocytes/macrophages (15, 17); and 4) EAE has been regarded as Th1 T cell-mediated autoimmune disease (1, 2), SR-PSOX/CXCL16 may induce chemotaxis of MOG_{35-55}-specific Th1-polarized activated CD4 T cells and/or CD8 T cells into the CNS, although we cannot deny the possibility that SR-PSOX-CXCL16 is also involved in accumulation, activation, and/or proliferation of MOG_{35-55} peptide-specific, Th1-poralized, activated CD4 T cells in the CNS.

Previous reports clearly indicated the essential role of MCP-1/CCL2 in adoptive transfer EAE (11, 13), and MCP-1/CCL2-attracted monocyte/macrophage may induce traffic of activated T cell into the CNS by the function of SR-PSOX/CXCL16. SR-PSOX/CXCL16 that induces chemotaxis and accumulation of MOG_{35-55}-specific T cells expressing CXCR6 (Figs. 5 and 6*D*) might be expressed on infiltrated monocyte/macrophage into the CNS. Actually, SR-PSOX/CXCL16 was shown to be expressed on activated macrophages (14) and was suggested to be expressed in infiltrated cells into the CNS of EAE mice (Fig. 6*B*). However, we could not detect significant expression of SR-PSOX/CXCL16 in the spinal cords before immunization by in situ hybridization (Fig. 6, *B* and *C*). These data suggest that adoptively transferred MOG-reactive T cells infiltrate into the spinal cords of unimmunized mice without using CXCR6 and SR-PSOX/CXCL16, although administration of anti-SR-PSOX/CXCL16 mAb into the recipient mice inhibits onset of transfer EAE, probably through inhibiting direct infiltration of the transferred MOG-reactive T cells into spinal cord. Low level expression of SR-PSOX/CXCL16, which could be slightly detected by RT-PCR (Fig. 6*D*) but not by in situ hybridization (Fig. 6*C*) in the spinal cords of unimmunized mice,

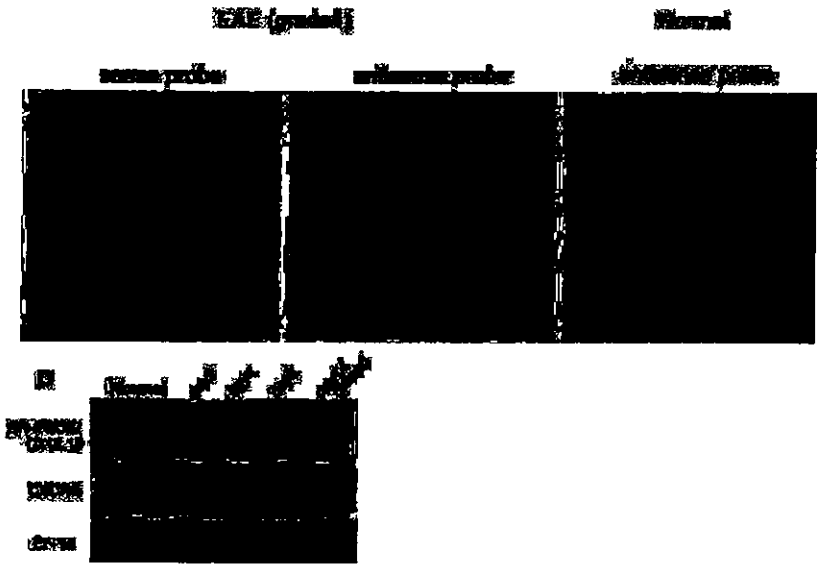

FIGURE 6. Expression of SR-PSOX/CXCL16 in the CNS of mice with EAE. *A–C*, Expression of SR-PSOX/CXCL16 mRNA was analyzed in spinal cord of EAE-induced mice 14 days after immunization or of control mice without immunization (normal) by in situ hybridization. *D*, mRNA of SR-PSOX/CXCL16 and CXCR6/Bonzo in spinal cord from EAE mice were measured by RT-PCR 2, 4, 6, and 14 days after immunization. Expression of elongation factor 1-α (EF1-α) mRNA was also measured as control.

might induce traffic of the transferred MOG-reactive T cells, although we cannot deny the possibility that SR-PSOX/CXCL16 does not play a role in infiltration of the adoptively transferred T cells into spinal cord.

MIP-1α/CCL3 and IP-10/CXCL10, which possess similar functions to SR-PSOX/CXCL16 against activated T cells, might be also involved in activated T cell traffic into the CNS in EAE (7, 8). However, two contradictory results were reported on the function of IP-10/CXCL10 for EAE, which indicated that administration of neutralizing Abs decreased or increased clinical disease incidence and severity, as well as infiltration of mononuclear cells into the CNS in transfer EAE, while anti-IP-10/CXCL10 did not show any effects on acute EAE (8, 10). SR-PSOX/CXCL16 and MIP-1α/CCL3 may coordinately and/or complementarily function in EAE together with or without IP-10/CXCL10 by inducing chemotaxis of activated Th1 T cells into the CNS, and/or accumulation of the activated T cells in the CNS.

Our findings in this report open the possibility that mAb-induced in vivo inhibition of biological activities of SR-PSOX/CXCL16, such as generation of Ag-specific T cells in primary immune response in acute EAE and traffic of Th1-poralized activated T cells into the CNS in transfer EAE, may be useful for clinical therapy of autoimmune diseases including MS.

Acknowledgments

We thank H. Tomimoto, K. Togi, K. Okamoto, K. Sakamaki, and K. K. Lee for their generous help.

References

1. Steinman, L. 1996. Multiple sclerosis: a coordinated immunological attack against myelin in the central nervous system. *Cell 85:299.*
2. Hemmer, B., S. Cepok, S. Nessler, and N. Sommer. 2002. Pathogenesis of multiple sclerosis: an update on immunology. *Curr. Opin. Neurol. 15:227.*
3. Sallusto, F., A. Lanzavecchia, and C. R. Mackay. 1998. Chemokines and chemokine receptors in T-cell priming and Th1/Th2-mediated responses. *Immunol. Today 19:568.*
4. Godessart, N., and S. L. Kunkel. 2001. Chemokines in autoimmune disease. *Curr. Opin. Immunol. 13:670.*
5. Zlotnik, A., and O. Yoshie. 2000. Chemokines: a new classification system and their role in immunity. *Immunity 12:121.*
6. Mackay, C. R. 2001. Chemokines: immunology's high impact factors. *Nat. Immunol. 2:95.*
7. Karpus, W. J., N. W. Lukacs, B. L. McRae, R. M. Strieter, S. L. Kunkel, and S. D. Miller. 1995. An important role for the chemokine macrophage inflammatory protein-1α in the pathogenesis of the T cell-mediated autoimmune disease, experimental autoimmune encephalomyelitis. *J. Immunol. 155:5003.*
8. Fife, B. T., K. J. Kennedy, M. C. Paniagua, N. W. Lukacs, S. L. Kunkel, A. D. Luster, and W. J. Karpus. 2001. CXCL10 (IFN-γ-inducible protein-10) control of encephalitogenic $CD4^+$ T cell accumulation in the central nervous system during experimental autoimmune encephalomyelitis. *J. Immunol. 166:7617.*
9. Juedes, A. E., P. Hjelmstrom, C. M. Bergman, A. L. Neild, and N. H. Ruddle. 2000. Kinetics and cellular origin of cytokines in the central nervous system: insight into mechanisms of myelin oligodendrocyte glycoprotein-induced experimental autoimmune encephalomyelitis. *J. Immunol. 164:419.*
10. Narumi, S., T. Kaburaki, H. Yoneyama, H. Iwamura, Y. Kobayashi, and K. Matsushima. 2002. Neutralization of IFN-inducible protein 10/CXCL10 exacerbates experimental autoimmune encephalomyelitis. *Eur. J. Immunol. 32:1784.*
11. Huang, D. R., J. Wang, P. Kivisakk, B. J. Rollins, and R. M. Ransohoff. 2001. Absence of monocyte chemoattractant protein 1 in mice leads to decreased local macrophage recruitment and antigen-specific T helper cell type 1 immune response in experimental autoimmune encephalomyelitis. *J. Exp. Med. 193:713.*
12. Izikson, L., R. S. Klein, I. F. Charo, H. L. Weiner, and A. D. Luster. 2000. Resistance to experimental autoimmune encephalomyelitis in mice lacking the CC chemokine receptor (CCR)2. *J. Exp. Med. 192:1075.*
13. Kohler, R. E., A. C. Caon, D. O. Willenborg, I. Clark-Lewis, and S. R. McColl. 2003. A role for macrophage inflammatory protein-3α/CC chemokine ligand 20 in immune priming during T cell-mediated inflammation of the central nervous system. *J. Immunol. 170:6298.*

14. Shimaoka, T., N. Kume, M. Minami, K. Hayashida, H. Kataoka, T. Kita, and S. Yonehara. 2000. Molecular cloning of a novel scavenger receptor for oxidized low density lipoprotein, SR-PSOX, on macrophages. *J. Biol. Chem. 275:40663.*
15. Matloubian, M., A. David, S. Engel, J. E. Ryan, and J. G. Cyster. 2000. A transmembrane CXC chemokine is a ligand for HIV-coreceptor Bonzo. *Nat. Immunol. 1:298.*
16. Wilbanks, A., S. C. Zondlo, K. Murphy, S. Mak, D. Soler, P. Langdon, D. P. Andrew, L. Wu, and M. Briskin. 2001. Expression cloning of the STRL33/BONZO/TYMSTRligand reveals elements of CC, CXC, and CX3C chemokines. *J. Immunol. 166:5145.*
17. Shimaoka, T., T. Nakayama, N. Kume, S. Takahashi, J. Yamaguchi, M. Minami, K. Hayashida, T. Kita, J. Ohsumi, O. Yoshie, and S. Yonehara. 2003. Cutting edge: SR-PSOX/CXC chemokine ligand 16 mediates bacterial phagocytosis by APCs through its chemokine domain. *J. Immunol. 171:1647.*
18. Shimaoka, T., T. Nakayama, N. Fukumoto, N. Kume, S. Takahashi, J. Yamaguchi, M. Minami, K. Hayashida, T. Kita, J. Ohsumi, et al. 2004. Cell surface-anchored SR-PSOX/CXC chemokine ligand 16 mediates firm adhesion of CXC chemokine receptor 6-expressing cells. *J. Leukocyte Biol. 75:267.*
19. Kim, C. H., E. J. Kunkel, J. Boisvert, B. Johnston, J. J. Campbell, M. C. Genovese, H. B. Greenberg, and E. C. Butcher. 2001. Bonzo/CXCR6 expression defines type 1-polarized T-cell subsets with extralymphoid tissue homing potential. *J. Clin. Invest. 107:595.*
20. Calabresi, P. A., S. H. Yun, R. Allie, and K. A. Whartenby. 2002. Chemokine receptor expression on MBP-reactive T cells: CXCR6 is a marker of IFNγ-producing effector cells. *J. Neuroimmunol. 127:96.*
21. Imai, T., K. Hieshima, C. Haskell, M. Baba, M. Nagira, M. Nishimura, M. Kakizaki, S. Takagi, H. Nomiyama, T. J. Schall, and O. Yoshie. 1997. Identification and molecular characterization of fractalkine receptor CX3CR1, which mediates both leukocyte migration and adhesion. *Cell 91:521.*
22. Okuda, Y., C. C. Bernard, H. Fujimura, T. Yamagihara, and S. Sakoda. 1998. Fas has a crucial role in the progression of experimental autoimmune encephalomyelitis. *Mol. Immunol. 35:317.*
23. Sun, Y., X. Lin, H. M. Chen, Q. Wu, S. K. Subudhi, L. Chen, and Y. X. Fu. 2002. Administration of agonistic anti-4-1BB monoclonal antibody leads to the amelioration of experimental autoimmune encephalomyelitis. *J. Immunol. 168:1457.*
24. Hisahara, S., T. Araki, F. Sugiyama, K. Yagami, M. Suzuki, K. Abe, K. Yamamura, J. Miyazaki, T. Momoi, T. Saruta, et al. 2000. Targeted expression of baculovirus p35 caspase inhibitor in oligodendrocytes protects mice against autoimmune-mediated demyelination. *EMBO J. 19:341.*
25. Saeki, Y., T. Mima, S. Sakoda, H. Fujimura, N. Arita, T. Nomura, and T. Kishimoto. 1992. Transfer of multiple sclerosis into severe combined immunodeficiency mice by mononuclear cells from cerebrospinal fluid of the patients. *Proc. Natl. Acad. Sci. USA 89:6157.*
26. Simmons, R. D., and D. O. Willenborg. 1990. Direct injection of cytokines into the spinal cord causes autoimmune encephalomyelitis-like inflammation. *J. Neurol. Sci. 100:37.*
27. Sethna, M. P., and L. A. Lampson. 1991. Immune modulation within the brain: recruitment of inflammatory cells and increased major histocompatibility antigen expression following intracerebral injection of interferon-γ. *J. Neuroimmunol. 34:121.*
28. Pal, E., T. Tabira, T. Kawano, M. Taniguchi, S. Miyake, and T. Yamamura. 2001. Costimulation-dependent modulation of experimental autoimmune encephalomyelitis by ligand stimulation of Vα14 NK T cells. *J. Immunol. 166:662.*
29. Godfrey, D. I., K. J. Hammond, L. D. Poulton, M. J. Smyth, and A. G. Baxter. 2000. NKT cells: facts, functions and fallacies. *Immunol. Today 21:573.*

Available online at www.sciencedirect.com
SCIENCE DIRECT®
Biochemical and Biophysical Research Communications 322 (2004) 700–704
BBRC
www.elsevier.com/locate/ybbrc

Direct demonstration of involvement of the adaptor protein ShcA in the regulation of Ca^{2+}-induced platelet aggregation☆

Tomohito Higashi[a], Akira Yoshioka[b,1], Ryutaro Shirakawa[a], Arata Tabuchi[b], Hiroaki Nishioka[b,2], Toru Kita[a], Hisanori Horiuchi[a,*]

[a] Department of Cardiovascular Medicine, Graduate School of Medicine, Kyoto University, Kyoto 606-8507, Japan
[b] Geriatric Medicine, Graduate School of Medicine, Kyoto University, Kyoto 606-8507, Japan

Received 20 May 2004

Abstract

Platelet aggregation is mediated by conformational change of integrin $\alpha_{IIb}\beta_3$. Tyrosine-phosphorylation of cytoplasmic domain of β_3 upon platelet activation has been demonstrated to play a critical role in this process. Recently, the adaptor protein ShcA has been shown to bind to the tyrosine-phosphorylated β_3, while it remains open whether ShcA plays any role in platelet aggregation. Here, we show that ShcA bound to tyrosine-phosphorylated β_3-tail peptide through its phosphotyrosine-binding domain in vitro. Then, we examined the involvement of ShcA in platelet aggregation by a previously established in vitro assay using platelets permeabilized with streptolysin-O, where exogenous addition of platelet cytosol is required for reconstitution of the Ca^{2+}-induced aggregation. When ShcA was specifically depleted with anti-ShcA antibody from the cytosol, this ShcA-depleted cytosol lost the aggregation-supporting activity, which was rescued by addition of purified recombinant ShcA. Thus, ShcA is essential for the Ca^{2+}-induced platelet aggregation.

Keywords: Platelet; Aggregation; Integrin; ShcA; Streptolysin-O; Phosphotyrosine-binding domain

Platelet aggregation is mediated by conformational change of integrin $\alpha_{IIb}\beta_3$ which is regulated by signals at its short cytoplasmic tails [1,2] that consist of 20 amino acids in α_{IIb} subunit and 47 in β_3 subunit [3]. Two tyrosine residues in β_3-tail are known to be phosphorylated during platelet activation [4] and platelets bearing mutations at these tyrosine residues exhibit impaired aggregation [5], indicating that these tyrosine residues are important for platelet aggregation. So far, myosin [6] and the adaptor protein ShcA [7] have been identified as tyrosine-phosphorylation-dependent β_3-tail binding proteins.

ShcA is the essential adaptor protein containing two phosphotyrosine-binding domains, the phosphotyrosine-binding (PTB) domain and Src-homology 2 (SH2) domain (Fig. 1A) [8]. ShcA mediates signals involved in cell growth [9] and cytoskeletal organization [10]. Accordingly, ShcA-deficient mice are embryonic lethal due to severe defects in heart development and establishment of mature blood vessels [10]. Upon platelet aggregation, ShcA has been demonstrated to be co-immunoprecipitated with tyrosine-phosphorylated $\alpha_{IIb}\beta_3$ [3] and to be phosphorylated at its tyrosine residues [11]. In platelets of mice with mutations on both tyrosine residues of β_3-tail, ShcA does not undergo aggregation-induced tyrosine-phosphorylation [7]. These results suggest that ShcA may be involved in the regulation of platelet aggregation. However, it remains open whether ShcA regulates platelet aggregation.

Here, we show that ShcA binds to the tyrosine-phosphorylated β_3 peptide through its PTB domain. Exogenous addition of cytosol is required for reconstitution of aggregation of permeabilized platelets in our previously established assay [12]. Using this assay, we directly demonstrate the involvement of ShcA in the regulation of platelet aggregation by showing that the aggregation-supporting activity of the added cytosol was abolished by immunodepletion of ShcA, which was rescued by addition of recombinant ShcA.

[*] *Abbreviations:* PTB, phosphotyrosine-binding; SH2, Src-homology 2; PCR, polymerase chain reaction; GST, glutathione *S*-transferase; SLO, streptolysin-O; BSA, bovine serum albumin, SDS-PAGE, sodium dodecyl sulfate-polyacrylamide gel electrophoresis; CH1, collagen-homology 1.

[*] Corresponding author. Fax: +81 75 751 3574.
E-mail address: horiuchi@kuhp.kyoto-u.ac.jp (H. Horiuchi).
[1] Present address: Department of Internal Medicine, Mitsubishi Kyoto Hospital, 615-8087 Kyoto, Japan.
[2] Present address: Sir William Dunn School of Pathology, University of Oxford, South Parks Rd., Oxford OX1 3RE, UK.

0006-291X/$ - see front matter © 2004 Elsevier Inc. All rights reserved.
doi:10.1016/j.bbrc.2004.07.177

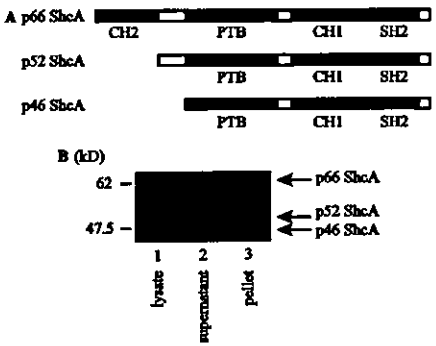

Fig. 1. ShcA is present in platelet cytosol. (A) Domain structures of p46, p52, and p66 ShcA isoforms are shown schematically. (B) Low speed supernatant of sonicated platelets (lane 1) was centrifuged at 4 °C for 30 min at 300,000*g*, and the comparable amounts of the supernatant (lane 2) and the pellet (lane 3) were analyzed by immunoblot with anti-ShcA antibody as described in the Experimental procedures. The data shown are the representative of three independent experiments with similar results.

Experimental procedures

Materials. The cDNA encoding p52 ShcA was generated by polymerase chain reaction (PCR) using Marathone cDNA of human bone marrow (Clontech) as a template and cloned into pGEX-2T (Amersham–Pharmacia) at the *Eco*RI site. The PTB (47–208) and SH2 (377–456) domains of p52 ShcA (PTB-ShcA and SH2-ShcA, respectively) were also generated by PCR with full length ShcA DNA as a template and cloned at the *Eco*RI site and the *Bam*HI–*Eco*RI site, respectively. Glutathione *S*-transferase (GST)-fusion proteins of ShcA, PTB-ShcA, and SH2-ShcA were produced in *Escherichia coli* strain BL21 and affinity-purified using glutathione–Sepharose (Amersham Pharmacia). cDNA encoding p52 ShcA was also cloned in pDEST (Invitrogen) and p52 ShcA was produced and purified as a GST-fusion protein in Sf9 insect cells using a Bac-to-Bac system (Invitrogen). The biotinylated β_3 cytoplasmic peptides (735–762) with or without tyrosine-phosphorylation at 747 and 759 were produced by Sawady Technology, Tokyo, Japan. They were biotin-ARAKWDTANNPLYKEATSTFTNITYRGT and biotin-ARAKWDTANNPLphospho-YKEATSTFTNITphospho-YRGT. The streptoavidin–agarose, glutathione–Sepharose, and protein A–agarose were purchased from Sigma, Amersham Pharmacia, and Roche, respectively. Anti-ShcA rabbit polyclonal and anti-GST (B-14) mouse monoclonal antibodies were purchased from BD-Transduction Laboratories and Santa Cruz Biotechnology, respectively. Horseradish peroxidase-labeled anti-rabbit and anti-mouse IgG polyclonal antibodies were from Amersham–Pharmacia, which were used as secondary antibodies for immunoblotting visualized by enhanced chemiluminescence method (Amersham). Unless otherwise specified, all the chemicals were purchased from Sigma, except for streptolysin-O (SLO), that was from Dr. S. Bhakdi, Mainz Univ., Mainz, Germany [13]. Supernatant of sonicated platelets after centrifuged at 100,000*g* for 60 min at 4 °C was used as the human platelet cytosol. All the recombinant proteins and platelet cytosol were dialyzed against Buffer A (50 mM Hepes–KOH, pH 7.4, 78 mM KCl, 4 mM $MgCl_2$, 0.2 mM $CaCl_2$, 2 mM EGTA, 1 mM dithiothreitol, and the calculated free $[Ca^{2+}]$ was approximately 20 nM [14]) and stored at −80 °C until use. The DNA sequences of all the PCR products were confirmed by DNA-sequencing using ABI PRIZM, 310 Genetic Analizer (Applied Biosystems).

The peptide affinity chromatography. The streptoavidin-coated beads (100 μl) were first incubated in Buffer A containing 0.1% Triton X-100, 1 mM Na_3VO_4, and 20 mM NaF at 4 °C for 30 min with 30 nmol of biotin and the biotin-tagged β_3 peptides. Then, the beads were washed with the same buffer and incubated at 4 °C for 3 h with the human platelet cytosol (8 mg of proteins) in the experiments for Fig. 2A, or with GST-ShcA, GST-PTB-ShcA, GST-SH2-ShcA, and GST (100 pmol) in the presence of 0.4 mg/ml BSA for Fig. 2B. Then, the beads were washed 5 times with the same buffer and added with the SDS-containing Laemmli's buffer for immunoblot analysis [15].

The aggregation assay using permeabilized platelets. The method of the aggregation assay was previously described [12], where platelets permeabilized with SLO were stimulated by $[Ca^{2+}]$ at 20 μM [14] in the presence of exogenous cytosol and an ATP regeneration system, and the light transmission was monitored.

Results and discussion

The adaptor protein ShcA consists of three isoforms with molecular weights of 66, 52, and 46 kDa which are produced by RNA splicing or alternative translational initiation [9,16,17]. All of these ShcA isoforms contain two phosphotyrosine-binding domains, PTB and SH2, and collagen homology domain 1 (CH1) (Fig. 1A) [8]. Among ShcA isoforms, p52 ShcA was predominant, and p46 and p66 ShcA were minor in platelets (Fig. 1B). Most of p52 ShcA was recovered in the supernatant after high-speed centrifugation of the sonicated platelets (Fig. 1B), indicating that p52 ShcA exists mainly in the cytosol in resting platelets.

First, to examine whether p52 ShcA could bind to β_3-tail in vitro, we incubated platelet cytosol with streptoavidin-beads coated with the biotinylated tyrosine-phosphorylated β_3-tail peptide (735–762) and the non-phosphorylated peptide. p52 ShcA was detected on the tyrosine-phosphorylated peptide-coated beads, but not on the non-phosphorylated peptide-coated beads (Fig. 2A). Then, we examined which phosphotyrosine-binding motif of ShcA, namely PTB or SH2

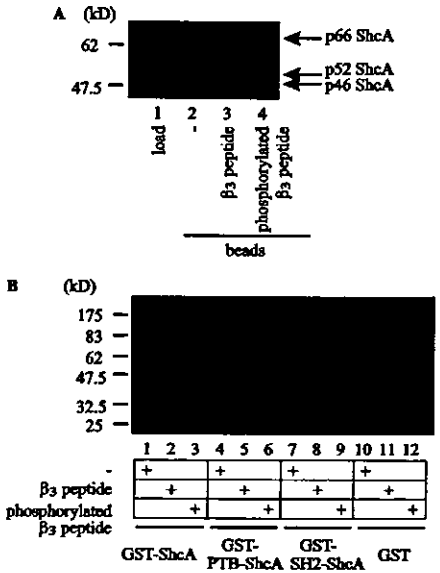

Fig. 2. ShcA binds to tyrosine-phosphorylated β_3 peptide through its PTB domain. (A) Streptoavidin beads alone (lane 2), and the beads coated with the tyrosine-phosphorylated (lane 4) and non-phosphorylated β_3 peptide (lane 3) were incubated with platelet cytosol (lane 1), and bead-associated ShcA was analyzed by immunoblot as described in the Experimental procedures. The data shown are the representative of three independent experiments with similar results. (B) Biotin-coated streptoavidin beads (lanes 1, 4, 7, and 10), and beads coated with the biotin-tyrosine-phosphorylated (lanes 3, 6, 9, and 12) and biotin-non-phosphorylated β_3 peptides (lanes 2, 5, 8, and 11) were incubated with 100 pmol GST-ShcA (lanes 1–3), GST-PTB-ShcA (lanes 4–6), GST-SH2-ShcA (lanes 7–9), and GST (lanes 10–12) and the bead-associated proteins were analyzed by immunoblot with anti-GST antibody as described in the Experimental Procedures. The data shown are the representative of three independent experiments with similar results.

domain, mediates the direct binding to the tyrosine-phosphorylated β_3 peptide. We generated and purified proteins of GST-ShcA, GST-PTB-ShcA, GST-SH2-ShcA, and GST in *E. coli*. Then, we incubated these proteins with streptoavidin-beads coated with β_3-tail peptides. As shown in Fig. 2B, PTB-ShcA bound to the phosphorylated β_3 peptide (lane 6), but not to the non-phosphorylated peptide (lane 5) or biotin (lane 4). On the other hand, SH2-ShcA did not bind to either of β_3 peptides (lanes 7–9). Thus, ShcA bound to the tyrosine-phosphorylated, but not non-phosphorylated, β_3 peptide through its PTB domain.

So far, myosin [6] and the adaptor protein ShcA [7] have been shown to bind to the tyrosine-phosphorylated β_3-tail. While binding of myosin requires phosphorylation of both tyrosine residues, ShcA-binding requires only Y759 phosphorylation [7]. The binding of proteins to the phosphotyrosine-containing motifs is known to depend upon the sequences around phosphorylated tyrosine. Although the sequence NITYRGT around Y759 of β_3 does not contain the SH2-domain-binding pYXNX motif, it contains the PTB-domain-binding NXXpY motif [18]. It is conceivable that ShcA interacts with the NITpY(759) of β_3 through its PTB domain.

We have previously established an assay for analyzing the Ca^{2+}-induced aggregation of platelets permeabilized with streptolysin-O using a light transmission aggregometer [12]. The aggregation of permeabilized platelets in the assay revealed similar responses in Ca^{2+}-sensitivity, time course, and involvement of the integrin to that of intact platelets [12]. Reconstitution of aggregation of permeabilized platelets in the assay required exogenous addition of platelet cytosol [12]. Since most of p52 ShcA was present in the cytosol of platelets (Fig. 1B), to examine whether ShcA is involved in the regulation of aggregation, we specifically depleted the platelet cytosol of ShcA with anti-ShcA antibody-coated beads (Fig. 3A). While the platelet cytosol treated with the control rabbit IgG-coated beads retained the supporting activity for the Ca^{2+}-induced platelet aggregation in the assay, the ShcA-depleted cytosol lost the aggregation-supporting activity (Fig. 3C). We produced GST-p52 ShcA with baculovirus-expression system and purified the protein from overexpressing Sf9 cells (Fig. 3B). As shown in Fig. 3C, addition of purified GST-ShcA concentration-dependently rescued the aggregation-supporting activity of the ShcA-depleted cytosol. Thus, ShcA is an essential factor in platelet cytosol for the Ca^{2+}-induced platelet aggregation.

By using this semi-intact aggregation assay, we previously demonstrated that PKCα is an essential cytosolic factor for platelet aggregation by showing that the PKC-depleted cytosol lost the aggregation-supporting activity that was rescued by addition of purified PKCα [12]. In that study, addition of PKCα alone without addition of any cytosol did not support the aggregation [12]. Therefore, we speculated that cytosolic factor(s) other than PKCα are also required for the aggregation [12]. With the results presented here, we could say that one of such factors is ShcA. It has been demonstrated that phosphorylation of ShcA by PKCα promotes its membrane translocation [19,20]. ShcA and PKCα might cooperatively regulate platelet aggregation.

Talin, an actin binding protein, has been demonstrated to bind to β_3-tail and regulate activity of the integrin $\alpha_{IIb}\beta_3$ [5,21,22]. CIB (calcium and integrin binding protein) [23,24] and β-endonexin [25] bind to α_{IIb}-tail and regulate this integrin activity. Here, we showed the involvement of ShcA in this regulation. Thus, the

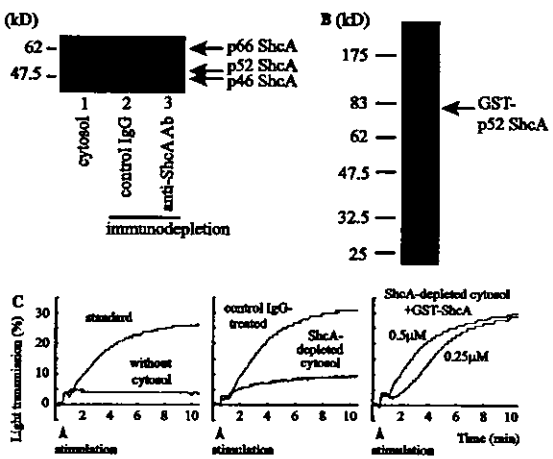

Fig. 3. ShcA-depleted cytosol loses the aggregation-supporting activity, which is rescued by addition of purified recombinant ShcA. (A) Platelet cytosol (lane 1) was incubated with anti-ShcA antibody (lane 3) or control IgG (lane 2)-coated beads, and, after removing these beads, the supernatants were analyzed by immunoblot with anti-ShcA antibody as described in Experimental procedures. (B) GST-p52 ShcA purified from Sf9 cells was analyzed in Coomassie-stained SDS–PAGE gel. (C) The Ca^{2+}-induced aggregation of the permeabilized platelets was examined in the presence of platelet cytosol, cytosol treated with the control IgG, and the ShcA-depleted cytosol in the absence or presence of 0.25 and 0.5 μM GST-ShcA purified from Sf9 cells as described in Experimental procedures. The data shown are the representative of three independent experiments with similar results.

activity of the integrin is regulated by multiple factors at its cytosolic tail. It is essential to elucidate the mechanism of how these factors cooperatively or independently regulate the integrin activation for further understanding of platelet aggregation.

In summary, we have directly demonstrated that the adaptor protein ShcA regulates the platelet aggregation most likely through direct interaction with tyrosine-phosphorylated β_3 subunit. Further investigation of the mechanism of ShcA-mediated platelet aggregation would provide a clue for understanding of the process of platelet aggregation.

Acknowledgments

We are also grateful to the Kyoto Red Cross Blood Center for providing platelet pellet and to T. Matsubara for excellent technical assistance. This work was supported by Research Grants from Ministry of Education, Culture, Sports, Science and Technology, Japan (No. 16-1244 to R.S., 12CE2006 and 16209031 to T.K., and No. 15590740 and 15081206 to H.H.,), Health and Labour Sciences Research Grants from Research Grants from Ministry of Health Labour and Welfare, Japan (Comprehensive Research on Aging and Health (H14-Tyouju-012) to T.K. and H.H.), and partially by grants from Takeda Science Foundation, Suzuken Memorial Foundation, Study Group of Molecular Cardiology and Novartis Foundation for Gerontological Research to H.H.

References

[1] R.O. Hynes, Integrins: bidirectional, allosteric signaling machines, Cell 110 (2002) 673–687.
[2] O. Vinogradova, A. Velyvis, A. Velyviene, B. Hu, T. Haas, E. Plow, J. Qin, A structural mechanism of integrin alpha(IIb)beta(3) "inside-out" activation as regulated by its cytoplasmic face, Cell 110 (2002) 587–597.
[3] D.R. Phillips, K.S. Prasad, J. Manganello, M. Bao, L. Nannizzi-Alaimo, Integrin tyrosine phosphorylation in platelet signaling, Curr. Opin. Cell Biol. 13 (2001) 546–554.
[4] D.A. Law, L. Nannizzi-Alaimo, D.R. Phillips, Outside-in integrin signal transduction. Alpha IIb beta 3-(GP IIb IIIa) tyrosine phosphorylation induced by platelet aggregation, J. Biol. Chem. 271 (1996) 10811-10815.
[5] D.A. Law, F.R. DeGuzman, P. Heiser, K. Ministri-Madrid, N. Killeen, D.R. Phillips, Integrin cytoplasmic tyrosine motif is required for outside-in alphaIIbbeta3 signalling and platelet function, Nature 401 (1999) 808–811.
[6] A.L. Jenkins, L. Nannizzi-Alaimo, D. Silver, J.R. Sellers, M.H. Ginsberg, D.A. Law, D.R. Phillips, Tyrosine phosphorylation of the beta3 cytoplasmic domain mediates integrin-cytoskeletal interactions, J. Biol. Chem. 273 (1998) 13878–13885.
[7] K.J. Cowan, D.A. Law, D.R. Phillips, Identification of shc as the primary protein binding to the tyrosine-phosphorylated beta 3 subunit of alpha IIbbeta 3 during outside-in integrin platelet signaling, J. Biol. Chem. 275 (2000) 36423–36429.

[8] G. Pelicci, L. Dente, A. De Giuseppe, B. Verducci-Galletti, S. Giuli, S. Mele, C. Vetriani, M. Giorgio, P.P. Pandolfi, G. Cesareni, P.G. Pelicci, A family of Shc related proteins with conserved PTB, CH1 and SH2 regions, Oncogene 13 (1996) 633–641.
[9] K.S. Ravichandran, Signaling via Shc family adapter proteins, Oncogene 20 (2001) 6322–6330.
[10] K.M. Lai, T. Pawson, The ShcA phosphotyrosine docking protein sensitizes cardiovascular signaling in the mouse embryo, Genes Dev. 14 (2000) 1132–1145.
[11] L. Bonfini, E. Migliaccio, G. Pelicci, L. Lanfrancone, P.G. Pelicci, Not all Shc's roads lead to Ras, Trends Biochem. Sci. 21 (1996) 257–261.
[12] A. Tabuchi, A. Yoshioka, T. Higashi, R. Shirakawa, H. Nishioka, T. Kita, H. Horiuchi, Direct demonstration of involvement of protein kinase Calpha in the Ca2+-induced platelet aggregation, J. Biol. Chem. 278 (2003) 26374–26379.
[13] M. Palmer, R. Harris, C. Freytag, M. Kehoe, J. Tranum-Jensen, S. Bhakdi, Assembly mechanism of the oligomeric streptolysin O pore: the early membrane lesion is lined by a free edge of the lipid membrane and is extended gradually during oligomerization, EMBO J. 17 (1998) 1598–1605.
[14] A. Fabiato, F. Fabiato, Calculator programs for computing the composition of the solutions containing multiple metals and ligands used for experiments in skinned muscle cells, J. Physiol. (Paris) 75 (1979) 463–505.
[15] U.K. Laemmli, Cleavage of structural proteins during the assembly of the head of bacteriophage T4, Nature 227 (1970) 680–685.
[16] G. Pelicci, L. Lanfrancone, F. Grignani, J. McGlade, F. Cavallo, G. Forni, I. Nicoletti, T. Pawson, P.G. Pelicci, A novel transforming protein (SHC) with an SH2 domain is implicated in mitogenic signal transduction, Cell 70 (1992) 93–104.
[17] E. Migliaccio, S. Mele, A.E. Salcini, G. Pelicci, K.M. Lai, G. Superti-Furga, T. Pawson, P.P. Di Fiore, L. Lanfrancone, P.G. Pelicci, Opposite effects of the p52shc/p46shc and p66shc splicing isoforms on the EGF receptor-MAP kinase-fos signalling pathway, EMBO J. 16 (1997) 706–716.
[18] W.M. Kavanaugh, L.T. Williams, An alternative to SH2 domains for binding tyrosine-phosphorylated proteins, Science 266 (1994) 1862–1865.
[19] L. Daulhac, A. Kowalski-Chauvel, L. Pradayrol, N. Vaysse, C. Seva, Ca2+ and protein kinase C-dependent mechanisms involved in gastrin-induced Shc/Grb2 complex formation and P44-mitogen-activated protein kinase activation, Biochem. J. 325 (Part 2) (1997) 383–389.
[20] C.K. Miranti, S. Ohno, J.S. Brugge, Protein kinase C regulates integrin-induced activation of the extracellular regulated kinase pathway upstream of Shc, J. Biol. Chem. 274 (1999) 10571–10581.
[21] D.A. Calderwood, B. Yan, J.M. de Pereda, B.G. Alvarez, Y. Fujioka, R.C. Liddington, M.H. Ginsberg, The phosphotyrosine binding-like domain of talin activates integrins, J. Biol. Chem. 277 (2002) 21749–21758.
[22] S. Tadokoro, S.J. Shattil, K. Eto, V. Tai, R.C. Liddington, J.M. de Pereda, M.H. Ginsberg, D.A. Calderwood, Talin binding to integrin beta tails: a final common step in integrin activation, Science 302 (2003) 103–106.
[23] U.P. Naik, P.M. Patel, L.V. Parise, Identification of a novel calcium-binding protein that interacts with the integrin alphaIIb cytoplasmic domain, J. Biol. Chem. 272 (1997) 4651–4654.
[24] S. Tsuboi, Calcium integrin-binding protein activates platelet integrin alpha IIbbeta 3, J. Biol. Chem. 277 (2002) 1919–1923.
[25] H. Kashiwagi, M.A. Schwartz, M. Eigenthaler, K.A. Davis, M.H. Ginsberg, S.J. Shattil, Affinity modulation of platelet integrin alphaIIbbeta3 by beta3-endonexin, a selective binding partner of the beta3 integrin cytoplasmic tail, J. Cell Biol. 137 (1997) 1433–1443.

Roles of thromboxane A_2 and prostacyclin in the development of atherosclerosis in apoE-deficient mice

Takuya Kobayashi,[1] Yoshio Tahara,[1] Mayumi Matsumoto,[1] Masako Iguchi,[1] Hideto Sano,[2] Toshinori Murayama,[3] Hidenori Arai,[2] Hiroji Oida,[4] Takami Yurugi-Kobayashi,[5] Jun K. Yamashita,[5] Hiroyuki Katagiri,[6,7] Masataka Majima,[7] Masayuki Yokode,[3] Toru Kita,[3] and Shuh Narumiya[1]

[1]Department of Pharmacology, [2]Department of Geriatric Medicine, and [3]Department of Clinical Innovative Medicine, Kyoto University Faculty of Medicine, Kyoto, Japan. [4]Fukui Safety Research Institute, Ono Pharmaceutical Co., Fukui, Japan. [5]Laboratory of Stem Cell Differentiation, Kyoto University Faculty of Medicine, Kyoto, Japan. [6]Department of Surgery and [7]Department of Pharmacology, Kitasato University School of Medicine, Kanagawa, Japan. [8]Department of Cardiovascular Medicine, Kyoto University Faculty of Medicine, Kyoto, Japan.

Production of thromboxane (TX) A_2 and PG I_2/prostacyclin (PGI_2) is increased in patients with atherosclerosis. However, their roles in atherogenesis have not been critically defined. To examine this issue, we cross-bred atherosclerosis-prone apoE-deficient mice with mice deficient in either the TXA receptor (TP) or the PGI receptor (IP). Although they showed levels of serum cholesterol and triglyceride similar to those of apoE-deficient mice, *apoE*$^{-/-}$*TP*$^{-/-}$ mice exhibited a significant delay in atherogenesis, and *apoE*$^{-/-}$*IP*$^{-/-}$ mice exhibited a significant acceleration in atherogenesis compared with mice deficient in apoE alone. The plaques in *apoE*$^{-/-}$*IP*$^{-/-}$ mice showed partial endothelial disruption and exhibited enhanced expression of ICAM-1 and decreased expression of platelet endothelial cell adhesion molecule 1 (PECAM-1) in the overlying endothelial cells compared with those of *apoE*$^{-/-}$*TP*$^{-/-}$ mice. Platelet activation with thrombin ex vivo revealed higher and lower sensitivity for surface P-selectin expression in platelets of *apoE*$^{-/-}$*IP*$^{-/-}$ and *apoE*$^{-/-}$*TP*$^{-/-}$ mice, respectively, than in those of *apoE*$^{-/-}$ mice. Intravital microscopy of the common carotid artery revealed a significantly greater number of leukocytes rolling on the vessel walls in *apoE*$^{-/-}$*IP*$^{-/-}$ mice than in either *apoE*$^{-/-}$*TP*$^{-/-}$ or *apoE*$^{-/-}$ mice. We conclude that TXA_2 promotes and PGI_2 prevents the initiation and progression of atherogenesis through control of platelet activation and leukocyte-endothelial cell interaction.

Introduction

It is now understood that atherosclerosis is an inflammation in the intima of large arteries that is triggered by high serum cholesterol and in which various types of cells including monocytes/macrophages, endothelial cells (ECs), smooth muscle cells (SMCs), T cells, and blood platelets exert a complex array of interaction (1). A variety of substances including cytokines, chemokines, and growth factors are suggested to induce, amplify, and modify this inflammatory process. One group of these mediators is prostanoids, which are produced from arachidonic acid by the action of COX and include various types of PGs and thromboxane (TX). Involvement of prostanoids in acute inflammation has been well documented based on the finding that aspirin-like NSAIDs are specific COX inhibitors. Among prostanoids, PG I_2/prostacyclin (PGI_2) and TXA_2 have attracted particular attention for their importance in cardiovascular diseases: the former, generated by vascular ECs, is a potent platelet inhibitor and vasodilator, and the latter, released from activated platelets, is a potent vasoconstrictor and platelet-aggregating agent. Indeed, low-dose aspirin that preferentially inhibits platelet-derived TXA_2 over endothelium-derived PGI_2 has been used as anti-platelet therapy for the prevention of myocardial infarction and recurrence of strokes. Although biosynthesis of PGI_2 and TXA_2 is increased in patients with atherosclerosis (2, 3), the roles of these molecules in the initiation and progression of atherosclerosis have not yet been critically examined.

The role played by prostanoids in atherogenesis has been studied mostly by examining the effects of various drugs in mice deficient in either apoE (*apoE*$^{-/-}$ mice) (4, 5) or the LDL receptor (LDLR) (*LDLR*$^{-/-}$ mice) (6). One group of such pharmacological studies has used low doses of aspirin in atherosclerotic model animals to evaluate the contribution of TXA_2. Cyrus et al. (7) fed *LDLR*$^{-/-}$ mice a high-fat diet, treated the mice with low-dose aspirin, and found that this dose of aspirin significantly retarded the development of atherosclerotic lesions, with a 64% reduction in an en face analysis and 29% in a cross-sectional analysis. In contrast, Cayatte et al. (8) used aspirin in *apoE*$^{-/-}$ mice and did not find retardation in the development of atherosclerotic lesions. This discrepancy could be attributed to the higher dose of aspirin used in the latter study, which may have inhibited prostanoid production in cells other than platelets, particularly PGI_2 in blood vessels. In the same study, Cayatte et al. (8) administered a TXA receptor (TP) antagonist, S-18886, to *apoE*$^{-/-}$ mice. They reported that administration of this drug indeed suppressed the extent of atherogenesis, but only marginally, by 21%. The other group of pharmacological studies has used isoform-specific COX inhibitors and has evaluated the roles of prostanoids in atherogenesis. COX exists as two isoforms encoded by two distinct genes (9): COX-1 is constitutively expressed in most tissues and mediates basal physiological functions, while COX-2 is induced by various types of stimuli and works "on demand" in such conditions as inflammation. There is now substantial evidence that the majority of PGI_2 is produced by COX-2 in vascular ECs, whereas production of TXA_2 by platelets is catalyzed by COX-1 (10). The COX-2–catalyzed PGI_2 production probably reflects induction of COX-2 by hemodynamic shear stress in the vasculature (11). The issue of whether COX-2–derived PGI_2 exerts any protective effect on atherosclerosis is important, given that many juvenile patients with arthritis are treated with selective COX-2 inhibitors (12) and a large-scale study (VIGOR) indicated an increased tendency for cardiovascular accidents associated with the use of such drugs versus the nonselective COX inhibitor naproxen (discussed in ref. 13). Experiments examining the effects of COX-2 inhibitors in atherogenesis have yielded conflicting results. One study in which an MF-tricyclic was administered to *apoE*$^{-/-}$ mice found exaggeration of atherosclerosis (14), and one study examining the effect of rofecoxib in *LDLR*$^{-/-}$ mice detected a small but significant suppression in the development of atherosclerosis (15). The former study (14) did not specify the gender of the mice studied and may be difficult to interpret. However, two other studies, one of nimesulide in *LDLR*$^{-/-}$ mice (16) and the other of SC-236 in *apoE*$^{-/-}$ mice (17), did not find significant effects. These studies, except for the study using MF-tricyclic (14), all detected similar suppression of PGI_2 production in animals given these drugs. However, the suppression remained partial,

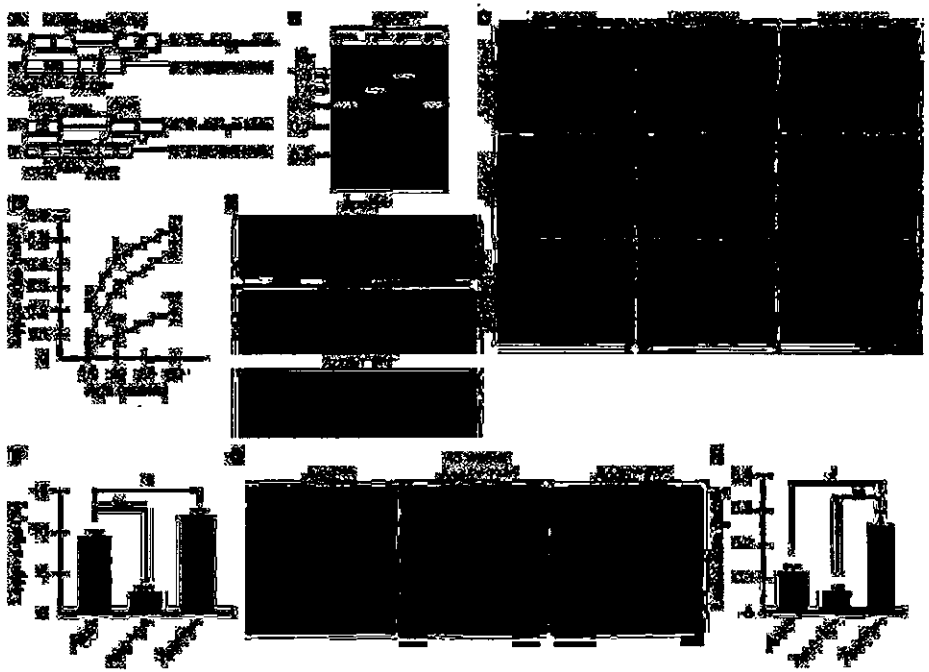

Figure 1
Generation and atherosclerotic lesions of *apoE*$^{+/-}$*TP*$^{+/-}$ and *apoE*$^{+/-}$*IP*$^{+/-}$ mice. (**A**) Strategy for PCR analysis of WT and targeted alleles of TP and IP. Primers are shown by arrowheads. Amplified fragments are shown by broken lines. Neo, neomycin-resistance gene. (**B**) Representative PCR for TP and IP alleles of *apoE*$^{+/-}$, *apoE*$^{+/-}$*TP*$^{+/-}$, and *apoE*$^{+/-}$*IP*$^{+/-}$ mice. (**C**) Representative oil red O staining of aortic sinus sections of *apoE*$^{+/-}$ (middle), *apoE*$^{+/-}$*TP*$^{+/-}$ (lower), and *apoE*$^{+/-}$*IP*$^{+/-}$ (upper) mice. Scale bar: 200 μm. (**D**) Time course of atherosclerotic lesion development in *apoE*$^{+/-}$ (open circles), *apoE*$^{+/-}$*TP*$^{+/-}$ (filled circles), and *apoE*$^{+/-}$*IP*$^{+/-}$ (filled squares) mice. Data are means ± SEM (n = 10 for 15-week-old *apoE*$^{+/-}$ and *apoE*$^{+/-}$*IP*$^{+/-}$ and 20-week-old *apoE*$^{+/-}$ and *apoE*$^{+/-}$*TP*$^{+/-}$ male mice; n = 6 for 15-week-old *apoE*$^{+/-}$*TP*$^{+/-}$, 20-week-old *apoE*$^{+/-}$*IP*$^{+/-}$, and 30-week-old *apoE*$^{+/-}$, *apoE*$^{+/-}$*TP*$^{+/-}$, and *apoE*$^{+/-}$*IP*$^{+/-}$ mice). *P < 0.05 and **P < 0.01 versus *apoE*$^{+/-}$ mice. (**E**) Representative Sudan IV staining of en face preparations of aortas from *apoE*$^{+/-}$, *apoE*$^{+/-}$*TP*$^{+/-}$, and *apoE*$^{+/-}$*IP*$^{+/-}$ mice at 20 weeks of age. Scale bars: 2 mm. (**F**) Quantification of en face atherosclerotic lesions in *apoE*$^{+/-}$, *apoE*$^{+/-}$*TP*$^{+/-}$ and *apoE*$^{+/-}$*IP*$^{+/-}$ mice at 20 weeks of age. Data are means ± SEM (n = 5 each). *P < 0.05 and **P < 0.01 for bracketed comparisons. (**G**) Representative hematoxylin and eosin staining of innominate artery sections of *apoE*$^{+/-}$, *apoE*$^{+/-}$*TP*$^{+/-}$, and *apoE*$^{+/-}$*IP*$^{+/-}$ mice at 45 weeks of age. Scale bar: 20 μm. (**H**) Quantitative analysis of innominate atherosclerotic areas in *apoE*$^{+/-}$, *apoE*$^{+/-}$*TP*$^{+/-}$, and *apoE*$^{+/-}$*IP*$^{+/-}$ mice at 45 weeks of age. Data are means ± SEM (n = 10 each). *P < 0.05 and **P < 0.01 for bracketed comparisons.

Nonstandard abbreviations used: EC, endothelial cell; HDLC, HDL-cholesterol; IP, PGI receptor; LDLC, LDL-cholesterol; LDLR, LDL receptor; PECAM-1, platelet endothelial cell adhesion molecule 1; PPA, paraformaldehyde; PGI_2, PG I_2/prostacyclin; PRP, platelet-rich plasma; SMC, smooth muscle cell; TC, total cholesterol; TG, total triglyceride; TP, TXA receptor; TX, thromboxane; VLDLC, VLDL-cholesterol; vWF, von Willebrand factor.

Conflict of interest: The authors have declared that no conflict of interest exists.

Citation for this article: *J. Clin. Invest.* 114:784–794 (2004). doi:10.1172/JCI200421446.

Table 1
Plasma cholesterol and triglyceride levels

Mouse (mg/dl)	TC (mg/dl)	TG (mg/dl)	VLDLC (mg/dl)	LDLC (mg/dl)	HDLC
C57BL/6 ($n = 8$)	99 ± 5	57 ± 4	6 ± 1	24 ± 3	58 ± 4
TP$^{-/-}$ ($n = 8$)	85 ± 9	50 ± 5	8 ± 1	19 ± 3	54 ± 4
IP$^{-/-}$ ($n = 8$)	90 ± 9	55 ± 6	7 ± 1	22 ± 3	56 ± 4
ApoE$^{-/-}$ ($n = 8$)	535 ± 43[A]	102 ± 6[A]	381 ± 36[A]	127 ± 5[A]	27 ± 4[B]
ApoE$^{-/-}$*TP*$^{-/-}$ ($n = 8$)	595 ± 53[A]	105 ± 10[A]	395 ± 60[A]	138 ± 5[A]	22 ± 4[B]
ApoE$^{-/-}$*IP*$^{-/-}$ ($n = 8$)	588 ± 52[A]	103 ± 8[A]	430 ± 44[A]	135 ± 11[A]	22 ± 4[B]

All data are shown as mean ± SEM. [A]$P < 0.01$ versus C57BL/6. [B]$P < 0.05$ versus C57BL/6.

supporting a view that both COX-1 and COX-2 contribute to PGI_2 production under pathological conditions such as atherosclerosis (3). Thus, pharmacological approaches using various drugs have produced variable and inconclusive results and have failed to provide a cohesive picture on the contribution of prostanoids, including PGI_2 and TXA_2, to atherogenesis. This probably reflects the inherent limitations associated with pharmacological studies, such as differences in the potency and specificity of individual drugs and differences in the experimental protocols and animal models. Moreover, it is difficult in principle to evaluate contribution of each prostanoid by the use of COX inhibitors, because each isoform is capable of producing more than one type of prostanoid in a variety of tissues. For example, TXA_2 is produced not only by COX-1 in blood platelets but also by COX-2 in macrophages, which is also believed to produce PGE_2 in atheromatous plaques. The importance of COX-2 in macrophages was suggested by the reduction in atherogenesis found in *LDLR*$^{-/-}$ mice reconstituted with *COX-2*$^{-/-}$ fetal liver cells (15).

In order to conquer these limitations, we have examined the development of atherosclerosis in mice deficient in prostanoid receptors for individual molecules (TXA_2 and PGI_2). TXA_2 and PGI_2 exert their effects through interaction with cell surface receptors specific to each molecule, TP and the PGI receptor (IP), respectively (18). These receptors are encoded by distinct genes and are expressed differentially in the body. With the use of homologous recombination, we have generated mice that lack either TP or IP individually and have subjected the mice to models of various diseases to analyze the roles of TXA_2 and PGI_2 (19–29). In this work, we have cross-bred TP- and IP-deficient (*TP*$^{-/-}$ and *IP*$^{-/-}$) mice with *apoE*$^{-/-}$ mice and have analyzed the roles played by TXA_2 and PGI_2 in atherosclerotic lesion development.

Results

Generation and lipid profile of apoE$^{-/-}$*TP*$^{-/-}$ *and apoE*$^{-/-}$*IP*$^{-/-}$ *double-KO mice.* *TP*$^{-/-}$ and *IP*$^{-/-}$ mice that had been backcrossed to the C57BL/6 background 10 times each were bred with *apoE*$^{-/-}$ mice that had been backcrossed to the C57BL/6 background 5 times. The resultant heterozygous mice, *apoE*$^{+/-}$*TP*$^{+/-}$ or *apoE*$^{+/-}$*IP*$^{+/-}$ mice, were cross-bred with each other, and compound mice deficient in both apoE and TP or both apoE and IP were generated. The genes encoding IP and apoE are both located on chromosome 7, with a genetic interval of approximately 1.5 cM. To generate recombination between the genes encoding IP and apoE, we mated pairs of *apoE*$^{+/-}$*IP*$^{+/-}$ double-heterozygous mice and selected offspring null either for *apoE* or *IP* (about 1% of the offspring) and cross-bred them with each other. Loss of TP or IP was assessed by PCR analysis (Figure 1, A and B) and was confirmed by examination of the platelet response to a TP or IP agonist (data not shown). The TP agonist I-BOP induced aggregation of platelets from *apoE*$^{-/-}$ mice but not of platelets from *apoE*$^{-/-}$*TP*$^{-/-}$ mice, whereas thrombin-induced aggregation occurred similarly in platelets from *apoE*$^{-/-}$ and *apoE*$^{-/-}$*TP*$^{-/-}$ mice. In contrast, the IP agonist cicaprost inhibited I-BOP–induced platelet aggregation in *apoE*$^{-/-}$ mice and this response was lost in *apoE*$^{-/-}$*IP*$^{-/-}$ platelets. The apoE deficiency in these mice was verified by measurement of plasma cholesterol levels and PCR analysis. At 20 weeks of age, *apoE*$^{-/-}$*TP*$^{-/-}$ and *apoE*$^{-/-}$*IP*$^{-/-}$ mice showed elevated levels of both total cholesterol (TC) and total triglyceride (TG) similar to those seen in *apoE*$^{-/-}$ mice (Table 1). Moreover, VLDL-cholesterol (VLDLC), LDL-cholesterol (LDLC), and HDL-cholesterol (HDLC) in *apoE*$^{-/-}$, *apoE*$^{-/-}$*TP*$^{-/-}$, and *apoE*$^{-/-}$*IP*$^{-/-}$ mice were almost identical. These findings suggest that loss of either TP or IP did not affect the hypercholesterolemia induced by apoE deficiency. *apoE*$^{-/-}$*TP*$^{-/-}$ and *apoE*$^{-/-}$*IP*$^{-/-}$ mice were fertile and apparently healthy. All animals were maintained on a normal chow diet and gained weight in a similar manner (data not shown).

Atherosclerotic lesion development in apoE$^{-/-}$*TP*$^{-/-}$ *and apoE*$^{-/-}$*IP*$^{-/-}$ *mice.* We used male mice of the three strains (*apoE*$^{-/-}$, *apoE*$^{-/-}$*TP*$^{-/-}$, and *apoE*$^{-/-}$*IP*$^{-/-}$) and examined atherosclerotic lesion development by analysis of cross-sections of the proximal aorta, en face analysis of the total aorta, and analysis of cross-sections of the innominate artery. The cross-sectional analysis of the proximal aorta was performed in the first 360 μm of the aortas of *apoE*$^{-/-}$, *apoE*$^{-/-}$*TP*$^{-/-}$, and *apoE*$^{-/-}$*IP*$^{-/-}$ mice at 15, 20, and 30 weeks of age. Typical oil red O staining in each strain of mice at the respective age is shown in Figure 1C. The quantitative analysis revealed significant acceleration and delay of lesion development in *apoE*$^{-/-}$*IP*$^{-/-}$ and *apoE*$^{-/-}$*TP*$^{-/-}$ mice, respectively, compared with that in *apoE*$^{-/-}$ mice (Figure 1D). At 15 and 20 weeks of age, the lesion areas of *apoE*$^{-/-}$*IP*$^{-/-}$ mice (0.206 ± 0.016 mm^2 and 0.420 ± 0.017 mm^2) were augmented significantly by 131% and 45%, respectively, compared with those of *apoE*$^{-/-}$ mice (0.089 ± 0.015 mm^2 and 0.290 ± 0.015 mm^2; $P < 0.05$, Tukey's *t* test following one-way ANOVA) (Figure 1D). After 20 weeks, lesion development in *apoE*$^{-/-}$*IP*$^{-/-}$ mice appeared to quickly reach a plateau and did not show a significant difference compared with that in *apoE*$^{-/-}$ mice at 30 weeks of age. In contrast, *apoE*$^{-/-}$*TP*$^{-/-}$ mice showed significant delay in the lesion development; their lesion areas at 20 and 30 weeks of age (0.087 ± 0.015 mm^2 and 0.183 ± 0.034 mm^2) were significantly suppressed, by 70% and 58%, respectively, compared with those of *apoE*$^{-/-}$ mice (0.290 ± 0.015 mm^2 and 0.438 ± 0.025 mm^2; $P < 0.01$, Tukey's *t* test following one-way ANOVA) (Figure 1D).

ApoE$^{-/-}$*IP*$^{-/-}$ and *apoE*$^{-/-}$*TP*$^{-/-}$ mice showed enhancement and suppression, respectively, of atherogenesis not only locally in the aortic sinus but also globally throughout aorta. En face analysis of aortic preparations of mice at 20 weeks of age revealed significant augmentation and reduction in atherosclerotic area in *apoE*$^{-/-}$*IP*$^{-/-}$ and *apoE*$^{-/-}$*TP*$^{-/-}$ mice, respectively, compared with that of *apoE*$^{-/-}$ mice (Figure 1E); the average lesion size in *apoE*$^{-/-}$*TP*$^{-/-}$ mice ($2.8\% \pm 0.4\%$) was reduced 71% compared with that in *apoE*$^{-/-}$ mice ($9.6\% \pm 0.9\%$; $P < 0.01$, Tukey's *t* test following one-way ANOVA), while that in

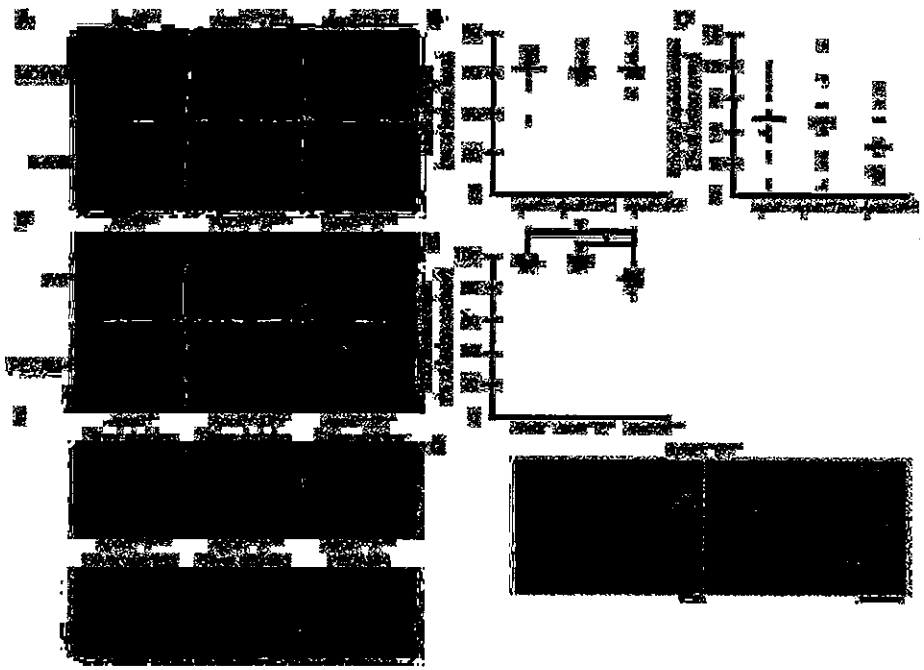

Figure 2
Effects of TP or IP deficiency on the abundance of macrophages and SMCs and EC integrity in aortic arch lesions of apoE-deficient mice at 20 weeks of age. (**A**) Representative immunostaining of macrophages and SMCs in aortic arch lesions of *apoE*$^{-/-}$ (left panels), *apoE*$^{-/-}$*TP*$^{-/-}$ (middle panels), and *apoE*$^{-/-}$*IP*$^{-/-}$ (right panels) mice. Lesions were stained with specific antibodies for macrophages (MOMA-2; upper) and for SMCs (α-actin; lower). White arrowheads indicate the external elastic lamina. Scale bars: 20 μm. (**B** and **C**) Quantitative analysis of the abundance of macrophages (**B**) and SMCs (**C**) in aortic arch lesions of *apoE*$^{-/-}$, *apoE*$^{-/-}$*TP*$^{-/-}$, and *apoE*$^{-/-}$*IP*$^{-/-}$ mice. Data are means ± SEM ($n = 10$ each). (**D**) Representative immunostaining of ECs in aortic arch lesions of *apoE*$^{-/-}$ (left panels), *apoE*$^{-/-}$*TP*$^{-/-}$ (middle panels), and *apoE*$^{-/-}$*IP*$^{-/-}$ (right panels) mice. Cross-sections were stained with specific antibodies for ECs (vWF, upper, and PECAM-1, red, lower) and SMCs (α-actin, green, lower). Black and white arrowheads indicate the site of endothelial disruption. Scale bars: 20 μm. (**E**) Quantitative analysis for endothelial integrity in aortic arch lesions of *apoE*$^{-/-}$, *apoE*$^{-/-}$*TP*$^{-/-}$, and *apoE*$^{-/-}$*IP*$^{-/-}$ mice by measurement of the vWF-positive signals overlying aortic lesions. Data are means ± SEM ($n = 10$ each). *$P < 0.05$ for bracketed comparisons. (**F**) Representative en face staining of aortic arch lesions of *apoE*$^{-/-}$, *apoE*$^{-/-}$*TP*$^{-/-}$, and *apoE*$^{-/-}$*IP*$^{-/-}$ mice. En face staining of aortic arch lesions with silver nitrate or anti–PECAM-1 was performed. Scale bars: 10 μm. (**G**) Representative scanning electron micrographs of aortic arches of *apoE*$^{-/-}$*IP*$^{-/-}$ mice. The right panel shows a higher magnification of the boxed area in the left panel. Scale bars: 50 μm.

apoE$^{-/-}$*IP*$^{-/-}$ mice (12.3% ± 1.0%) was augmented 28% compared with that in *apoE*$^{-/-}$ mice ($P < 0.05$, Tukey's *t* test following one-way ANOVA) (Figure 1F). Atherosclerotic lesions in *apoE*$^{-/-}$ mice were seen in the lesser curvature of the aortic arch and at the ostium of the brachiocephalic artery as well as in the abdominal aorta. The lesions in *apoE*$^{-/-}$*TP*$^{-/-}$ at this age were limited mostly to the aortic arch region, where the extent was much less. In contrast, atherosclerotic lesions in *apoE*$^{-/-}$*IP*$^{-/-}$ mice were more extensive than in *apoE*$^{-/-}$ mice in every region examined (Figure 1E).

Although analysis of atherogenesis in *apoE*$^{-/-}$ mice is carried out mostly in the aorta, atherosclerotic lesions in this strain of mice are not limited to the aorta. We noted the atherosclerotic lesion at the ostium of the brachiocephalic (innominate) artery in our en face analysis of 20-week-old mice described above. Recently, Rosenfeld et al. (30) examined the distribution of atherosclerotic lesions throughout the arterial tree of *apoE*$^{-/-}$ mice and found a highly advanced, clinically significant lesion in the innominate artery in mice 30–60 weeks of age. We therefore examined atherosclerotic lesion development in the innominate artery by cross-sectional analysis in *apoE*$^{-/-}$, *apoE*$^{-/-}$*TP*$^{-/-}$, and *apoE*$^{-/-}$*IP*$^{-/-}$ mice 45 weeks of age. As shown in the hematoxylin and eosin staining in Figure 1G, the lesion was found in all three strains of mice but the extent differed significantly. Whereas the plaques protruded into the arterial lumen only partially in *apoE*$^{-/-}$ and *apoE*$^{-/-}$*TP*$^{-/-}$ mice, those in

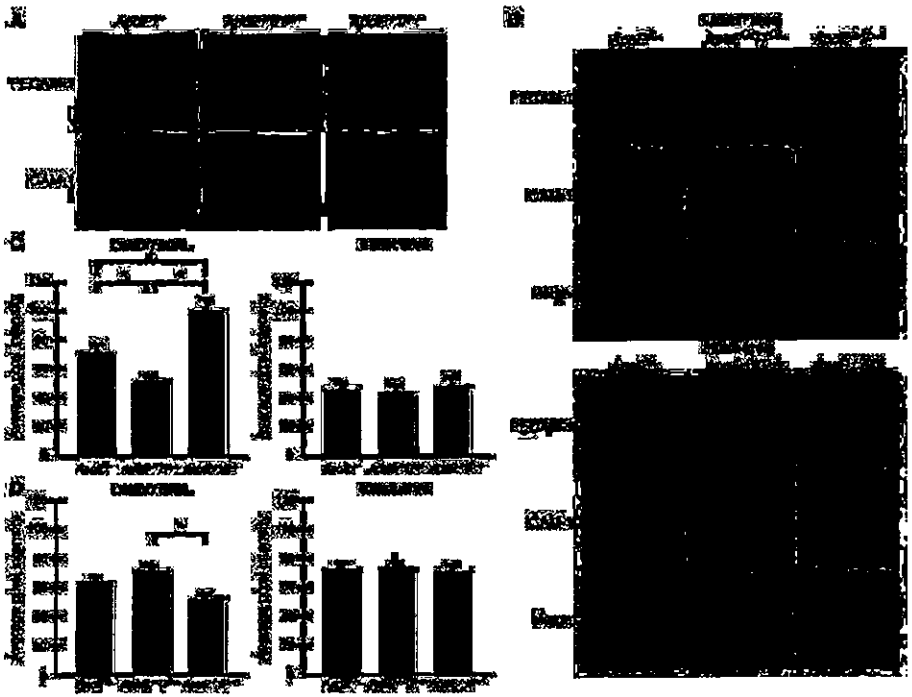

Figure 3
Effects of TP or IP deficiency on ICAM-1 and PECAM-1 expression in the ECs overlying atheromatous lesions of apoE-deficient mice. (A) Representative immunostaining for ICAM-1 and PECAM-1 in cross-sections from *apoE*$^{-/-}$ (left panels), *apoE*$^{-/-}$*TP*$^{-/-}$ (middle panels), and *apoE*$^{-/-}$*IP*$^{-/-}$ (right panels) mice. Mice were sacrificed at 20 weeks of age. Cross-sections were stained with specific antibodies against ICAM-1 (red; lower panels), PECAM-1 (red; upper panels), and smooth muscle α-actin (green). Scale bars: 20 μm. (B) Representative immunostaining of aortic arch lesions and neighboring intact areas for ICAM-1 and PECAM-1 in en face preparations of *apoE*$^{-/-}$ (left panels), *apoE*$^{-/-}$*TP*$^{-/-}$ (middle panels) and *apoE*$^{-/-}$*IP*$^{-/-}$ (right panels) mice. En face preparations were stained with specific antibodies against ICAM-1 (middle panels) and PECAM-1 (upper panels). Mice were sacrificed at 20 weeks of age. Scale bars: 10 μm. Merge, merged images. (C and D) Quantification of ICAM-1 (C) and PECAM-1 (D) expression in ECs overlying aortic arch lesions and neighboring intact areas of *apoE*$^{-/-}$, *apoE*$^{-/-}$*TP*$^{-/-}$, and *apoE*$^{-/-}$*IP*$^{-/-}$ mice. Data are means ± SEM (n = 8 each). *P < 0.05 and **P < 0.01 for bracketed comparisons.

apoE$^{-/-}$*IP*$^{-/-}$ mice grew extensively to partially occlude the lumen. Quantitative analysis revealed significant acceleration and delay in lesion development, respectively, in *apoE*$^{-/-}$*IP*$^{-/-}$ and *apoE*$^{-/-}$*TP*$^{-/-}$ mice compared with *apoE*$^{-/-}$ mice (Figure 1H).

Impaired EC integrity in atheromatous plaques of apoE$^{-/-}$*IP*$^{-/-}$ *mice.* To investigate whether loss of TP or IP signaling had any effect on the cell composition in atheromatous plaques, we stained macrophages, SMCs, and ECs in the plaques at the aortic arches of 20-week-old mice with antibodies against the respective marker proteins. Quantification of macrophage and SMC abundance in the plaques and of endothelial integrity on the lesion surface was performed on the ten sections taken every 18 μm as described in Methods (Figure 2). Cells staining positive for MOMA-2 were found throughout the plaques in all of *apoE*$^{-/-}$, *apoE*$^{-/-}$*TP*$^{-/-}$, and *apoE*$^{-/-}$*IP*$^{-/-}$ mice at this stage. Quantification revealed that MOMA-2–stained cells occupied about 60% of the total plaque area and there were no significant differences among the three strains (Figure 2, A and B). The fact that the area inside the plaque was stained homogenously with oil red O suggested that these MOMA-2–positive cells represented macrophage-derived foam cells and the space not occupied by macrophages represented mostly lipid cores. SMCs staining positive for α-actin accumulated and formed a layer at the top of the lesion beneath the EC layer (Figure 2A and data not shown). Quantification revealed that they comprised about 7% of the total plaque area in *apoE*$^{-/-}$ and *apoE*$^{-/-}$*TP*$^{-/-}$ mice (Figure 2C). The proportion of SMCs in *apoE*$^{-/-}$*IP*$^{-/-}$ mice tended to be lower than that in the other two strains of mice, but there was no significant difference. This SMC phenotype of *apoE*$^{-/-}$*IP*$^{-/-}$ mice is at odds with the suppression

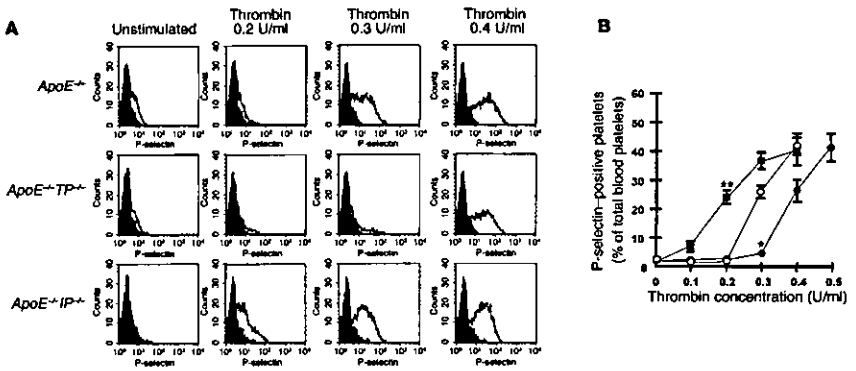

Figure 4
Platelet reactivity for thrombin-induced surface expression of P-selectin. (A) Representative histograms of thrombin-induced P-selectin expression in platelets from *apoE*$^{+/+}$ (upper panels), *apoE*$^{+/+}$*TP*$^{+/+}$ (middle panels), and *apoE*$^{+/+}$*IP*$^{+/+}$ (lower panels) mice. Platelets were either left unstimulated or were stimulated with 0.2, 0.3, or 0.4 U/ml of thrombin. They were then labeled with FITC-conjugated anti–P-selectin and were analyzed by flow cytometry. Filled histograms indicate background signal. (B) Quantification analysis. Concentration-dependent effect of thrombin for P-selectin expression was determined in platelets from *apoE*$^{+/+}$ (open circles), *apoE*$^{+/+}$*TP*$^{+/+}$ (filled circles), and *apoE*$^{+/+}$*IP*$^{+/+}$ (filled squares) mice. Data are means ± SEM (n = 9 each). *P < 0.05 and **P < 0.01 versus *apoE*$^{+/+}$ mice.

of SMC proliferation by a PGI_2 analog (cicaprost) in vitro (22) as well as the enhanced proliferative response found in IP-deficient mice subjected to chronic hypoxia (23) or catheter-induced carotid vascular injury (31). Impaired SMC proliferation in the absence of IP may suggest that SMC proliferation is under more complex regulation in atherosclerosis or that it may be unique to the apoE-deficient mice. These points should be clarified in future studies.

EC integrity on the plaque surface was then examined by staining of the cross-sections for two endothelial markers: von Willebrand factor (vWF) and platelet endothelial cell adhesion molecule 1 (PECAM-1). As expected, the staining was seen as a linear signal in the EC layer over the plaques. There was occasional loss of staining of these two markers in the plaques of *apoE*$^{-/-}$*IP*$^{-/-}$ mice, especially on the "shoulder" of atherosclerotic lesions (Figure 2D). In contrast, no such irregularity in EC staining on the plaque surface was seen in *apoE*$^{-/-}$ and *apoE*$^{-/-}$*TP*$^{-/-}$ mice. Quantification of vWF staining on the plaque surface revealed a significant reduction in *apoE*$^{-/-}$*IP*$^{-/-}$ mice (85.5% ± 0.7%) compared with *apoE*$^{-/-}$ mice (98.0% ± 0.5%, P < 0.05, Tukey's t test following one-way ANOVA) and *apoE*$^{-/-}$*TP*$^{-/-}$ mice (98.5% ± 0.5 %, P < 0.05, Tukey's t test following one-way ANOVA) (Figure 2E). Compatible with these findings in the cross-sections, staining of en face preparations with silver nitrate as well as anti-PECAM revealed loss of ECs which was consistently associated with the "shoulder" of a plaque in *apoE*$^{-/-}$*IP*$^{-/-}$ mice (Figure 2F). Such EC loss was rarely seen in *apoE*$^{-/-}$ and *apoE*$^{-/-}$*TP*$^{-/-}$ mice (observations of 5 mice of each strain). Scanning electron microscopy of the aortic arch region revealed again focal endothelial disruption in the "shoulder" of atheromatous plaques of all of three *apoE*$^{-/-}$*IP*$^{-/-}$ mice examined, while none of three *apoE*$^{-/-}$ or *apoE*$^{-/-}$*TP*$^{-/-}$ mice showed such lesions. In some cases, the lesion of endothelial disruption formed a crater in which monocyte/macrophage-like cells accumulated (Figure 2G). These findings suggest that the EC loss had already occurred in vivo and was not an artifact created during sample preparation.

ICAM-1 and PECAM-1 expression on ECs in apoE$^{-/-}$*TP*$^{-/-}$ *and apoE*$^{-/-}$*IP*$^{-/-}$ *mice.* To explore endothelium activation in *apoE*$^{-/-}$*TP*$^{-/-}$ and *apoE*$^{-/-}$*IP*$^{-/-}$ mice, we stained for ICAM-1 and PECAM-1 in ECs overlying the lesions of the three lines of mice. In cross-sections, PECAM-1 expression was found more or less homogenously through the EC monolayer overlying the lesions, while ICAM-1 expression by endothelium was most intense at borders and the "shoulder" of the lesions in all of the three strains of mice (Figure 3A). We then performed quantitative analysis using en face confocal microscopy images (Figure 3B). In the ECs overlying the lesions, *apoE*$^{-/-}$*TP*$^{-/-}$ mice had a significant decrease in ICAM-1 expression (53.9 ± 1.8 versus 73.1 ± 4.1; P < 0.05, Tukey's t test following one-way ANOVA; values measured in arbitrary units based on fluorescence intensity per pixel) compared with that of *apoE*$^{-/-}$ mice, whereas ICAM-1 expression in *apoE*$^{-/-}$*IP*$^{-/-}$ mice significantly increased (100.5 ± 7.6; P < 0.01, Tukey's t test following one-way ANOVA) (Figure 3C). In contrast, there was no difference in ICAM-1 expression in ECs in intact areas among the three strains of mice, which was low compared with that in the atherosclerotic lesions. As for PECAM-1 expression in the atherosclerotic lesions, expression in *apoE*$^{-/-}$*TP*$^{-/-}$ mice or *apoE*$^{-/-}$*IP*$^{-/-}$ mice tended to increase or decrease, respectively, compared with that in *apoE*$^{-/-}$ mice, and there was a significant difference in expression between *apoE*$^{-/-}$*IP*$^{-/-}$ and *apoE*$^{-/-}$*TP*$^{-/-}$ mice (52.4 ± 3.2 versus 68.3 ± 1.7; P < 0.05, Tukey's t test following one-way ANOVA) (Figure 3D). There was also no difference in PECAM-1 expression in the ECs of intact areas among the three strains of mice.

Reactivity of platelets in apoE$^{-/-}$, *apoE*$^{-/-}$*TP*$^{-/-}$, *and apoE*$^{-/-}$*IP*$^{-/-}$ *mice.* Because TXA_2 and PGI_2 are potent activators and suppressors, respectively, of blood platelets, chronic loss of their actions may cause alterations in platelet reactivity to an aggregating agent. Reactivity of blood platelets was therefore compared among *apoE*$^{-/-}$, *apoE*$^{-/-}$*TP*$^{-/-}$, and *apoE*$^{-/-}$*IP*$^{-/-}$ mice by whole-blood flow cytometry (32, 33). Briefly,

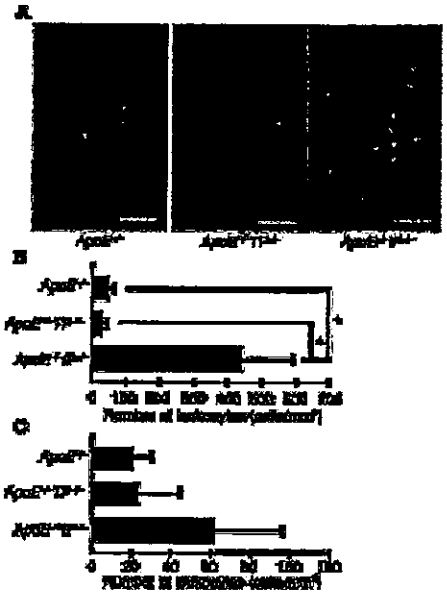

Figure 5
Intravital microscopy for leukocyte rolling and adhesion. (A) Fluorescence images of rolling and adherent leukocytes. Black and white arrows indicate rolling and adherent leukocytes, respectively. Vessel lumens are outlined by broken lines. Scale bars: 0.1 mm. (B) Quantitative analysis of rolling leukocytes. Data are means ± SEM ($n = 5$ each). *$P < 0.05$ versus *apoE*$^{+/+}$ and *apoE*$^{+/-}$*TP*$^{+/+}$ mice. (C) Quantitative analysis for adherent leukocytes as described in B.

diluted blood was activated with various concentrations of thrombin and expression of P-selectin on the platelet surface was evaluated by flow cytometry. Expression of P-selectin was barely detected on unstimulated platelets, but the number of blood platelets showing surface P-selectin expression increased with increasing concentrations of thrombin. P-selectin expression was induced significantly with 0.3 U/ml thrombin and increased with 0.4 U/ml thrombin on the platelets of *apoE*$^{-/-}$ mice (Figure 4, A and B), whereas its expression was only marginally induced at 0.3 U/ml thrombin in the platelets of *apoE*$^{-/-}$*TP*$^{-/-}$ mice (Figure 4, A and B). In contrast, an increase in the P-selectin expression was detected at doses as low as 0.1 U/ml and increased significantly with 0.2 U/ml thrombin in the platelets of *apoE*$^{-/-}$*IP*$^{-/-}$ mice (Figure 4, A and B). These results indicate that the platelets of *apoE*$^{-/-}$*TP*$^{-/-}$ and *apoE*$^{-/-}$*IP*$^{-/-}$ mice have lower and higher sensitivity to thrombin, respectively, than those of *apoE*$^{-/-}$ mice.

Leukocyte adherence in the common carotid arteries of apoE$^{-/-}$*IP*$^{-/-}$ *mice.* Finally, we examined the leukocyte-EC interaction by intravital microscopy. Rhodamine 6G was injected i.v. into *apoE*$^{-/-}$, *apoE*$^{-/-}$*TP*$^{-/-}$, and *apoE*$^{-/-}$*IP*$^{-/-}$ mice to label leukocytes in vivo, and interaction of the leukocytes with the wall of the common carotid artery was examined by intravital microscopy. Leukocytes rolling or adhering were seen as fluorescent dots on the wall of the artery (Figure 5A). Quantitative analysis revealed a significantly greater number of leukocytes rolling on the walls of arteries in *apoE*$^{-/-}$*IP*$^{-/-}$ mice than in either *apoE*$^{-/-}$ or *apoE*$^{-/-}$*TP*$^{-/-}$ mice (Figure 5B). Additionally, adhesion of leukocytes also tended to be higher in *apoE*$^{-/-}$*IP*$^{-/-}$ mice (Figure 5C). Although rhodamine 6G also labeled platelets, we did not see thrombus formation or detachment in any strain of mice during our observation period.

Discussion

TXA_2 and PGI_2 are two major prostanoids in the cardiovascular system, being abundantly produced by blood platelets and vascular endothelium, respectively. Previous studies found that TXA_2 and PGI_2 biosynthesis is increased in patients with atherosclerosis (2, 3). In this work, we generated compound mice, *apoE*$^{-/-}$*TP*$^{-/-}$ and *apoE*$^{-/-}$*IP*$^{-/-}$, and examined the roles of TXA_2 and PGI_2 in the initiation and progression of atherosclerosis. *ApoE*$^{-/-}$ mice develop a spectrum of atherosclerotic lesions similar to that of humans (34). They also show elevated production of TXA_2 and PGI_2, as seen in humans (35). Thus, the *apoE*$^{-/-}$ mouse is a suitable animal model for evaluation of the roles of TXA_2 and PGI_2 in atherosclerosis. Previously, the involvement of these prostanoids in atherosclerosis was examined by the use of various COX inhibitors in this and similar animal models. However, the results obtained by those studies were variable (7, 8, 14–17). In addition, a study using a TP antagonist in *apoE*$^{-/-}$ mice showed only a marginal reduction in atherogenesis (8). In contrast to those findings in the previous studies, our study here using genetically engineered mice has demonstrated significant suppression and significant enhancement of atherosclerosis in *apoE*$^{-/-}$*TP*$^{-/-}$ and *apoE*$^{-/-}$*IP*$^{-/-}$ mice, respectively, suggesting strongly proatherogenic and antiatherogenic actions of TXA_2 and PGI_2, respectively. TP deficiency suppressed the extent of atherosclerosis at both 20 and 30 weeks of age. Suppression of atherosclerosis by TP deficiency is much more robust (70% at 20 weeks of age and 58% at 30 weeks of age) than that found after treatment with the TP antagonist S-18886 (about 20%) (8). We have also examined the effects of TP or IP deficiency on the development of vascular lesions in the innominate arteries of 45-week-old *apoE*$^{-/-}$ mice. Rosenfeld et al. (30) previously noted more-advanced vascular lesions in the innominate arteries in *apoE*$^{-/-}$ mice. In this study we have not only confirmed their findings in *apoE*$^{-/-}$ mice but also found that this lesion was far more advanced in *apoE*$^{-/-}$*IP*$^{-/-}$ mice, whereas the disease progression appeared to be retarded in *apoE*$^{-/-}$*TP*$^{-/-}$ mice.

It is noteworthy that atherogenesis was significantly accelerated and reached a plateau early in *apoE*$^{-/-}$*IP*$^{-/-}$ mice compared with *apoE*$^{-/-}$ mice. These results indicate that signaling from PGI_2 to IP is important in preventing the initiation of atherosclerosis. Impaired PGI_2 function, moreover, appeared to affect the progression and nature of atherosclerotic plaques. Our analysis detected frequent loss of ECs in the plaques of *apoE*$^{-/-}$*IP*$^{-/-}$ mice. In addition to ECs, we also found that the abundance of SMCs tended to be lower in the plaques of *apoE*$^{-/-}$*IP*$^{-/-}$ mice (Figure 2). Lesions with impaired EC integrity and weaker fibrous caps are suggested to be prone to rupture (36). Recently, Cipollone and colleagues found that COX-2 and membrane-bound PGE synthetase are upregulated in macrophages in atheromatous plaques of humans and induce expression of matrix metalloproteinase-9 and proposed that this pathway leads to plaque instability (37, 38). It is interesting in this context that PGI_2 can suppress expression of this matrix metalloproteinase isoform in vitro and in vivo (39, 40). Lesion rupture, when it occurs in vivo, then precipitates thrombosis, which is further accelerated in the absence of IP. Disruption of IP is known to increase the risk of thrombosis (20). Thus, PGI_2 appears to exert important inhibitory actions on the initiation and progression of atherosclerosis, and the reduction in PGI_2 in the presence of normal TXA_2 formation is likely to lead an increased risk of atherosclerosis and thrombosis. Currently, an important question concerning COX-2 inhibitors is whether the selective reduction in PGI_2 increases the risk of atherosclerosis. Our findings support that conclusion. However, our findings cannot be directly extrapolated to the clinical outcome of patients treated with COX-2 inhibitors. Although the majority of PGI_2 under basal conditions is derived from COX-2 catalysis, both COX-1 and COX-2 contribute to the increase in PGI_2 in patients with atherosclerosis as well as in *apoE*$^{-/-}$ mice (3, 17), and selective inhibition of COX-2 usually results in only partial inhibition of PGI_2 production (15–17). In addition, TXA_2 can be derived also from COX-2 in atherosclerotic plaques. COX-2 is expressed by monocytes/macrophages in mouse atherosclerotic lesions (15). Macrophages contain TX synthase and release large amounts of TXA_2 when transformed into foam cells with modified LDL (41).

What, then, are the underlying mechanisms of the actions of TXA_2 and PGI_2 in atherogenesis? Activation and inhibition of blood platelets by TXA_2 and PGI_2, respectively, may certainly be one of the mechanisms. Activated platelets were found in the circulating blood of patients with atherosclerosis (42–44) and hypercholesterolemia (45, 46). We have examined this issue by using whole-blood flow cytometry for thrombin-induced P-selectin expression in platelets (32). This method has been used frequently to evaluate platelet reactivity in patients with various cardiovascular disorders (33). Our analysis has revealed that platelets of *apoE*$^{-/-}$*TP*$^{-/-}$ and *apoE*$^{-/-}$*IP*$^{-/-}$ mice have lower and higher reactivity, respectively, than those of *apoE*$^{-/-}$ mice, which is consistent with the atherosclerotic phenotypes observed in the three strains of mice.

Here, we have further examined effects of TP or IP disruption on expression of adhesion molecules on ECs. Adhesion molecules on ECs play important roles in the migration of monocytes/macrophages through the EC monolayer and the initiation of atheromatous plaques. Indeed, ICAM-1 is strongly expressed in atherosclerotic plaques of humans (47) and the level of soluble ICAM-1 correlates with the severity of atherosclerosis (48). In *apoE*$^{-/-}$ mice, ICAM-1 expression is high in atherosclerosis-prone sites of the aorta, and deficiency in ICAM-1 in apoE-deficient mice significantly reduces atherosclerotic lesions (49). We have found that ICAM-1 expression on ECs overlying the plaques of *apoE*$^{-/-}$*TP*$^{-/-}$ mice is significantly lower, while that of *apoE*$^{-/-}$*IP*$^{-/-}$ mice is significantly higher, than ICAM-1 expression in *apoE*$^{-/-}$ mice (Figure 3). The changes in the ICAM-1 expression in the presence of TP or IP deficiency are consistent with the reported in vitro actions of TXA_2 and PGI_2. ICAM-1 expression is induced by proinflammatory cytokines from activated macrophages such as TNF-α or IL-1β (50). Signaling from PGI_2 to IP is known to inhibit TNF-α production by activated macrophages (21) and to reduce IL-1–induced ICAM-1 expression on ECs (51). In contrast, stimulation of TP induces ICAM-1 expression in cultured ECs in vitro (52, 53), suggesting that TXA_2 formed in situ in atheromatous plaques acts on ECs to induce ICAM-1 expression to amplify atherogenesis. Interestingly, TXA_2 and PGI_2 appear to have effects opposite to those of ICAM-1 on the expression of PECAM-1 on the plaque ECs, which was up- and downregulated in *apoE*$^{-/-}$*TP*$^{-/-}$ and *apoE*$^{-/-}$*IP*$^{-/-}$ mice, respectively. PECAM-1 was first described as an adhesion molecule essential in the transmigration of leukocytes through endothelial monolayer (54). However, recent analyses of *PECAM-1*$^{-/-}$ mice in various models showed that PECAM-1 deficiency did not block but instead enhanced leukocyte accumulation at inflammation sites (55–57). Given its intracellular domain, PECAM-1 is now suggested to be an inhibitory signaling molecule (58). Intriguingly, regulation of PECAM-1 expression is opposite to that of ICAM-1. For example, a previous report showed that the expression of PECAM-1 and ICAM-1 on cultured human umbilical vein ECs was down- and upregulated, respectively, after activation with TNF-α plus IFN-γ (59). Such opposite modes of expression may explain the changes in the patterns of ICAM-1 and PECAM-1 expression found in the atherosclerosis phenotypes of *apoE*$^{-/-}$*TP*$^{-/-}$ and *apoE*$^{-/-}$*IP*$^{-/-}$ mice.

The above findings on the reactivity of platelets and the expression of adhesion molecules in ECs in *apoE*$^{-/-}$, *apoE*$^{-/-}$*TP*$^{-/-}$, and *apoE*$^{-/-}$*IP*$^{-/-}$ mice suggest that TP or IP deficiency can affect the interaction of ECs with platelets and leukocytes. We examined this issue by intravital microscopy. Although we did not detect significant platelet adhesion to the blood vessels of any of the three lines of mice under basal conditions, we found significant leukocyte adherence to the wall of the common carotid artery in *apoE*$^{-/-}$*IP*$^{-/-}$ mice. This may be relevant to the higher platelet reactivity and enhanced ICAM-1 expression in this line of animals. Platelet P-selectin is suggested to play an important role in mediating the leukocyte-EC interaction (60). It may be also relevant to the EC disruption observed in *apoE*$^{-/-}$*IP*$^{-/-}$ mice.

In conclusion, using the IP-deficient and TP-deficient mice, we were able to evaluate separately the contributions of PGI_2 and TXA_2 to the development of atherosclerosis. The information presented here will aid in the interpretation of clinical findings and the evaluation of risk in atherosclerotic patients treated with various drugs modulating the arachidonate cascade. Our findings also indicate that the administration of PGI mimetics and TP antagonists may be useful in the prevention of atherosclerosis. This line of genetic approach may also help to identify the contributions of PGs other than PGI_2 and TXA_2 to atherosclerosis.

Methods

Generation of apoE$^{-/-}$*TP*$^{-/-}$ *and apoE*$^{-/-}$*IP*$^{-/-}$ *double-KO mice.* *ApoE*$^{-/-}$ mice (129Ola × C57BL/6 mixed background) were a generous gift from Edward M. Rubin (University of California at Berkeley, Berkeley, California, USA) (4). Mice lacking TP or IP individually were generated as described (19, 20). *ApoE*$^{-/-}$, *TP*$^{-/-}$, and *IP*$^{-/-}$ mice were backcrossed 5, 10, and 10 times, respectively, to C57BL/6CrSlc mice (Japan SLC). *TP*$^{-/-}$ and *IP*$^{-/-}$ mice were then cross-bred with *apoE*$^{-/-}$ mice. Functional disruption of the gene encoding apoE was confirmed by markedly elevated plasma cholesterol levels. Genotype analyses of *apoE*$^{-/-}$, *TP*$^{-/-}$, and *IP*$^{-/-}$ mice were performed by PCR using genomic DNA isolated from tail snip samples as a template. PCR analysis was performed for apoE alleles with the sense primers exon2 (5′-GTGCTGTTGGTCACATTGCTGACA-3′) and Neo1 (5′-ATGGGATCGGCCATTGAACA-3′) for WT and mutant alleles, respectively, and the antisense primer exon3 (5′-TCAGTTCTTGTGTGACTTGGGAGC-3′); for TP alleles with the sense primers ML139 (5′-ACTTTGTTGCAGACACCACCTGTC-3′) and Neo2 (5′-TGATATTGCTGAAGAGCTTGGCGGCGA-3′) for WT and mutant alleles, respectively, and the antisense primer ML136 (5′-AAGCTTGGGTTTCAGGGACCT-3′); and for IP alleles with the sense primer CY37 (5′-GTATCTTTCAGTACCTGAGGACTG-3′) and

the antisense primers CY41 (5′-GAGCAGAAAAATTCCCAGAGGCTT-3′) and Neo17 (5′-TGACCGCTTCCTCGTGCTTTAC-3′) for WT and mutant alleles, respectively (Figure 1A). Reaction mixtures contained 10 mM Tris-HCl, pH 8.3, 50 mM KCl, 1.5 mM $MgCl_2$, 0.1% Triton X-100, 10% DMSO, 0.25 mM dNTPs, 20 pmol of each primer, and 1 U of Taq DNA polymerase (Toyobo) in a total volume of 20 μl. After a denaturation step at 94°C for 3 minutes, 35 cycles of the amplification step (94°C for 60 seconds, 58°C for 60 seconds, and 72°C for 80 seconds) were carried out, followed by a final elongation step of 3 minutes at 72°C. For apoE alleles, primers exon2 and exon3 amplify a 0.7-kb WT allele fragment, and primers Neo1 and exon3 amplify a 0.4-kb mutant allele fragment. For TP alleles, primers ML139 and ML136 amplify a 0.9-kb WT allele fragment, and primers Neo2 and ML136 amplify a 1.1-kb mutant allele fragment (Figure 1A). For IP alleles, primers CY37 and CY41 amplify a 1.3-kb WT allele fragment, and primers CY37 and Neo17 amplify a 0.9-kb mutant allele fragment (Figure 1A). Mice were kept on a 12-hour light/dark cycle and were fed a normal chow diet (F2; Funabashi Farm). Food and water were available ad libitum. All experiments were performed in male mice. All experimental procedures were approved by the Committee on Animal Research of Kyoto University Faculty of Medicine.

Preparation of mouse platelets and platelet aggregation assay. Platelet aggregation was examined as described previously (61). Blood (1.0 ml) was drawn by cardiac puncture of ether-anesthetized mice with a syringe containing 50 μl of 3.8% trisodium citrate. Blood pooled from 3–4 animals was diluted with an equal volume of modified Tyrode-HEPES buffer, pH 7.4 (20 mM HEPES, 140 mM NaCl, 5 mM $MgCl_2$, and 5 mM KCl). Platelet-rich plasma (PRP) was prepared by centrifugation at 160 *g* for 5 minutes at room temperature. Platelet-poor plasma was obtained by further centrifugation of the blood after PRP was removed at 1,500 *g* for 10 minutes at room temperature. The number of platelets in the PRP was adjusted to 3×10^5 platelets/μl. Platelet aggregation was measured with an aggregometer (NBS Hema Tracer 601; Tokyo Koden). I-BOP, a TP agonist, was used to activate platelets, and cicaprost, an IP agonist, was used to inhibit platelet aggregation.

Lipid and lipoprotein analyses. Blood (1.0 ml) was drawn by cardiac puncture of ether-anesthetized mice into a tube containing EDTA (final concentration, 5 mM). Plasma was isolated by centrifugation at 1,500 *g* for 10 minutes and was maintained at 4°C. Plasma cholesterol and triglyceride were measured using Toyobo enzymatic assay kits (Toyobo). For quantification of the cholesterol content of each lipoprotein, lipoproteins were separated at buoyant densities of 1.019 g/ml and 1.063 g/ml by ultracentrifugation. VLDLC is the difference between TC and cholesterol with a density greater than 1.019 g/ml; HDLC is cholesterol with a density of more than 1.063 g/ml cholesterol; LDLC is the difference between TC and the sum of VLDLC and HDLC.

Quantification of atherosclerosis. Atherosclerotic lesions were quantified by en face analysis of the whole aorta and by cross-sectional analysis of the proximal aorta and the innominate artery. For en face preparations of the aorta, a cannula was inserted into the left ventricle and the aortic tree was fixed by perfusion for 10 min with ice-cold PBS containing 4% paraformaldehyde (PFA), 5% sucrose, 20 μM butylated hydroxytoluene, and 2 μM EDTA, as described previously (62, 63). The aorta was opened longitudinally, from the heart to the iliac arteries, while still attached to the heart and major branching arteries in the body. The primary incision followed the ventral side of the aorta and the inner curvature of the arch. To obtain a flat preparation for imaging, a second incision was made along the outer curvature of the arch. The aorta (from the heart to the iliac bifurcation) was then removed and was "pinned out" on a black wax surface in a dissecting pan using stainless steel pins 0.2 mm in diameter. After overnight fixation with the PFA solution described above and a 12-hour rinse in PBS, the aortas were briefly rinsed in 70% ethanol; immersed for 6 minutes in a filtered solution containing 0.5% Sudan IV, 35% ethanol, and 50% acetone; and destained for 5 minutes in 80% ethanol. The Sudan IV–stained aortas were photographed and were used for quantification of atherosclerotic lesions.

For cross-sectional analysis of the aorta, hearts were isolated from mice sacrificed by cervical dislocation, were washed in PBS, and were embedded in OCT compound. The OCT-embedded hearts were sectioned with a cryostat, and 6-μm sections in the proximal aorta were obtained sequentially beginning at the aortic valve. Sections were transferred onto a Superfrost slide (Matsunami) and were stained with oil red O followed by counterstaining with hematoxylin (4). Ten sections obtained every 36 μm from the aortic sinus were used for quantification of lesion areas with Image Pro Plus software (Media Cybernetics). The average lesion area of the ten sections from each heart was taken as a value to represent that animal, and the means of the average lesion areas from each group were compared as described previously (64, 65).

Atherosclerotic lesions in the innominate artery were quantified by cross-sectional analysis. Innominate arteries were isolated from 45-week-old male mice sacrificed by cervical dislocation, were washed in PBS, and were embedded in OCT compound. OCT-embedded innominate arteries were sectioned with a cryostat and 8-μm sections were obtained sequentially. Sections were transferred onto a Superfrost slide and were stained with hematoxylin and eosin. Ten sections obtained every 80 μm were used for quantification of lesion areas with Image Pro Plus software. The average lesion area of the 10 sections from each innominate artery was taken as a value to represent that animal and the means of the average lesion areas from 10 mice were compared.

Immunohistochemistry. For cross-sectional analyses, the aortic tree was perfused with ice-cold PBS containing 5 mM EDTA via a cannula inserted into the left ventricle for 10 minutes. The aortic arch was isolated, embedded in OCT compound, and sectioned at a thickness of 6 μm with a cryostat. Sections containing atherosclerotic plaques were identified by microscopy. These sections were then fixed in 4% PFA at 4°C for 10 minutes, were immersed in PBS for 5 minutes for rehydration of the tissues, and were blocked overnight at 4°C with 2% skim milk (BD) in PBS. For evaluation of the abundance of macrophages and SMCs and the expression of ICAM-1 (CD54) and PECAM-1 (CD31) in the lesions, sections were incubated overnight at 4°C with a 1:200 dilution of rat MOMA-2 mAb against mouse macrophages (Accurate Chemical and Scientific Co.); a 1:200 dilution of mouse 1A4 mAb against human α-smooth muscle actin, labeled with FITC (Dako); a 1:200 dilution of armenian hamster mAb against mouse ICAM-1, labeled with Texas Red (BD); and a 1:200 dilution of rat mAb against mouse PECAM-1, labeled with FITC or Texas Red (BD). Sections incubated with MOMA-2 antibody were then washed and incubated with a 1:400 dilution of goat anti-rat IgG, labeled with Texas Red (BD). For vWF staining, endogenous peroxidase activity was blocked by incubation of sections at 4°C for 30 minutes with 0.3% (volume/volume) H_2O_2 in PBS. The sections were then incubated overnight at 4°C with a 1:200 dilution of mouse mAb against human vWF, labeled with HRP (Sigma-Aldrich). After a thorough washing, staining was developed with diaminobenzidine followed by counterstaining with hematoxylin. Ten sections obtained every 18 μm from aortic arch were used for quantification of the macrophages and SMCs and EC density of the lesions with Image-Pro Plus software. The macrophages and SMCs were quantified by measurement of the area that stained positive for the respective markers, as described previously (7). EC density was determined by the ratio of the vWF-positive luminal surface length to the total luminal surface length of each cross-sectional plaque. The average of the 10 sections was taken to represent 1 animal, and the means of the averages from each group were compared.

For the en face analysis, the aortic tree was first washed by perfusion with ice-cold PBS containing 5 mM EDTA and then was fixed by perfusion with ice-cold PBS containing 4% PFA via a cannula inserted into the left ventricle, each perfusion for 10 minutes. The aortic arch was isolated and opened longitudinally. En face preparations were blocked overnight at 4°C with 2% skim milk in PBS and were incubated overnight at 4°C with a 1:500 dilution of rat mAb against mouse PECAM-1, labeled with FITC, and armenian hamster mAb against mouse ICAM-1, labeled with Texas Red. Because activation of ECs occurs on the "shoulder" of plaques (66), five images (1,024 × 1,024 pixels/image) were obtained randomly from the EC monolayer on the "shoulder" of plaques with a Bio-Rad MRC-1024 confocal microscope. The average pixel intensity of the five images was taken as a value to represent that animal, and the means of the average pixel intensity from each group were compared as described previously (60).

Silver nitrate staining of en face endothelial cells. The aortic tree was washed, stained, and fixed as described previously (67, 68) by successive perfusion in the following solutions: 10 ml of 5% glucose; 4 ml of 0.25% silver nitrate; 2 ml of 5% glucose; 8 ml of 3% cobalt bromide and 1% ammonium bromide; 2 ml of 5% glucose; 4 ml of 4% PFA; 10 ml of distilled water; 2 ml of hematoxylin; and 10 ml of distilled water. The aortic arch was isolated, opened longitudinally, and mounted with the endothelium upward on a Superfrost slide.

Scanning electron microscopy. The aortic trees of 20-week-old male mice were washed at 37°C for 10 minutes with PBS and were fixed at room temperature for 10 minutes with PBS containing 1% glutaraldehyde by perfusion, as described previously (69). The aortic tree was then excised, opened longitudinally, additionally fixed by immersion in PBS containing 1% glutaraldehyde at room temperature for 24 hours, dehydrated in ethanol, and processed by critical point drying with CO_2. The aortic tree specimens were then oriented with the lumens exposed, mounted with carbon paint, and coated with gold for scanning electron microscopy (T-330; Nippon Denshi).

Flow cytometry for platelet reactivity. Platelet reactivity was examined by whole-blood flow cytometry (32, 33). Blood (1.0 ml) was drawn by cardiac puncture of ether-anesthetized mice with a syringe containing 50 μl of 3.8% trisodium citrate. Within 10 minutes of being drawn, the blood was diluted 1:4 in modified Tyrode-HEPES buffer, pH 7.4, and the diluted blood was activated at 37°C for 10 minutes with 0.1–0.5 U/ml thrombin, incubated at room temperature for 30 minutes with a 1:100 dilution of rat mAb against mouse P-selectin, labeled with FITC, and fixed at 4°C for 2 hours with ice-cold PBS containing 1% PFA. Samples were then analyzed using a FACSVantage flow cytometer (BD).

Intravital microscopy. Leukocyte-EC interaction was examined by intravital microscopy using rhodamine 6G that stained in vivo leukocytes, as described previously (29, 60, 69). Five male mice 25–30 weeks of age were used for each strain. Rhodamine 6G was injected i.v., and the numbers of leukocytes rolling on and adhering to the wall of the common carotid artery were examined "off-line" during video playback analysis. A leukocyte was defined as rolling if it migrated along the vessel wall at a rate less than 200 μm/s and as adhering if it remained stationary for more than 20 seconds. We counted the number of leukocyte rolling and adhering in the artery per microscope field (×100) and expressed the results as the number of leukocytes observed per mm^2 area per minute.

Statistical analysis. Data are presented as means ± SEM. Comparison of two groups was analyzed by Student's *t* test. For comparison of more than two groups with comparable variances, one-way ANOVA was performed, followed by Tukey's *t* test to evaluate pair-wise group differences. An associated probability (*P* value) of less than 0.05 was considered significant. Analyses were performed with the use of GraphPad Software Prism 3.0.

Acknowledgments

We are grateful to H. Wise for helpful discussions; K. Deguchi, T. Fujiwara, and N. Kitagawa for animal care and breeding; and T. Arai, H. Nose, and Y. Kitagawa for secretarial assistance. This work was supported in part by Grants-in-Aid for Scientific Research from the Ministry of Education, Science, Sports and Culture of Japan and by grants from the Organization for Pharmaceutical Safety and Research and the Kowa Life Science Foundation.

Received for publication March 1, 2004, and accepted in revised form July 27, 2004.

Address correspondence to: Shuh Narumiya, Department of Pharmacology, Kyoto University Faculty of Medicine, Yoshida, Sakyo-ku, Kyoto 606-8501, Japan. Phone: +81-75-753-4392; Fax: +81-75-753-4693; E-mail: snaru@mfour.med.kyoto-u.ac.jp.

1. Ross, R. 1999. Atherosclerosis is an inflammatory disease. *Am. Heart J.* **138**:S419–S420.
2. FitzGerald, G.A., Smith, B., Pedersen, A.K., and Brash, A.R. 1984. Increased prostacyclin biosynthesis in patients with severe atherosclerosis and platelet activation. *N. Engl. J. Med.* **310**:1065–1068.
3. Belton, O., Byrne, D., Kearney, D., Leahy, A., and Fitzgerald, D.J. 2000. Cyclooxygenase-1 and -2-dependent prostacyclin formation in patients with atherosclerosis. *Circulation.* **102**:840–845.
4. Plump, A.S., et al. 1992. Severe hypercholesterolemia and atherosclerosis in apolipoprotein E-deficient mice created by homologous recombination in ES cells. *Cell.* **71**:343–353.
5. Zhang, S.H., Reddick, R.L., Piedrahita, J.A., and Maeda, N. 1992. Spontaneous hypercholesterolemia and arterial lesions in mice lacking apolipoprotein E. *Science.* **258**:468–471.
6. Ishibashi, S., et al. 1993. Hypercholesterolemia in low density lipoprotein receptor knockout mice and its reversal by adenovirus-mediated gene delivery. *J. Clin. Invest.* **92**:883–893.
7. Cyrus, T., et al. 2002. Effect of low-dose aspirin on vascular inflammation, plaque stability, and atherogenesis in low-density lipoprotein receptor-deficient mice. *Circulation.* **106**:1282–1287.
8. Cayatte, A.J., et al. 2000. The thromboxane receptor antagonist S18886 but not aspirin inhibits atherogenesis in apo B-deficient mice: evidence that eicosanoids other than thromboxane contribute to atherosclerosis. *Arterioscler. Thromb. Vasc. Biol.* **20**:1724–1728.
9. Vane, J.R., Bakhle, Y.S., and Botting, R.M. 1998. Cyclooxygenases 1 and 2. *Ann. Rev. Pharmacol. Toxicol.* **38**:97–120.
10. McAdam, B.F., et al. 1999. Systemic biosynthesis of prostacyclin by cyclooxygenase (COX)-2: the human pharmacology of a selective inhibitor of COX-2. *Proc. Natl. Acad. Sci. U. S. A.* **96**:272–277.
11. Topper, J.N., Cai, J., Falb, D., and Gimbrone, M.A., Jr. 1996. Identification of vascular endothelial genes differentially responsive to fluid mechanical stimuli: cyclooxygenase-2, manganese superoxide dismutase, and endothelial cell nitric oxide synthase are selectively up-regulated by steady laminar shear stress. *Proc. Natl. Acad. Sci. U. S. A.* **93**:10417–10422.
12. Foeldvari, I. 2002. A selective COX-2 inhibitor, meloxicam, as a treatment option in patients with juvenile idiopathic arthritis and gastrointestinal side effects from naproxen [letter]. *Clin. Exp. Rheumatol.* **20**:874.
13. Mukherjee, D., Nissen, S.E., and Topol, E.J. 2001. Risk of cardiovascular events associated with selective COX-2 inhibitors. *JAMA.* **286**:954–959.
14. Rott, D., et al. 2003. Effects of MF-tricyclic, a selective cyclooxygenase-2 inhibitor, on atherosclerosis progression and susceptibility to cytomegalovirus replication in apolipoprotein-E knockout mice. *J. Am. Coll. Cardiol.* **41**:1812–1819.
15. Burleigh, M.E., et al. 2002. Cyclooxygenase-2 promotes early atherosclerotic lesion formation in LDL receptor-deficient mice. *Circulation.* **105**:1816–1823.
16. Pratico, D., Tillmann, C., Zhang, Z.B., Li, H., and FitzGerald, G.A. 2001. Acceleration of atherogenesis by COX-1-dependent prostanoid formation in low density lipoprotein receptor knockout mice. *Proc. Natl. Acad. Sci. U. S. A.* **98**:3358–3363.
17. Belton, O.A., Duffy, A., Toomey, S., and Fitzgerald, D.J. 2003. Cyclooxygenase isoforms and platelet vessel wall interactions in the apolipoprotein E knockout mouse model of atherosclerosis. *Circulation.* **108**:3017–3023.
18. Narumiya, S., Sugimoto, Y., and Ushikubi, F. 1999. Prostanoid receptors: structures, properties, and functions. *Physiol. Rev.* **79**:1193–1226.
19. Kabashima, K., et al. 2003. Thromboxane A_2 modulates interaction of dendritic cells and T cells and regulates acquired immunity. *Nat. Immunol.* **4**:694–701.
20. Murata, T., et al. 1997. Altered pain perception and inflammatory response in mice lacking

prostacyclin receptor. *Nature.* 388:678–682.
21. Shinomiya, S., et al. 2001. Regulation of TNFα and interleukin-10 production by prostaglandins I_2 and B_2: studies with prostaglandin receptor-deficient mice and prostaglandin E-receptor subtype-selective synthetic agonists. *Biochem. Pharmacol.* 61:1153–1160.
22. Fujino, T., et al. 2002. Effects of the prostanoids on the proliferation or hypertrophy of cultured murine aortic smooth muscle cells. *Br. J. Pharmacol.* 136:530–539.
23. Hoshikwa, Y., et al. 2001. Prostacyclin receptor-dependent modulation of pulmonary vascular remodeling. *Am. J. Respir. Crit. Care. Med.* 164:314–318.
24. Xiao, C.Y., et al. 2001. Roles of prostaglandin I_2 and thromboxane A_2 in cardiac ischemia-reperfusion injury: a study using mice lacking their respective receptors. *Circulation.* 104:2210–2215.
25. Takahashi, Y., et al. 2002. Augmentation of allergic inflammation in prostanoid IP receptor deficient mice. *Br. J. Pharmacol.* 137:315–322.
26. Nagao, K., et al. 2003. Role of prostaglandin I_2 in airway remodeling induced by repeated allergen challenge in mice. *Am. J. Respir. Cell Mol. Biol.* 29:314–320.
27. Arai, K., et al. 2003. Endogenous prostaglandin I_2 regulates the neural emergency system through release of calcitonin gene related peptide. *Gut.* 52:1242–1249.
28. Yamada, T., et al. 2003. Thromboxane A_2 regulates vascular tone via its inhibitory effect on the expression of inducible nitric oxide synthase. *Circulation.* 108:2381–2386.
29. Katagiri, H., et al. 2004. Role of thromboxane derived from COX-1 and -2 in hepatic microcirculatory dysfunction during endotoxemia in mice. *Hepatology.* 39:139–150.
30. Rosenfeld, M.E., et al. 2000. Advanced atherosclerotic lesions in the innominate artery of the apoE knockout mouse. *Arterioscler. Thromb. Vasc. Biol.* 20:2587–2592.
31. Cheng, Y., et al. 2002. Role of prostacyclin in the cardiovascular response to thromboxane A_2. *Science.* 296:539–541.
32. Nakashima, Y., Plump, A.S., Raines, E.W., Breslow, J.L., and Ross, R. 1994. ApoE-deficient mice develop lesions of all phases of atherosclerosis throughout the arterial tree. *Arterioscler. Thromb.* 14:133–140.
33. Pratico, D., Cyrus, T., Li, H., and FitzGerald, G.A. 2000. Endogenous biosynthesis of thromboxane and prostacyclin in 2 distinct murine models of atherosclerosis. *Blood.* 96:3823–3826.
34. Libby, P., Schoenbeck, U., Mach, F., Selwyn, A.P., and Ganz, P. 1998. Current concepts in cardiovascular pathology: the role of LDL cholesterol in plaque rupture and stabilization. *Am. J. Med.* 104:14S–18S.
35. Hartung, H.P., Kladetzky, R.G., Melnik, B., and Hennerici, M. 1986. Stimulation of the scavenger receptor on monocytes-macrophages evokes release of arachidonic acid metabolites and reduced oxygen species. *Lab. Invest.* 55:209–216.
36. Fitzgerald, D.J., Roy, L., Catella, F., and FitzGerald, G.A. 1986. Platelet activation in unstable coronary disease. *N. Engl. J. Med.* 315:983–989.
37. Cipollone, F., et al. 2001. Overexpression of functionally coupled cyclooxygenase-2 and prostaglandin E synthase in symptomatic atherosclerotic plaques as a basis of prostaglandin E_2-dependent plaque instability. *Circulation.* 104:921–927.
38. Cipollone, F., et al. 2003. The receptor RAGE as a progression factor amplifying arachidonate-dependent inflammatory and proteolytic response in human atherosclerotic plaques: role of glycemic control. *Circulation.* 108:1070–1077.
39. Kitahara, M., et al. 2001. Prostacyclin inhibits the production of MMP-9 induced by phorbol ester through protein kinase A activation, but does not affect the production of MMP-2 in human cultured mesangial cells. *Kidney Blood Press. Res.* 24:18–26.
40. Schermuly, R. T., et al. 2004. Antiremodeling effects of iloprost and the dual-selective phosphodiesterase 3/4 inhibitor tolafentrine in chronic experimental pulmonary hypertension. *Circ. Res.* 94:1101–1108.
41. Trip, M.D., Cats, V.M., van Capelle, F.J., and Vreeken, J. 1990. Platelet hyperreactivity and prognosis in survivors of myocardial infarction. *N. Engl. J. Med.* 322:1549–1554.
42. van Zanten, G.H., et al. 1994. Increased platelet deposition on atherosclerotic coronary arteries. *J. Clin. Invest.* 93:615–632.
43. Broijersen, A., Hamsten, A., Eriksson, M., Angelin, B., and Hjemdahl, P. 1998. Platelet activity in vivo in hyperlipoproteinemia-importance of combined hyperlipidemia. *Thromb. Haemost.* 79:268–275.
44. Broijersen, A., Karpe, F., Hamsten, A., Goodall, A.H., and Hjemdahl, P. 1998. Alimentary lipemia enhances the membrane expression of platelet P-selectin without affecting other markers of platelet activation. *Atherosclerosis.* 137:107–113.
45. Poston, R.N., Haskard, D.O., Coucher, J.R., Gall, N.P., and Johnson-Tidey, R.R. 1992. Expression of intercellular adhesion molecule-1 in atherosclerotic plaques. *Am. J. Pathol.* 140:665–673.
46. Morisaki, N., et al. 1997. New indices of ischemic heart disease and aging: studies on the serum levels of soluble intercellular adhesion molecule-1 (ICAM-1) and soluble vascular cell adhesion molecule-1 (VCAM-1) in patients with hypercholesterolemia and ischemic heart disease. *Atherosclerosis.* 131:43–48.
47. Collins, R.G., et al. 2000. P-Selectin or intercellular adhesion molecule (ICAM)-1 deficiency substantially protects against atherosclerosis in apolipoprotein E-deficient mice. *J. Exp. Med.* 191:189–194.
48. Springer, T.A. 1990. Adhesion receptors of the immune system. *Nature.* 346:425–434.
49. Della Bella, S., et al. 2001. Novel mode of action of iloprost: in vitro down-regulation of endothelial cell adhesion molecules. *Prostaglandins Other Lipid Mediat.* 65:73–83.
50. Ishizuka, T., et al. 1998. Stimulation with thromboxane A_2 (TXA_2) receptor agonist enhances ICAM-1, VCAM-1 or ELAM-1 expression by human vascular endothelial cells. *Clin. Exp. Immunol.* 112:464–470.
51. Mitsuhashi, M., et al. 2001. Necessity of thromboxane A_2 for initiation of platelet-mediated contact sensitivity: dual activation of platelets and vascular endothelial cells. *J. Immunol.* 166:617–623.
52. Muller, W.A., Weigl, S.A., Deng, X., and Phillips, D.M. 1993. PECAM-1 is required for transendothelial migration of leukocytes. *J. Exp. Med.* 178:449–460.
53. Duncan, G.S., et al. 1999. Genetic evidence for functional redundancy of platelet/endothelial cell adhesion molecule-1 (PECAM-1): CD31-deficient mice reveal PECAM-1 dependent and PECAM-1-independent functions. *J. Immunol.* 162:3022–3030.
54. Graesser, D., et al. 2002. Altered vascular permeability and early onset of experimental autoimmune encephalomyelitis in PECAM-1-deficient mice. *J. Clin. Invest.* 109:383–392. doi:10.1172/JCI200213595.
55. Ensminger, S.M., et al. 2002. Platelet-endothelial cell adhesion molecule-1 (CD31) expression on donor endothelial cells attenuates the development of transplant arteriosclerosis. *Transplantation.* 74:1267–1273.
56. Newman, P.J. 1999. Switched at birth: a new family for PECAM-1. *J. Clin. Invest.* 103:5–9.
57. Rival, Y., Del Maschio, A., Rabiet, M.J., Dejana, E., and Duperray, A. 1996. Inhibition of platelet endothelial cell adhesion molecule-1 synthesis and leukocyte transmigration in endothelial cells by the combined action of TNF-α and IFN-γ. *J. Immunol.* 157:1233–1241.
58. Ma, H., et al. 2001. Increased bleeding tendency and decreased susceptibility to thromboembolism in mice lacking the prostaglandin E receptor subtype EP3. *Circulation.* 104:1176–1180.
59. Palinski, W., et al. 1994. ApoE-deficient mice are a model of lipoprotein oxidation in atherogenesis. Demonstration of oxidation-specific epitopes in lesions and high titers of autoantibodies to malondialdehyde-lysine in serum. *Arterioscler. Thromb.* 14:605–616.
60. Tangirala, R.K., Rubin, E.M., and Palinski, W. 1995. Quantitation of atherosclerosis in murine models: correlation between lesions in the aortic origin and in the entire aorta, and differences in the extent of lesions between sexes in LDL receptor-deficient and apolipoprotein E-deficient mice. *J. Lipid Res.* 36:2320–2328.
61. Sano, H., et al. 2001. Functional blockade of platelet-derived growth factor receptor-β but not of receptor-α prevents vascular smooth muscle cell accumulation in fibrous cap lesions in apolipoprotein E-deficient mice. *Circulation.* 103:2955–2960.
62. Murayama, T., et al. 2000. Over expression of low density lipoprotein receptor eliminates apolipoprotein B100-containing lipoproteins from circulation and markedly prevents early atherogenesis in apolipoprotein E-deficient mice. *Atherosclerosis.* 153:295–302.
63. Nakashima, Y., Raines, E.W., Plump, A.S., Breslow, J.L., and Ross, R. 1998. Upregulation of VCAM-1 and ICAM-1 at atherosclerosis-prone sites on the endothelium in the ApoE-deficient mouse. *Arterioscler. Thromb. Vasc. Biol.* 18:842–851.
64. Huo, Y., et al. 2003. Circulating activated platelets exacerbate atherosclerosis in mice deficient in apolipoprotein E. *Nat. Med.* 9:61–67.
65. Furchgott, R.F., and Zawadzki, J.V. 1980. The obligatory role of endothelial cells in the relaxation of arterial smooth muscle by acetylcholine. *Nature.* 288:373–376.
66. Poole, J.C.F., Sanders, A.G., and Florey, H.W. 1958. The regeneration of aortic endothelium. *J. Pathol. Bacteriol.* 75:133–143.
67. Massberg, S., et al. 2003. A crucial role of glycoprotein VI for platelet recruitment to the injured arterial wall in vivo. *J. Exp. Med.* 197:41–49
68. Furman, M.I., et al. 1998. Increased platelet reactivity and circulating monocyte-platelet aggregates in patients with stable coronary artery disease. *J. Am. Coll. Cardiol.* 31:352–358.
69. Michelson, A.D., and Furman, M.I. 1999. Laboratory markers of platelet activation and their clinical significance. *Curr. Opin. Hematol.* 6:342–348.

Circ J 2004; **68**: 1160–1164

Combined Measurements of Cardiac Troponin T and N-Terminal Pro-Brain Natriuretic Peptide in Patients With Heart Failure

Ryoji Taniguchi, MD; Yukihito Sato, MD*; Tasuku Yamada, MD; Muneo Ooba, MD; Hirokazu Higuchi, MD; Akira Matsumori, MD; Takeshi Kimura, MD; Toru Kita, MD

Background To examine the prognostic contribution of combined cardiac troponin T (cTnT) and N-terminal pro-brain natriuretic peptide (NT-proBNP) in patients with heart failure (CHF) in the absence of acute coronary syndrome.

Methods and Results Between July 2001 and March 2002, 71 consecutive patients (mean age=68.4±1.4 years, 37 men), hospitalised for heart failure, were studied during hospitalisation and follow up until December 2002. Serum cTnT and NT-proBNP were measured on admission. Actuarial rates of adverse cardiac events, including sudden or CHF death, or rehospitalisation for CHF during follow up were compared with patients grouped according to initial serum cTnT and/or NT-proBNP concentrations. The adverse cardiac event-free rate among the 20 patients with cTnT≥0.01 ng/ml was significantly lower than the 51 patients with cTnT<0.01 ng/ml ($P<0.05$). Similarly, the adverse cardiac event-free rate among the 36 patients with NT-proBNP≥1,357 pg/ml (median) was significantly lower than the 35 patients with NT-proBNP<1,357 pg/ml ($P<0.01$). The 16 patients with high concentrations of both cTnT and NT-proBNP had a lower adverse cardiac event-free rate than the 31 patients with low cTnT and low NT-proBNP upon commencement of the study ($P<0.005$).

Conclusion Measurements of serum cTnT and NT-proBNP were reliable prognostic markers of adverse cardiac event in patients with CHF. (*Circ J* 2004; **68**: 1160–1164)

Key Words: Heart failure; Pro-brain natriuretic peptide; Prognosis; Troponin

Chronic heart failure (CHF) is associated with a dismal long-term prognosis and remains a major health concern world wide[1,2] While various management strategies have become available, clinical tools to stage CHF remain few. The New York Heart Association (NYHA) functional classification, along with several tests, including chest roentgenogram, echocardiogram, myocardial scintigraphy, cardiopulmonary exercise, and hemodynamic measurements are useful to estimate the degree of CHF, although they are subject to inter-observer variations in interpretation[3,4] Serial measurements of reliable and objective biochemical markers would be advantageous to monitor the long-term prognosis of patients with CHF.

The troponin complex consists of 3 proteins attached to the actin thin filament, known as subunits I, T, and C, which regulate the force and velocity of muscle contraction. Cardiac troponin T (cTnT) is a highly sensitive and specific marker of myocardial injury in acute coronary syndromes, and a revised definition of acute myocardial infarction has been developed, based on rises in cardiac troponins in the blood[5,6] We found that patients with idiopathic dilated cardiomyopathy, who had a particularly poor prognosis, had increased serum concentrations of cTnT in the absence of significant coronary stenoses[7–10] Most patients with poor outcomes had persistently high cTnT. This often occurred during periods when CHF was stabilised by conventional treatment, and there was no evidence of dyspnea, roentgenographic and auscultatory signs of pulmonary congestion[8,9] Therefore, an increase in serum cTnT concentrations seems to be a reliable indicator of ongoing subclinical myocyte injury rather than an indicator

Table 1 Demographic and Baseline Clinical Characteristics of Study Population (n=71)

Age, mean±SE (years)	*68.4±1.4*
M/F	*37/34*
NYHA functional class I/II/III/IV	*10/22/22/17*
Underlying heart disease	
Dilated cardiomyopathy	*20 (28)*
Hypertrophic cardiomyopathy	*8 (11)*
Ischemic	*8 (11)*
Congenital or valvular	*22 (31)*
Hypertensive	*9 (13)*
Other	*4 (6)*
Oral drug regimen	
β-adrenergic blockade	*24 (34)*
ACEI or ARB	*33 (46)*
Spironolactone	*33 (46)*
Furosemide	*49 (69)*

Unless indicated otherwise, values are number (%) of patients. Other heart diseases include incessant tachyarrythmias (n=2), cardiac amyloidosis (n=1) and restrictive cardiomyopathy (n=1).
ACEI, angiotensin converting enzyme inhibitor; ARB, angiotensin receptor blocker; NYHA, New York Heart Association.

(Received June 7, 2004; revised manuscript received September 10, 2004; accepted September 22, 2004)
*Department of Cardiovascular Medicine, Graduate School of Medicine, Kyoto University, Kyoto, *Department of Cardiovascular Medicine, Hyogo Prefectural Amagasaki Hospital, Hyogo, Japan*
Mailing address: Yukihito Sato, MD, Department of Cardiovascular Medicine, Hyogo Prefectural Amagasaki Hospital, 1-1-1 Higashidaimotsu-cho, Amagasaki, Hyogo 660-0828, Japan. E-mail: cardioys@kuhp.kyoto-u.ac.jp

Table 2 Mean NT-ProBNP, CK, Age, and LVEF Among Patients With High and Low cTnT Values at Time of Hospital Admission

	NT-proBNP (pg/ml)	*CK (IU/L)*	*Age (years)*	*LVEF (%)*
cTnT high (n=20)	*13,260±5,035**	*90.2±9.2*	*68.5±3.5*	*49.6±3.1*
cTnT low (n=51)	*1,847±311*	*91.8±6.1*	*68.3±1.5*	*53.9±2.7*

**P<0.001, other between-group differences are not statistically significant.*
CK, creatine kinase; cTnT, cardiac troponin T; LVEF, left ventricular ejection fraction; NT-proBNP, N-terminal pro-brain natriuretic peptide.

Table 3 Comparison Between Patients With and Without Cardiac Decompensation

	Decompensation (+) (n=45)	*Decompensation (–) (n=26)*
Age, mean±SE (years)	*70.4±1.7*	*64.8±2.4*
M/F	*21/24*	*16/10*
LVEF (%)	*49.5±2.5*	*58.1±3.6*
NYHA functional class I/II/III/IV	*0/12/16/17*	*10/10/6/0*
TnT positive (%)	*16/45 (35)*	*4/26 (15)*
Mean TnT of positive patients (ng/ml)	*0.037±0.004*	*0.038±0.002*
NT-proBNP (pg/ml)	*7,233±2,369*	*1,303±291**
Creatinine (mg/dl)	*1.1±0.1*	*1.0±0.1*
Underlying heart disease		
Dilated cardiomyopathy	*14 (31)*	*6 (23)*
Ischemic	*5 (11)*	*3 (11)*
Congenital or valvular	*14 (31)*	*8 (31)*
Hypertensive	*8 (17)*	*1 (4)*
Oral drug regimen		
β-adrenergic blockade	*12 (27)*	*12 (46)*
ACEI or ARB	*22 (48)*	*11 (42)*
Spironolactone	*26 (58)*	*7 (27)**
Furosemide	*37 (82)*	*12 (46)***
Cardiac event (%)	*10 (22)*	*0 (0)**

**P<0.05, **P<0.01*
ACEI, angiotensin converting enzyme inhibitor; ARB, angiotensin receptor blockers; LVEF, left ventricular ejection fraction; NT-proBNP, N-terminal pro-bruin natriuretic peptide; NYHA, New York Heart Association; TnT, Troponin T.

of circulatory congestion.

However, N-terminal pro-brain natriuretic peptide (NT-proBNP) represents the N-terminal fragment of pro-BNP, the high molecular weight precursor of biologically active BNP. N-terminal pro-brain natriuretic peptide has a relatively long half-life and is stable in whole blood. Concentrations of NT pro-BNP are increased in patients with CHF and correlate with prognosis[11–13] Since CHF is a complex clinical syndrome, a single biomarker may not reflect all of its characteristics. Theoretically, cTnT is a marker of myocyte injury while NT-proBNP reflects cardiac load.

This study examines the contribution of combined measurements of cTnT and NT-proBNP in patients with CHF in absence of acute coronary syndrome.

Methods

Subjects

The study population consisted of 71 consecutive patients admitted to our hospital between July 2001 and March 2002 for the management or evaluation of decompensated CHF. No patient had suffered a myocardial infarction or unstable angina pectoris within 3 months prior to hospitalisation, and no electrocardiographic changes or increase in creatine kinase (CK) were present upon admission. The criteria for a diagnosis of left heart decompensation on initial presentation used in this study were: (1) dyspnea or orthopnea requiring emergency hospitalisation, intravenous furosemide, and infusion of nitrates or inotropic agents, and (2) roentgenographically apparent pulmonary oedema and presence of moist rales on auscultation. Patients with cancer and undergoing hemodialysis were excluded. The demographic and baseline clinical characteristics of the study population are presented in Table 1.

Serum cTnT and NT-proBNP were measured with commercially available immunoassay kits (Roche Diagnostics, Tokyo, Japan). All study procedures were in accordance with the ethical institutional guidelines of Kyoto University.

Long-Term Clinical Events

The subsequent incidence of adverse cardiac events was recorded until December 2002. Significant adverse cardiac events were defined as sudden death without apparent ischemia, death from CHF, or rehospitalisation of the patient for management of cardiac decompensation with pulmonary oedema. Information pertinent to a patient's death occurring outside the hospital between follow-up visits was obtained from the family.

Statistical Analysis

Data are expressed as mean±standard error. The study variables were compared by factorial analysis of variance for continuous variables. A receiver–operator characteristic (ROC) curve was used to determine the cut-off value of NT-proBNP which predicts cardiac decompensation and cardiac events. Adverse cardiac event-free rate, were constructed by Kaplan–Meier's method, log-rank test. A P value<0.05 was considered statistically significant.

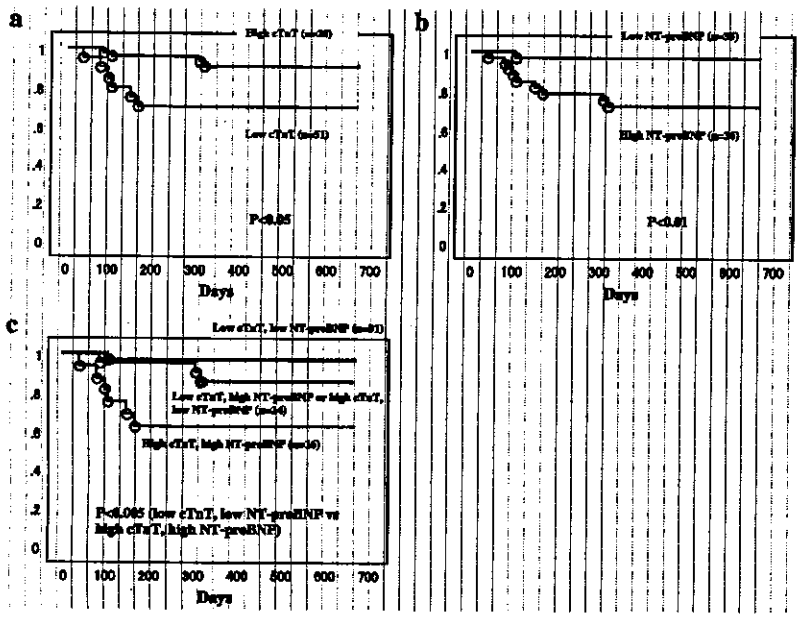

Fig 1. (a) Adverse cardiac event-free rate of patients with cTnT concentrations ≥0.01 ng/ml vs patients with cTnT concentrations <0.01 ng/ml. (b) Adverse cardiac event-free rate of patients with NT-proBNP concentrations ≥1,357 pg/ml vs patients with NT-proBNP concentrations <1,357 pg/ml. (c) Adverse cardiac event-free rate of patients with combined measurements of cTnT and NT-proBNP concentrations.

Results

Measurements of NT-ProBNP and TnT

The mean serum NT-proBNP concentration upon hospital admission of the 71 patients was 5,062±1,537 pg/ml (median=1,357 pg/ml). The mean NT-proBNP concentrations in patients of the NYHA functional class I, II, III, and IV were 954±361 (n=10), 1,673±473 (n=22), 2,902±771 (n=22), and 14,659±5,839 pg/ml (n=17), respectively. The cut-off value determined by ROC analysis for cardiac decompensation and cardiac events was 1,050 pg/ml (sensitivity 80%, specificity 67%) and 2,000 pg/ml (sensitivity 59%, specificity 67%), respectively. Age, CK concentration, and left ventricular ejection fraction and enddiastolic dimension measured echocardiographically did not correlate with NT-proBNP in this small population (data not shown).

The serum concentration of cTnT upon admission into the hospital was ≥0.01 ng/ml in 20 of the 71 patients (0.037±0.003 ng/ml). Cardiac troponin T was ≥0.01 ng/ml in 0/10 (0%), 6/22 (27%; 0.037±0.004 ng/ml), 7/22 (31%; 0.031±0.005 ng/ml) and 7/17 (41%; 0.046±0.008 ng/ml) patients in the NYHA functional classes I, II, III, and IV, respectively.

The mean serum concentration of NT-proBNP in the group of patients with high cTnT was significantly higher than in patients with low cTnT values (P<0.001). In contrast, age, CK and left ventricular ejection fraction were similar in both cTnT groups (Table 2). Comparisons between patients with and without cardiac decompensation are shown in Table 3. Concentrations of NT-proBNP in patients with cardiac decompensation were significantly higher than those in patients without (P<0.05).

Measurements of cTnT and NT-ProBNP, and Adverse Cardiac Events

Adverse cardiac events were observed in 10 patients (2 deaths from CHF and 8 cases of rehospitalisation for the management of cardiac decompensation with pulmonary oedema). The patients were divided into groups according to values of cTnT and NT-proBNP. The adverse cardiac event-free rate among the 20 patients with cTnT concentrations ≥0.01 ng/ml was significantly lower than the 51 patients with cTnT concentrations <0.01 ng/ml (P<0.05, Fig 1a). Similarly, the adverse cardiac event-free rate among the 36 patients with NT-proBNP concentrations ≥1,357 pg/ml was significantly lower than the 35 patients with NT-proBNP <1,357 pg/ml (P<0.01, Fig 1b). When groups were allocated according to both cTnT and NT-proBNP measurements, the 16 patients with high concentrations of both cTnT and NT-proBNP had a significantly lower adverse cardiac event-free rate than the 31 patients who had low cTnT and low NT-proBNP concentrations upon commencement of the study (P<0.005, Fig 1c).

Table 4 Hypothesis of Relationship Between Measurements of NT-ProBNP and TnT

	Low TnT	*High TnT*
Low NT-proBNP	*Without ongoing myocyte injury or myocardial load.*	*No myocardial load however, subclinical myocyte injury is ongoing. Patient is at risk of heart failure in the near future.*
High NT-proBNP	*Patient has heart failure without ongoing myocyte injury. Patient will stabilize with optimal treatment for heart failure.*	*Patient has heart failure with ongoing myocyte injury. If TnT concentrations do not decrease, heart failure may progress*

NT-proBNP, N-terminal pro-brain natriuretic peptide; TnT, Troponin T.

Discussion

In the present study, cTnT and NT-proBNP were reliable prognostic markers, both singly and in combination. Serum concentrations of cTnT≥0.01 ng/ml were considered significant[14] Assay of NT-proBNP is a new technology and normal values were reported approximately as 20 pg/ml![5,16] In our study, while mean NT-proBNP rose in the NYHA functional class, a similar correlation was not observed with mean cTnT concentrations. Moreover, 65% of patients with cardiac decompensation did not have a high serum cTnT concentration, and 15% had elevated concentrations despite being in a compensated state (Table 3). Troponin T seems to be a less sensitive marker of congestion.

We recently hypothesised that when managing heart failure, the therapeutic goals should be: (1) the relief of circulatory congestion and rapid lowering of markers of myocardial load, and (2) the mitigation of myocyte injury and lowering of markers of myocyte injury during long-term follow up![17] In this hypothesis, cTnT and NT-proBNP are important biochemical markers. The relationship between TnT and BNP and heart failure, based on our hypothesis, is shown in Table 4. These markers are easy to determine within a few hours and can be repeated for patient follow up, without inter-observer variability. In the future, the combination of these tests may be used in bedside clinical settings![18,19] Unfortunately, a multivariate analysis was not used to evaluate the prognostic value of these parameters because of our small sample numbers. Recently, Ishii et al reported that elevated cTnT and BNP on admission independently correlated with an increase in cardiac event rates in patients who were admitted to the coronary care unit for worsening chronic heart failure![14]

Although the mechanism of myocyte injury and the release of cTnT in CHF is not completely understood, cTnT seems to reflect ongoing myocyte injury even during compensated periods of CHF![7–10] Whether this indicates irreversible or reversible myocyte injury requires further investigation. The cytosolic pool for cTnT has been estimated at 6–8%. The release of protein may be because of a transient leak from the cytosol due to loss of sarcolemmal integrity during reversible ischemia, or from its continuous release when ischemic injury is irreversible![20,21]

No guidelines have been issued regarding the use of biochemical markers as part of the management of CHF. Recently, Maeda et al reported that BNP after optimized treatment for heart failure, rather than BNP before treatment, is an independent risk factor for morbidity and mortality in patients with congestive heart failure![22] We were unable to obtain follow up NT-proBNP data. While further studies are necessary, we anticipate that these assays will become the new monitoring standards in this patient population.

References

1. Shiba N, Watanabe J, Shinozaki T, Koseki Y, Sakuma M, Kagaya Y, et al. Analysis of chronic heart failure registry in the Tohoku district. Third year follow-up. *Circ J* 2004; **68:** 427–434.
2. Tsuchibayashi M, Tsutsui H, Kodama K, Kasagi F, Takeshita A. Clinical characteristics and prognosis of hospitalized patients with congestive heart failure: A study in Fukuoka, Japan. *Circ J* 2000; **64:** 953–959.
3. Hunt SA, Baker DW, Chin MH, Cinquegrani MP, Feldman AM, Francis GS, et al American College of Cardiology; American Heart Association. ACC/AHA guidelines for the evaluation and management of chronic heart failure in the adult: Executive summary. *J Heart Lung Transplant* 2002; **21:** 189–203.
4. Remme WJ, Swedberg K. Task force for the diagnosis and treatment of chronic heart failure, European Society of Cardiology: Guidelines for the diagnosis and treatment of chronic heart failure. *Eur Heart J* 2001; **22:** 1527–1560.
5. Alpert JS, Thygesen K, Antman E, Bassand JP. Myocardial infarction redefined-a consensus document of the Joint European Society of Cardiology/American College of Cardiology Committee for the redefinition of myocardial infarction. *J Am Coll Cardiol* 2000; **36:** 959–969.
6. Jaffe AS, Ravkilde J, Roberts R, Naslund U, Apple FS, Galvani M, et al. It's time for a change to a troponin standard. *Circulation* 2000; **102:** 1216–1220.
7. Sato Y, Kataoka K, Matsumori A, Sasayama S, Yamada T, Ito H, et al. Measuring serum aminoterminal type III procollagen peptide, 7S domain of type IV collagen, and cardiac troponin T in patients with idiopathic dilated cardiomyopathy and secondary cardiomyopathy. *Heart* 1997; **78:** 505–508.
8. Sato Y, Yamada T, Taniguchi R, Kataoka K, Sasayama S, Matsumori A, et al. Serum concentration of cardiac troponin T in patients with cardiomyopathy: A possible mechanism of acute heart failure. *Heart* 1998; **80:** 209–210.
9. Sato Y, Yamada T, Taniguchi R, Nagai K, Makiyama T, Okada H, et al. Persistently increased serum concentrations of cardiac troponin T in patients with idiopathic dilated cardiomyopathy are predictive of adverse outcomes. *Circulation* 2001; **103:** 369–374.
10. Sato Y, Taniguchi R, Makiyama T, Nagai K, Okada H, Yamada T, et al. Serum cardiac troponin T and plasma brain natriuretic peptide in patients with cardiac decompensation. *Heart* 2002; **88:** 647–648.
11. Richards AM, Doughty R, Nicholls MG, MacMahon S, Sharpe N, Murphy J, et al Australia-New Zealand Heart Failure Group. Plasma N-terminal pro-brain natriuretic peptide and adrenomedullin: Prognostic utility and prediction of benefit from carvedilol in chronic ischemic left ventricular dysfunction. Australia-New Zealand Heart Failure Group. *J Am Coll Cardiol* 2001; **37:** 1781–1787.
12. Bay M, Kirk V, Parner J, Hassager C, Nielsen H, Krogsgaard K, et al. NT-proBNP: A new diagnostic screening tool to differentiate between patients with normal and reduced left ventricular systolic function. *Heart* 2003; **89:** 150–154.
13. Fisher C, Berry C, Blue L, Morton JJ, McMurray J. N-terminal pro B type natriuretic peptide, but not the new putative cardiac hormone relaxin, predicts prognosis in patients with chronic heart failure. *Heart* 2003; **89:** 879–881.
14. Ishii J, Nomura M, Nakamura Y, Naruse H, Mori Y, Ishikawa T, et al. Risk stratification using a combination of cardiac troponin T and brain natriuretic peptide in patients hospitalized for worsening chronic heart failure. *Am J Cardiol* 2002; **89:** 691–695.
15. Seino Y, Ogawa A, Yamashita T, Fukushima M, Ogata K, Fukumoto H, et al. Application of NT-proBNP and BNP measurements in cardiac care: A more discerning marker for the detection and evaluation of heart failure. *Eur J Heart Fail* 2004; **6:** 295–300.
16. Swedberg KB, Hall C, Nielsen OW, Wu AHB, Apple FS, Collinson

PO. New frontiers in cardiovascular management clinical experiences and state-of-the-art research on N-terminal pro-brain natriuretic prptide (NT-proBNP). A report by the division of cardiology St. Michael's hospital, University of Toronto, Canada 2003. Toronto: University of Canada.
17. Sato Y, Kita T, Takatsu Y, Kimura T. Biochemical markers of myocyte injury in heart failure: Review. *Heart* 2004; **90:** 1110–1113.
18. Fonarow GC, Horwich TB. Combining natriuretic peptides and necrosis markers in determining prognosis in heart failure. *Rev Cardiovasc Med* 2003; **4**(Suppl): S20–S28.
19. Koh E, Nakamura T, Takahashi H. Troponin-T and brain natriuretic peptide as predictors for adriamycin-induced cardiomyopathy in rats. *Circ J* 2004; **68:** 163–167.
20. Piper HM, Schwartz P, Spahr R, Hutter JF, Spieckermann PG. Early enzyme release from myocardial cells is not due to irreversible cell damage. *J Mol Cell Cardiol* 1984; **16:** 385–388.
21. Katus HA, Remppis A, Scheffold T, Diederich KW, Kuebler W. Intracellular compartmentation of cardiac troponin T and its release kinetics in patients with reperfused and nonreperfused myocardial infarction. *Am J Cardiol* 1991; **67:** 1360–1367.
22. Maeda K, Tsutamoto T, Wada A, Mabuchi N, Hayashi M, Tsutsui T, et al. High levels of plasma brain natriuretic peptide and interleukin-6 after optimized treatment for heart failure are independent risk factors for morbidity and mortality in patients with congestive heart failure. *J Am Coll Cardiol* 2000; **36:** 1587–1593.

Available online at www.sciencedirect.com
SCIENCE DIRECT®
Biochemical and Biophysical Research Communications 323 (2004) 1116–1123
BBRC
www.elsevier.com/locate/ybbrc

Peroxisome proliferator-activated receptor α ligands activate transcription of lectin-like oxidized low density lipoprotein receptor-1 gene through GC box motif☆

Kazutaka Hayashida, Noriaki Kume*, Manabu Minami, Atsuko Inui-Hayashida, Eri Mukai, Masako Toyohara, Toru Kita

Department of Cardiovascular Medicine, Graduate School of Medicine, Kyoto University, Japan

Received 25 August 2004

Abstract

Lectin-like oxidized low-density lipoprotein receptor-1 (LOX-1) is a receptor for oxidized LDL. Peroxisome proliferator-activated receptors (PPARs) are nuclear receptors regulating transcription of various genes. We examined effects of PPAR ligands on LOX-1 expression and their transcriptional regulation in vascular endothelial cells. PPARα-specific ligands, such as fenofibrate and WY-14643, but not PPARγ-specific ligands induced LOX-1 expression. Reduced expression of PPARα by antisense oligonucleotides directed to PPARα blocked fenofibrate-induced LOX-1 expression. Luciferase reporter gene assays with deletion and point mutations in the LOX-1 promoter revealed that transcriptional activity of LOX-1 gene by fenofibrate was localized in the −114/−106 GC box. Electrophoretic mobility shift assays with the radiolabeled GC box sequence showed inducible bands by PPARα ligands, which is competitively suppressed by unlabeled GC box motif and by an antibody to PPARα. In conclusion, PPARα appears to be one of the key regulators that induce LOX-1 expression, utilizing the GC box as a promoter.

Keywords: Lectin-like oxidized low-density lipoprotein receptor-1; Peroxisome proliferators-activated receptors α; Vascular endothelial cells; GC box like motif; Oxidized LDL

Receptor-mediated endocytosis of oxidized LDL (Ox-LDL) may be crucial in the actions of Ox-LDL on vascular cells in atherogenesis. Among several different classes of receptors for atherogenic Ox-LDL, lectin-like oxidized low-density lipoprotein receptor-1 (LOX-1) is a 40–50 kDa type II membrane glycoprotein with a C-type lectin-like extracellular domain and a short cytoplasmic tail [1]. Expression of LOX-1 can be found in vascular endothelial cells, in addition to macrophages, and activated vascular smooth muscle cells [2–4]. More importantly, LOX-1 expression is not constitutive, but drastically inducible by proinflammatory cytokines, such as tumor necrosis factor α (TNFα) [3,5] and transforming growth factor β (TGFβ) [6], and fluid shear stress [7]. Moreover, LOX-1 expression in vivo is highly upregulated in endothelial cells covering early atherosclerotic lesions, as well as macrophages and smooth muscle cells accumulated in the intima of advanced atherosclerotic lesions [8]. However, transcriptional regulatory mechanisms of the LOX-1 gene have not yet been elucidated.

Peroxisome proliferator-activated receptors (PPARs) are members of the nuclear receptor superfamily, which can activate the transcription of various genes by heterodimer formation with the retinoid X receptor (RXR) in ligand-activated manners, and play key roles in lipid and carbohydrate metabolism [9]. PPARα appears to play a key role in lipid metabolism to regulate the gene expression involved in lipid metabolism [10]. PPARs are also expressed by vascular endothelial and smooth muscle cells [11–14] as well as macrophages [15].

PPARγ ligands can stimulate macrophage differentiation and induce expression of CD36, a receptor for Ox-LDL [15]. PPARα ligands, including fibrates [16], can suppress expression of proinflammatory genes, such as VCAM-1 [17] and IL-6 [14], in vascular endothelial and smooth muscle cells. By contrast, recent studies showed oxidized phospholipids could directly activate PPARα [18,19] to induce MCP-1 and IL-8 in vascular endothelial cells [19]. To further explore the direct action of PPARs on vascular cells, we sought to determine whether PPARα ligands can modulate expression of LOX-1 which is endocytic receptor for Ox-LDL in cultured vascular endothelial cells. We also explored transcriptional regulatory mechanisms involved in this process.

Materials and methods

Cell culture and reagents. DMEM was obtained from Nissui and fetal bovine serum (FBS) was from Irvine Scientific. WY14643 was purchased from Calbiochem–Novabiochem. Fenofibrate and 15-deoxy-12,14-prostaglandin J_2 was purchased from Sigma. Troglitazone was kindly provided by Sankyo. Bovine aortic endothelial cells (BAECs) were isolated by scraping the inner surface of bovine aortas with a razor blade and cultured in DMEM containing 10% (vol/vol) FBS.

Immunoblot analysis. Cells were washed with PBS and lysed in a buffer containing 50 mM Tris–HCl, pH 6.8, 2% SDS, 10% glycerol, and 0.01% bromophenol blue. After heated at 98 °C for 5 min, equal protein concentrations of the cell lysates were subjected to SDS-polyacrylamide (10%) gel electrophoresis and transferred onto nitrocellulose membranes (Hybond-N+, Amersham) by electroblotting. After preincubation with blocking reagent (PBS containing 0.1% Tween 20 and 5% nonfat dried milk) for 2 h at room temperature, blotted membranes were incubated with an anti-bovine LOX-1 monoclonal antibody for 2 h at room temperature, followed by washing twice with blocking reagent. Membranes were then incubated with a horseradish peroxidase-conjugated anti-mouse IgG (Amersham) for 1 h at room temperature, washed twice in PBS containing 0.04% Tween 20, and visualized by ECL Western blotting detection reagents (Amersham Biosciences).

Northern blot analysis. Total cellular RNA was isolated by Trizol reagent (Invitrogen). Total cellular RNA (15 μg) was subjected to electrophoresis through 1% agarose gel containing formaldehyde and transferred onto nitrocellulose membranes (Pro-Tran, Schleicher & Schuell). Membranes were hybridized with an *Xho*I fragment of bovine LOX-1 cDNA which had been labeled with [α-^{32}P]dCTP (DuPont-New England Nuclear) using random hexanucleotide primers (DNA labeling kit, Amersham Biosciences).

Cellular uptake of DiI-labeled Ox-LDL. LDL (density: 1.019–1.063 g/ml) was isolated by sequential ultracentrifugation of human plasma. Oxidative modification of LDL was carried out with cupric ion in vitro as previously described [20]. Oxidation was monitored by measuring the amount of thiobarbituric acid-reactive substances (TBARS). Our Ox-LDL contained approximately 10 nmol malondialdehyde equivalent/mg protein. Agarose gel electrophoresis showed increased electrophoretic mobility and minimal aggregation of Ox-LDL particles. Labeling of LDL with 1,1′-dioctadecyl-3,3,3′,3′-tetramethyl-indocarbocyanine perchlorate (DiI, Molecular Probes) was performed as previously described [21]. To examine cellular uptake of Ox-LDL, BAECs were incubated with DiI-labeled Ox-LDL (5 μg/ml) with 500 μg/ml (the 100-fold excess amount) of unlabeled acetylated LDL (Ac-LDL) in DMEM/10% FBS for additional 2 h after treatment of the indicated reagents for 12 h, and washed three times with the cell culture medium. Fluorescence microscopy was performed to detect DiI-Ox-LDL accumulated in cytoplasm. To quantify the fluorescence intensity, DiI was extracted from the cells by isopropanol, and the fluorescence intensity was measured in Fluoroscan II (Flow Laboratories). Acetylation of LDL was carried out using acetic anhydride as previously described [1].

Antisense oligonucleotides directed to PPARα. Antisense, sense, missense, and scrambled phosphorothionate oligonucleotides (ODNs) directed to 5′-coding sequence of the bovine PPARα mRNA were designed and manufactured by Fasmac. The sequences of ODNs were as follows: antisense; 5′-GGGCTTTCCGTGTCCACCAT, sense; 5′-ATGGTGGACACGGAAAGCCC, missense; 5′-GGCCTTGCCG TATCCATCAT, and scramble; 5′-TACCACCTGTGCCTTTCG GG. Transfection into BAECs was performed at the concentration of 1 μM of sODNs with lipofectamine 2000 (Invitrogen). After transfected cells were incubated with or without 100 μM fenofibrate for 12 h, the whole cell lysates were subjected to immunoblotting with an anti-LOX-1 monoclonal antibody.

RT-PCR for PPARα mRNA expression. Total RNA (1 μg) extracted from BAECs was reverse-transcribed with oligo(dT) and Superscript II (Invitrogen). The reverse-transcribed material (3 μl) was amplified with Ex-taq (Takara) by use of pairs of primers specific to bovine PPARα (forward primer: GGATCAGATGGCTCCGTTATT ACAG, reverse primer: GCTCCAGTGCATTGAACTTCATTG) and bovine glyceraldehyde-phosphate-dehydrogenase (forward primer: TCTGGCAAAGTGGACATCG, reverse primer: GGTCATAAGTC CCTCCACGAT). PCR products were 925 and 456 bp, for PPARα and GAPDH, respectively. For PCR, 30 cycles were used at 94 °C for 40 s, 55 °C for 1 min, and 72 °C for 1 min. PCR amplified products were visualized on 1.0% agarose gel electrophoresis by ethidium bromide staining.

Luciferase reporter gene plasmid constructs. Promoter regions of human LOX-1 gene from −3141 to +31, from −2423 to +31, and −167 to +31 were amplified from genomic DNA isolated from Jurkat cells by PCR and subcloned into PGL3-Basic (Promega), and were designated PGL3 −3141/+31, PGL3 −2433/+31, and PGL3 −167/+31, respectively. Reporter plasmids containing promoter regions from −1662 to +31 and from −1136 to +31 were generated by self-ligation of PGL3 −2423/+31 after digestion with *Sma*I and *Eco*RV. Plasmid containing from −527 to +31 was generated by self-ligation of PGL3 −2423/+31 after digestion with *Sma*I and *Spe*I followed by blunting. A point mutation with transversion of G–T at −107 in GC box related sequence located between −114 and −106 was generated by LA PCR in vitro mutagenesis kit (Takara).

Promoter–reporter gene assay. Confluent BAECs cultured in 24-well plates were transiently transfected with 2 μg of a luciferase reporter gene construct containing human LOX-1 5′ promoter region in 100 μl of Optimem (Invitrogen) and 0.2 μg pRL-TK plasmid (Promega) simultaneously as an internal transfection control using lipofectamine 2000 (Invitrogen). Luciferase activities were determined by dual-luciferase assay kit (Promega), and transfection efficiencies were normalized by *Renilla* luciferase activities.

Nuclear protein extraction and electrophoretic mobility shift assay (EMSA). Nuclear proteins were extracted, as previously described [22], from BAECs. Binding reactions were carried out in a total volume of 10 μl containing 10 μg of nuclear extracts, 1 μg of salmon testis DNA (Sigma), and ^{32}P-labeled oligonucleotide probes at room temperature for 30 min. Sequences of the used oligonucleotides were as

☆ *Abbreviations:* LOX-1, lectin-like oxidized low-density lipoprotein receptor-1; Ox-LDL, oxidized low-density lipoprotein; PPAR, peroxisome proliferators-activated receptor; PMA, phorbol 12-myristate 13-acetate; BAEC, bovine aortic endothelial cell.

* Corresponding author. Fax: +81 75 751 4094.
E-mail address: nkume@kuhp.kyoto-u.ac.jp (N. Kume).

0006-291X/$ - see front matter © 2004 Elsevier Inc. All rights reserved.
doi:10.1016/j.bbrc.2004.08.193